Electrical Characterization of Microwire-Polymer Assemblies for Solar Water Splitting Applications

by

IMAN YAHYAIE

A Thesis submitted to the Faculty of Graduate Studies of

The University of Manitoba

in partial fulfilment of the requirements of the degree of

DOCTOR OF PHILOSOPHY

Department of Electrical and Computer Engineering

University of Manitoba

Winnipeg

Abstract

The increasing demand for energy and the pressure to reduce reliance on fossil fuels encourages the development of devices to harness clean and renewable energy. Solar energy is a large enough source to fulfill these demands, however, in order to overcome its daily and seasonal variability, it has been proposed that sunlight be harvested and stored in the form of chemical fuels. One potential approach is the photosynthetic splitting of water to store solar energy in the simplest chemical bond, H–H, using a device that includes: semiconducting microwire arrays as light harvesting components, redox catalysts, and a membrane barrier for separating the products of water redox reactions..

However, the harvested solar energy can be lost across the system and it is critical to characterize the electrical properties of each component within the system to quantify how much of this energy will ultimately be coupled to the water splitting reactions. The aim of this research is to develop approaches for characterization of a proposed system of this kind, incorporating individual semiconductor microwires as photoelectrodes (with no redox catalysts) embedded into a candidate conducting polymer membrane to form a single functional unit.

Semiconductor microwires were isolated and using a novel contact formation approach with tungsten probes in a standard probe station, and their current versus voltage properties were characterized. This approach is of particular interest when

considering the limitations of conventional contact formation approaches (e.g. thermal evaporation of contact metals), arising from the small dimensions of the microwires and also the incompatibility of these techniques with many microwire/polymer structures due to the unwanted interactions between polymers, photoresists, etchants and the high temperature lithographic processes.

The electrical properties of different microwires and also the junctions between microwires and two candidate polymers were studied. Specifically, the combination of methyl-terminated silicon microwires and PEDOT:PSS:Nafion demonstrated promising behavior, with a total DC resistance of approximately 720 kΩ (i.e. losses < 16 mV at maximum available photocurrent), making it a suitable candidate for the use in the proposed system. The outcome of these research may be applied to many applications including semiconducting microstructures and conducting polymers.

Acknowledgements

I wish to express my sincere appreciation to my advisors Dr. Derek Oliver and Dr. Douglas Thomson for their support, direction, and encouragement during my studies. I am always grateful for the opportunity to have carried out this multidisciplinary research under their guidance. I am also indebted to Drs. Michael Freund and Nate Lewis for their advice and ongoing support throughout this research. I sincerely thank the members of my advisory committee, Drs. Greg Bridges, Douglas Buchanan, John Page and Can-Ming Hu for supervising my work and providing constructive feedback. I also wish to thank Dr. Peter Mascher for agreeing to be my external examiner.

During the course of my studies I have had the privilege of working with many wonderful students and postdoctoral fellows. My special thanks go to Dr. Kevin McEleney, Dr. Shaune McFarlane and Michael McDonald in Freund group, for generously dealing with my countless enquiries. I would like to thank Dr. Michael Walter, Dr. Ronald Grimm and Dr. Shane Ardo, postdoctoral fellows in Lewis group, for providing the microwire samples and for all the useful discussions.

I am grateful to Dwayne Chrusch, the nanosystems fabrication laboratory manager, and James Dietrich of the Advanced RF Systems Lab for their assistance during different steps of this research. I would like to thank Dr. Arkady Major for generously providing the setup for solar source calibration. I appreciate the assistance of Allan McKay and all the technical staff, in particular, Cory Smit, Allen Symmons, Mount-First Ng and

Ravinder Sidhu. I wish to thank our department office staff: Amy Dario, Judy Noble, and Karin Kroeker for their assistance with everyday departmental matters.

I wish to thank my friends at the University of Manitoba, Graham Ferrier, Jun Hui Zhao, Auxence Minko, Pommy Patel, Sharmistha Bhadra, Arezoo Emadi, Gustavo Bello, Md. Obaej Tareq, Farhad Yahyaie, Amir Hossein Birjandi and many others who have walked beside me in support.

I wish to acknowledge the financial support from the Natural Sciences and Engineering Research Council (NSERC) of Canada, the Manitoba Research and Innovation Fund and the University of Manitoba. In addition, this research made use of the Manitoba Materials and Surface Characterization Facility.

For her unwavering love and support, I would like to thank my wife, Nasim, who stood by me through the good times and bad and never stopped cheering me. Finally, but not least, I wish to express my profound gratitude to Amin, Elham and my parents, who have done everything for me and no word can describe the extent of my love for them. Thank you!

Contents

List of Tables

List of Figures

List of Copyrighted Material for which Permission was Obtained

Notations and Abbreviations

Symbols and Constants

e^-	electron
a	lattice constant
f	frequency
h	Planck constant
h^+	hole
hv	photon energy
k_B	Boltzmann constant
m	mass
m^*	effective mass
n	electron density in the conduction band
p	hole density in the valence band
q	charge on an electron
s	spacing
α	absorption coefficient, modifier of the Richardson constant
ΔE^0	electrochemical potential difference under standard conditions
ΔG	free energy change
η	ideality factor of the diode
η_{ext}	external quantum efficiency
λ	wavelength
μ	minority carrier mobility
ρ	resistivity
τ	minority carrier lifetime

Φ_b	barrier height
A	cross-sectional area
A^{**}	modified Richardson constant
Au	gold
B	boron
BCl_3	boron trichloride
C	carbon; capacitance
CdS	cadmium sulfide
CH_2Cl_2	dichloromethane
CH_3	methyl
CH_3CN	acetonitrile
CH_3MgBr	methylmagnesium bromide
CO_2	carbon dioxide
Cu	copper
D	minority carrier diffusion coefficient
$E^0(A/A^-)$	standard potential for the reduction of A to A^-
E_a	activation energy
E_c	conduction band-edge energy
E_d	activation energy required for producing point defect sites
E_F	Fermi level energy
E_g	bandgap energy
E_v	valence band-edge energy
F	Fluorine
Fe_2O_3	iron (III) oxide
$FeCl_3$	iron (III) chloride
Ga	Gallium
GaAs	gallium arsenide
$GaInP_2$	gallium indium phosphide

GaP	gallium phosphide
H_2	hydrogen
H_2O_2	hydrogen peroxide
$H_3PMo_{12}O_{40}$	phosphomolybdic acid
HCl	hydrogen chloride
HF	hydrofluoric acid
I	current
I_0	reverse saturation current
In	indium
InP	indium phosphide
J	current density
J_0	reverse saturation current density
J_{sc}	short-circuit current density
K	potassium
KOH	potassium hydroxide
L	length
L_D	minority carrier diffusion length
N_C	effective density of states in the conduction band
Ni	nickel
O_2	oxygen
P	phosphorus
Pd	palladium
Pt	platinum
$-q^{E0}(A/A^-)$	standard reduction potential of A to A^- in eV
R	resistance
R_C	junction resistance
$R_{C\text{-}n}$	n-Si microwire/polymer junction resistance
$R_{Contact}$	W probe/microwire contact resistance
$R_{C\text{-}p}$	p-Si microwire/polymer junction resistance

R_L	microwire resistance per unit length
$R_{n\text{-}wire}$	n-Si microwire resistance
$R_{polymer}$	polymer film resistance
$R_{p\text{-}wire}$	p-Si microwire resistance
R_{total}	total measured resistance of solar water splitting cell
R_{wire}	microwire resistance
Si	silicon
SiC	silicon carbide
SiO_2	silicon dioxide
$SrTiO_3$	strontium titanate
T	absolute temperature in Kelvin
TiO_2	titanium dioxide
V	voltage
Voc	open-circuit voltage
W	tungsten
WO_3	tungsten trioxide

Abbreviations

AES	auger electron spectroscopy
AM	Air Mass standardized solar irradiance
aq.	aqueous
BE	binding energy
Caltech	California Institute of Technology
CCI	Center for Chemical Innovation
CPS	counts per second
CVD	chemical vapor deposition
DC	direct current
DI	deionized
EBL	electron beam lithography

EDOT	3,4-ethylenedioxythiophene
EFM	electrostatic force microscopy
EHP	electron-hole pair
FIB	focused ion beam
FWHM	full width at half maximum
HER	hydrogen evolution reaction
In/Ga	indium-gallium metal eutectic
IPA	isopropyl alcohol
IR	Infrared
NHE	normal hydrogen electrode
OER	oxygen evolution reaction
PEC	photoelectrochemical cell
PEDOT	poly(3,4-ethylenedioxythiophene)
PEDOT:PMA	poly(3,4-ethylenedioxythiophene):phosphomolybdic acid
PEDOT:PSS	poly(3,4-ethylenedioxythiophene):poly(styrenesulfonate)
pH	potential hydrogen
PMA	phosphomolybdic acid
PPy	polypyrrole
PSS	poly(styrenesulfonate)
PTCDA	3,4,9,l0-perylenetetracarboxylic dianhydride
PV	photovoltaic
RPM	revolutions Per minute
RSF	relative sensitivity factor
SAW	surface acoustic wave
SC	semiconductor
SEM	scanning electron microscopy
SPCM	scanning photocurrent microscopy
SPM	scanning probe microscopy
UV	ultraviolet

VLS	vapor-liquid-solid
XPS	X-ray photoelectron spectroscopy

Units

°C	degrees Celsius
A	ampere
eV	electron volt
g	gram
Hz	hertz
J	joule
kg	kilogram
L	liter
m	meter
min	minute
mol	mole, 6.02×10^{23} elementary entities of a substance
Ω	ohm
N	newton
s	second
S	siemens
V	volt
W	watt

Chapter 1

Introduction

1.1 Solar Water Splitting Systems

The supply of clean and sustainable energy is arguably one of the most important scientific and technical challenges in the 21st century. Worldwide primary energy consumption is predicted to increase from 13.5 terawatt (TW) in 2001 to 27 TW by 2050 and 43 TW by 2100 [1,2]. The estimated fossil energy resources could support a ~30 TW global energy consumption rate for at least several centuries; however, consumption of fossil energy at this rate will produce a potentially significant global issue associated with the increased carbon (C) emission rates [3].

Energy harvested directly from sunlight offers a desirable approach toward fulfilling energy demands with minimal environmental impact. The earth and its atmosphere continuously receive ~1.7×10^{17} W of solar power [4], part of which is reflected by the atmosphere, yet the amount reaching the earth's surface is equal to 130 million 500 MW power plants [5]. However, the efficient utilization of sunlight as an energy source is limited by small solar power density at the earth's surface (~1 $kW.m^{-2}$ [6,7]), its daily and seasonal variations and difficulties in storage and/or transportation.

In order to overcome these limitations, solar energy must be efficiently captured, converted, and stored. Capture and conversion may be accomplished by photovoltaics (PVs) [8-10] although, cost-effective storage of solar electricity is still a significant challenge that is preventing its use as a primary energy source for society. One proposed method is to store solar energy in the form of chemical bonds and produce cheap solar fuels. Plants are working examples of this approach, using solar energy harvested through functionalized molecules in their chloroplast to reduce C from atmospheric carbon dioxide (CO_2) to saccharides; a process known as photosynthesis [11,12]. Borrowing this idea from nature, the photoelectrolysis of water to store solar energy in the simplest chemical bond, H_2, can be regarded as an important step in solar energy conversion and storage [5,13,14]. One technique of solar water splitting involves application of semiconductors as both the light absorber and energy converter, to evolve oxygen as one product and a reduced fuel (H_2) as the other [3,5,13]. More specifically, a photoelectrochemical water splitting cell, including stable semiconductors designed to split water directly at the semiconductor/liquid surface, has the potential to turn into an industrial technology [15]. This will be possible partly through the elimination of significant fabrication costs associated with the use of separate electrolyzers connected to p-n junction solar cells [16]; and by providing the possibility of forming an electric field at the semiconductor/liquid junction which will greatly assist the water separation reactions [17].

The process of solar water splitting in these photoelectrochemical cells is a multi-electron redox process promoted by photocatalyst and light. Despite the notable achievements in explaining the single electron-transfer reactions, an advancement so

significant that two Nobel Prizes were awarded for it [18,19], a similar level of understanding of multi-electron redox reactions has yet to be realized. Water splitting cells require semiconductor materials that are able to harvest a large portion of the solar spectrum and efficiently transfer photogenerated charge carriers to the semiconductor/aqueous interface with long-term chemical and electrical stability and minimal loss across the system [5].

Although a maximum photosynthetic efficiency of approximately 4.5% has been reported for the conversion of light (photons with approximate wavelengths of 680 nm) to stored chemical energy (dry carbon matter) [20-22], this value is rarely reached. The overall photosynthetic efficiency is affected by a range of factors. These factors include losses in photochemical and biochemical pathways, leaf reflectivity, the spectral distribution of light and the fact that there is a limited usable photon energy depending on the absorption properties of the light absorbing elements [14]. Only in exceptional cases, such as intensely cultivated sugarcane in tropical climates, will dry matter yield of photosynthesis exceed 1 or 2% and normally, agricultural crops yield biomass at efficiencies less than 1% [14,23]. On a global basis, the efficiency of photosynthesis is significantly lower (~0.2%) owing to seasonal changes and the existence of large areas of land on our planet, which do not sustain vegetation [14].

Many scientific and technical issues have to be addressed for photosynthetic water splitting technology to attain its useful generation potential. In addition, fast and reliable characterization techniques must be sought to identify all sources of energy loss in the ultimate system and to guarantee a reasonable efficiency.

1.2 Contributions

This thesis presents a study on the suitability of micro-scale semiconductor rods and their hetero-junctions with conducting polymers, from an electronic perspective, for the use in a proposed solar water splitting system. Systematic approaches were developed to form single microwire/polymer cell models of the ultimate envisioned device. Furthermore, a novel characterization technique was developed to investigate the electrical properties of these individual cells, with a focus on the potential losses across the cell.

Considering the existence of multiple electrical junctions within the proposed system and the limited amount of driving potential for water splitting reaction (i.e. the photogenerated potential), electrical loss across these components is anticipated to have critical impact on the final efficiency of the system. Electrical characterization of individual water splitting cells provides data that cannot be precisely determined from the bulk measurements. As a result, this technique can be reliably used to define and tune the electrical properties of different elements for the use in the ultimate solar water splitting device. Specifically:

- A novel characterization technique was developed in which an ohmic contact between the tungsten probes in a standard probe station and single semiconductor microwires was produced by applying mechanical force. This alleviated the need for lithography or high temperature processes to form a metal/semiconductor ohmic contact.
- The technique was first calibrated through measurements on individual semiconductor microwires. Silicon (Si) microwires doped with both p- and n-type dopants with resistivity values ranging from 0.02 to 13.51 Ω.cm were

investigated and a range of basic electrical properties of these individual microstructures, such as their resistivity and doping concentration as well as the uniformity of doping along the length, were extracted. Existing literature on single microwire measurements using conventional techniques were used as a benchmark to confirm the veracity of these results.

- The technique was also used to characterize the hetero-junctions between Si microwires and candidate conducting polymers that are of interest for the use in a proposed solar water splitting device. Specifically, structures including Poly(3,4-ethylenedioxythiophene) conducting polymer with two different oxidizing agents were investigated.
- Long-term electrical stability of the Si microwire/conducting polymer hetero-junctions may be a key feature in reducing the total implementation cost and as a result, justify their use in the proposed solar powered water splitting device. Therefore, in the final stages of this research, temporal changes in the microwire/polymer junction electrical properties as a measure of the stability of these combinations were also investigated using this technique. In a sequence of measurements, the individual p-Si microwire/polymer/n-Si microwire structures were studied over a period of 30 days and approaches to improve electrical stability in these junctions, such as passivation of microwire surfaces, were examined.

1.3 Thesis Outline

The remainder of this thesis is divided into four chapters. The second chapter provides a literature review of the areas of research spanned by this thesis and covers the basic theoretical background. It begins with a general overview of the photoelectrolysis systems and their different configurations. It is followed by a brief review of the novel photoelectrolysis cells based on micro- and nanostructures. The second section of chapter two is dedicated to an introduction to the Center for Chemical Innovation (CCI) collaborative project, covering some of the important aspects of the proposed system: the product-separating membrane materials (section 2.2.1) and the micro-scale semiconductor light absorbers (section 2.2.2). These sections focus on conducting polymer composites as the main candidates to be used as product-separating membrane and Si as the primary light absorbing photoelectrode material. Considering the importance of the semiconductor light absorber junctions with product-separating membrane materials, the final section of this chapter presents a discussion on the Si/polymer junctions and different approaches for characterizing these junctions will be discussed.

The third chapter details the experimental methods employed in the microwire/conducting polymer hetero-junction characterization. Approaches to isolate individual light absorbing microstructures are presented, followed by a description of the novel technique developed for ohmic contact formation to these individual microstructures. The second section of this chapter details the conducting polymer film preparation and semiconductor microstructure/polymer contact formation. General

figures of merit for these junctions are separately discussed in section 3.2.3. The third chapter concludes with a list of the apparatus used for the measurements.

The results of experimental work and a discussion of the results are presented in the fourth chapter. The results are presented in two main categories: the measurements on the individual light absorbing microstructures (sections 4.1 and 4.2) and microstructure/polymer junction characterization (sections 4.3 and 4.4). In the first section, different electrical properties of light absorbing microstructures are extracted using the novel contact formation technique. The measurement results are presented in four sub-sections and in a comparative manner. The second section details the microwire/polymer junction characterization for different combinations of candidate materials.

The fifth and final chapter concludes the thesis. A summary of the work is presented and potential future directions are explored. Five appendices follow. The calculation of the minimum required conductivity of the conducting polymer membrane is explained in Appendix A. Initial steps to prepare the semiconducting microstructure for the measurements are presented in Appendix B. The conducting polymer solution preparation procedure is described in Appendix C. The solar simulator lamp output power measurements and calibration are presented in Appendix D. The solar lamp was used to simulate the solar spectrum for the photocurrent measurements. Finally, the detailed results of the X-ray photoelectron spectroscopy (XPS) analysis carried on the n-type Si microstructures are presented in Appendix E.

1.4 Publications Arising From This Work

Journal papers:

1. I. Yahyaie, S. Ardo, D.R. Oliver, D.J. Thomson, M.S. Freund and N.S. Lewis, "Impact of Silicon Surface Functionalization on the Photoelectrical Properties of Individual Silicon Microwire/Polymer Assemblies for Water Splitting Application," Accepted for publication in *Energy and Environmental Science*, September 2012.

2. I. Yahyaie, K. McEleney, M.G. Walter, D.R. Oliver, D.J. Thomson, M.S. Freund and N.S. Lewis, "Characterization of the Electrical Properties of Individual p-Si Microwire/Polymer/n-Si Microwire Assemblies," *Physical Chemistry C*, Vol. 115, No. 50, pp. 24945-24950, November 2011.

3. I. Yahyaie, K. McEleney, M.G. Walter, D.R. Oliver, D.J. Thomson, M.S. Freund and N.S. Lewis, "Electrical Characterization of Si Microwires and of Si Microwire/Conducting Polymer Composite Junctions," *Physical Chemistry Letters*, Vol. 2, No. 6, pp. 675–680, March 2011.

4. S. H. Park, S. Ardo, I. Yahyaie, D. R. Oliver, D. J. Thompson, M. S. Freund and N. S. Lewis, "A > 90% Optically Transparent Composite Membrane for Tandem Microwire Array Solar Fuel Devices," In Preparation.

Conference proceedings:

1 S. Ardo, S. H. Park, E. L. Warren, I. Yahyaie, B. S. Brunschwig, D. R. Oliver, H. A. Atwater and N. S. Lewis, "Photoelectrosynthetic Hydrogen Evolution from Free-Standing Si Microwire Arrays," in *Gordon Research Conference - Renewable Energy: Solar Fuels*, Renaissance Tuscany II Ciocco Resort, Lucca (Barga), Italy, May 2012.

2 I. Yahyaie, K. McEleney, D.R. Oliver, D.J. Thomson and M.S. Freund, "Impact of Surface Functionalization on the Photoelectrical Properties of Individual p-Si Microwire/Polymer/n-Si Microwire Assemblies," in *2012 CCISolar Retreat*, Hilton Huntington Beach, CA, USA, January, 2012.

3 I. Yahyaie, K. McEleney, M. Walter, D.R. Oliver, D.J. Thomson, M.S. Freund and N.S. Lewis, "Electrical Characterization of Si Microwires and their Junction with Conducting Polymer Composite," in *15th Canadian Semiconductor Science and Technology Conference*, University of British Columbia, Vancouver, BC, Canada, August 2011.

4 D.R. Oliver, I. Yahyaie, B.P. Rakesh, G.E. Bridges, D.J. Thomson and M.S. Freund, "Local High-Frequency Electrostatic Probing of Candidate Conducting Polymer Membranes for Photovoltaic Applications," in *2nd International Workshop on SPM for Energy Applications*, Max Planck Institute for Polymer Research, Mainz, Germany, June 2011.

5 I. Yahyaie, K. McEleney, D.R. Oliver, D.J. Thomson and M.S. Freund, “Electrical Characterization of Semiconducting Microwires and Their Junction with Ionic and Electronic Conducting Polymers,” in *2011 CCISolar Retreat*, Hilton Huntington Beach, CA, USA, January, 2011.

6 I. Yahyaie, K. McEleney, D.R. Oliver, D.J. Thomson and M.S. Freund, “Electrical Characterization of Semiconducting Microwires and Their Junction with Ionic and Electronic Conducting Polymers,” in *Gordon Research Conference - Renewable Energy: Solar Fuels*, Ventura Beach, CA., USA, January 2011.

7 K. McEleney, I. Yahyaie, D.R. Oliver, D.J. Thomson and M.S. Freund, “Electrical Characterization of Semiconducting Microwires and their Junction with Ionic and Electronic Conducting Polymer Composites,” in *Materials Research Society, Fall Meeting*, Boston, MA., USA, November 2010.

8 I. Yahyaie, K. McEleney, D.R. Oliver, D.J. Thomson and M.S. Freund, “Characterization of the Electrical Junction between Silicon Microwires and Conductive Polymers,” in *2010 CCISolar Retreat*, Hilton Huntington Beach, CA, USA, January 2010.

Chapter 2

Literature Review and Theory

2.1 Photoelectrolysis

Photoelectrolysis is the conversion of light into an electrical current (electrical energy), and the use of this current in the division of a molecule; H_2O in the case of photosynthetic water-splitting cells [5]. The change in free energy associated with the conversion of one molecule of H_2O into H_2 and ½ O_2 is ΔG = 237.2 kJ.mol^{-1} (2.48 eV per molecule of H_2O), corresponding to an electrochemical potential difference (ΔE^0) of 1.23 V per electron transferred [5,13]:

$$H_2O + 2h^+ \rightarrow ½\ O_2 + 2H^+ \qquad \textit{Oxygen Evolution Reaction (OER)}$$

$$2H^+ + 2e^- \rightarrow H_2 \qquad \textit{Hydrogen Evolution Reaction (HER)}$$

$$H_2O \rightarrow ½\ O_2 + H_2 \qquad \Delta G = 237.2\ kJ.mol^{-1}$$

Semiconductor materials could be used as solar energy absorbers to provide the required photogenerated current directly from sunlight and drive the photosynthetic water splitting reactions. Ideally, a semiconductor with large enough bandgap energy (E_g) to

split water, and a conduction band energy (E_c) and valence band energy (E_v) that supports both the electrochemical potentials $E^{\circ}(H^+/H_2)$ and $E^{\circ}(O_2/H_2O)$, can drive the hydrogen evolution reaction (HER) and oxygen evolution reaction (OER) using electrons/holes generated under illumination. More specifically, p-type semiconductors with more negative conduction bands compared to the normal hydrogen electrode are well suited to drive HER and n-type semiconductors having a sufficiently positive valence band compared to normal hydrogen electrode[*] are ideal to drive OER [5].

To achieve this, the semiconductor must absorb photons with energies greater than 1.23 eV ($\lambda \leq$ ~1000 nm) and generate two electron-hole pairs (EHPs) per molecule of H_2 (2 × 1.23 eV = 2.46 eV) or four EHPs per molecule of O_2 (4 × 1.23 eV = 4.92 eV). To avoid recombination prior to water splitting reactions, photogenerated free charge carriers must travel to the semiconductor/liquid interface where they must react only with solution species. The charge transfer process at the semiconductor/liquid interface involves losses due to the concentration and kinetic overpotentials[†], therefore the energy required for photoelectrolysis at a semiconductor photoelectrode is reported to be 1.6-2.4 eV per electron-hole pair generated, to account for these losses [16,24]. The practical need for higher amount of energy in excess of the theoretical electrochemical potential difference to effectively drive water splitting motivates the use of multiple semiconductors with different energy gaps.

[*] A redox electrode which is used as a standard reference for the thermodynamic scale of oxidation-reduction potentials. To form a basis for comparison with all other electrode reactions, normal hydrogen electrode potential (E^0) is declared to be zero at all temperatures.
† Potentials required for photoelectrolysis, in excess of the required theoretical potential of 1.23 V.

2.1.1 Photoelectrolysis Cell Configurations

A basic photoelectrochemical water splitting device can be constructed in a range of different configurations. A single p-type or n-type semiconductor will form a single bandgap photoelectrolysis configuration. Two semiconductors connected in series or a semiconductor is in series with a PV cell will construct a dual bandgap configuration [5]. The single semiconductor configuration, forming a single bandgap device, requires two photons to produce one molecule of H_2 [24]. Depending on the device configurations, dual bandgap water splitting cells require two or four photons to produce one molecule of H_2 [5].

Fig. 2.1 depicts the energy band diagrams of basic photoelectrolysis cell configurations with a single (Fig. 2.1a) or a dual bandgap (Fig. 2.1b) structure. The back-to-back design in Fig. 2.1 was first demonstrated by Nozik in a "photochemical diode" using a p-n photoelectrochemical (PEC) device [25]. In Fig. 2.1, the photogenerated minority charge carriers are shown to be driven to the semiconductor/aqueous solution interface due to the electric field formed at the semiconductor/liquid contact. However, the majority carriers are either recombine at ohmic contacts between the photoelectrodes, or transferred to a metal cathode/anode to carry out the complementary redox step [25].

To generate the open circuit potentials (V_{OC}) required to split water, a single bandgap device requires a semiconductor with E_g of 1.6 to 1.7 eV which, considering voltage-loss mechanisms in the system, increases the required E_g to above 2 eV [26]. An oxygen-evolving n-type semiconductor photoanode electrically connected to a metal electrode for hydrogen evolution would form a single bandgap photosynthetic water splitting cell as depicted in Fig. 2.1a.

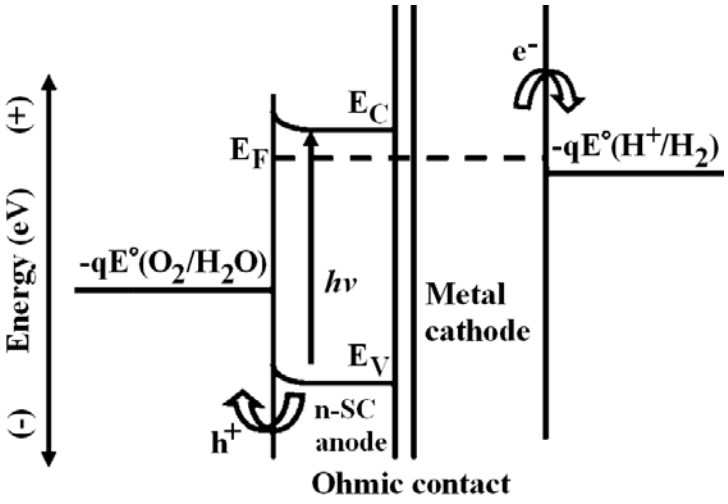

(a)

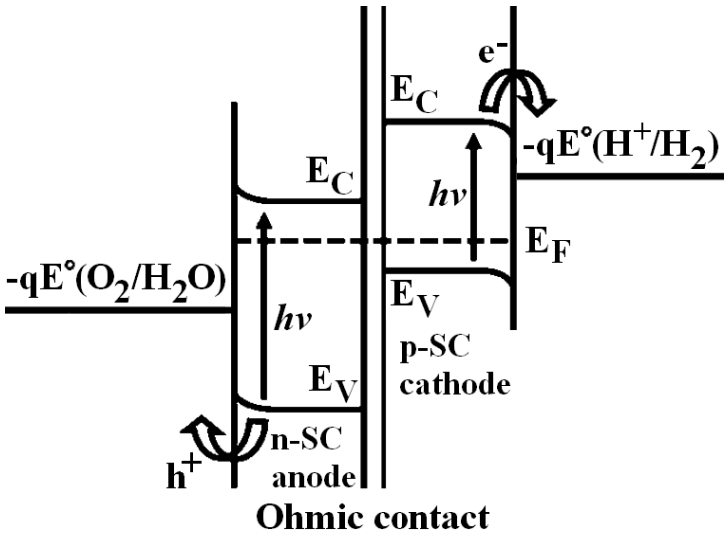

(b)

Figure 2.1: Energy diagrams for (a) a single bandgap photoelectrolysis cell with a photoanode in the form of n-type semiconductor (n-SC) and a metal cathode back contact; (b) a dual bandgap p/n-photoelectrolysis cell configuration with n-type and p-type photoelectrodes electrically connected in series. Adapted with permission from [5]. Copyright (2010) American Chemical Society.

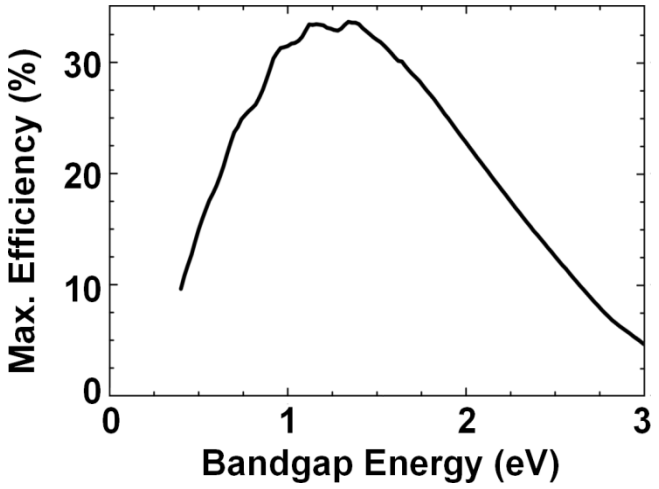

Figure 2.2: Maximum attainable solar conversion efficiency of a single bandgap solar cell, dictated by the Shockley-Queisser limit [27].

A single bandgap water splitting configuration can also be realized using a hydrogen-evolving p-type semiconductor photocathode and a metallic photoanode for oxygen evolution. However, many p-type semiconductors with high absorption in the visible region of the solar spectrum do not have sufficiently positive valence band potentials to oxidize water. In order to supply the extra photovoltage for water splitting, single bandgap photoelectrolysis cells can include a PV cell connected in series to form a dual bandgap device [5].

It is important to note that the maximum attainable solar conversion efficiency of a single bandgap solar cell, dictated by the Shockley-Queisser limit, is approximately 30% assuming a single p-n junction with a band gap of 1.1 eV, which is typical for Si [27]. As shown in Fig. 2.2, materials with bandgaps larger than 1.1 eV have lower conversion efficiencies. As a result, employing a single bandgap device for water splitting will be inefficient as materials with E_g > 2 eV would have to be employed, reducing the maximum theoretical efficiency by more than 33%.

Multiple bandgap cells employing several semiconductor materials with smaller bandgaps have been shown to outperform the Shockley-Queisser limit [28-32]. The increased efficiency in tandem structures is mainly due to the fact that each bandgap in these structures can be tuned to a different wavelength of light to span the solar spectrum, reducing an inherent source of loss [33]. In a set of infinite number of solar cells with a smoothly varying series of bandgaps (from 0 to ∞), the conversion efficiency is predicted to reach a theoretical limit of 86.8% under heavily concentrated sunlight [34]. Independent of the material bandgap, the conversion efficiency in this case will only be limited by the cell temperature and the geometrical factor which takes into account that the sun is seen only under a limited solid angle.

For water splitting devices, this means that a dual bandgap photoelectrolysis cell configuration would provide the ability to explore various combinations of smaller bandgap semiconductor materials. These materials will have wider combined range of light absorption, providing more efficient water splitting devices with a higher obtainable photovoltage [24,26]. A dual bandgap photoanode/photocathode configuration also allows partitioning of the water splitting half-reactions (i.e. OER and HER) between two semiconductor/liquid interfaces, efficiently separating water splitting reaction products (H_2 and O_2).

Since the absorption of one photon per semiconductor photoelectrode will generate one electron that is capable of fuel production, the maximum system external quantum efficiency (η_{ext}) in the dual bandgap structures is limited to 50% and, as a result, four photons are required to produce one molecule of H_2 and eight photons are required to produce one molecule of O_2 [5]. In addition, it is important to note that, commonly, two

surface electrocatalysts are required at the semiconductor-liquid junctions to reduce the required potential for each electrode, especially at the photoanode where losses often exceed 0.5 V [5,35-38].

In an early investigation, Honda and Fujishima suggested that the water splitting efficiency could be increased by coupling a p-type photocathode to a TiO_2 photoanode [39]. Increased light absorption through the use of a smaller bandgap semiconductor, along with generation of enough photovoltage to drive the hydrogen evolution reaction are the immediate results of such dual bandgap configuration [40]. However, in the specific case of TiO_2 with a bandgap energy of ~ 3 eV, the conversion efficiency (see Fig. 2.2) and consequently the amount of photocurrent that can be generated under white light illumination is small.

Since then, numerous reports have examined different types of photoelectrode materials. Photocathodes made of p-GaP have been reported in combination with n-type TiO_2 [25,41,42] and n-Fe_2O_3 [43] photoanodes. Stability issues due to the degradation of the p-GaP electrodes as well as the poor electrical performance and quantum efficiency of the n-Fe_2O_3 limit the viability of these combinations. A dual bandgap structure comprising a p-type InP and an n-type GaAs electrode has demonstrated reasonable electrical efficiency [44,45], however the materials used in this device included indium (In), a non-earth abundant material, suggesting expensive large-scale production. In another configuration, wide bandgap semiconductors, p-SiC (E_g ~ 2.9 eV) and n-TiO_2 (E_g ~ 3.0 eV) were used [46], however the wide bandgap limited the available operating photocurrent to the maximum output of the higher bandgap photoelectrode. As shown in Fig. 2.2, the maximum solar conversion efficiency will also be limited to about 5% for

these bandgap energies. It is worth mentioning that, with a bandgap of 3.4 eV, $SrTiO_3$ can split water by itself, albeit with lower efficiencies (maximum solar conversion efficiency < 5%, see Fig. 2.2) compared to a dual bandgap configuration [47]. A photoelectrolysis cell composed of p-type and n-type Fe_2O_3 photoelectrodes has also been reported [48] in which the poor photo-response and carrier transport of p-type Fe_2O_3 severely limited the efficiency of the cell. An n-type, nanostructured WO_3 photoanode combined with a p-type $GaInP_2$ photocathode [49] could not split water with light intensities <1 Wcm^{-2}, due to the low absorption of visible light by the WO_3.

Silicon is an attractive material choice for constructing a solar water splitting system because of its earth-abundance and prevalence in the electronics and PV industries. Silicon offers a good balance between low cost and narrow band gap (high conversion efficiency). With a band gap of 1.12 eV, p-Si is a desirable small bandgap absorber for possible use in dual bandgap water splitting cells for hydrogen evolution [5]. It has been demonstrated that planar p-Si photocathodes, combined with a variety of catalysts, reduce the voltage required to electrochemically produce H_2 [50-52]. Photon to hydrogen conversion efficiencies as high as 6% (under 633 nm illumination) have been reported for p-Si combined with Pt nanoparticles used as catalysts [51]. In this calculation of efficiency, the ratio of the stored potential energy as H_2 and O_2 to the incident optical power was defined as photon to hydrogen conversion efficiency. The stored potential energy is the product of the useful photogenerated voltage and photocurrent, where the useable photovoltage was the extent to which the photoelectrode potential is more positive than $E^0(H^+/H_2)$ at a nonzero photocurrent [51,53-56].

Application of Si as a potential photoanode material for light-assisted water oxidation, combined with iron oxide [57] or cobalt-based photocatalysts [58], has also attracted recent attention. This is mainly due to the robustness and abundance of Si electrode and the potential for direct processing of the metallic photocatalysts which presents a low technical barrier for manufacturing of these structures.

Direct solar energy to fuel conversion has been recently demonstrated using amorphous silicon combined with earth-abundant catalyst materials [59,60]. These catalysts have been interfaced directly with a commercial triple-junction amorphous silicon (3jn-a-Si) solar cell and solar to fuel conversion efficiencies as high as 2.5% have been reported. Considering these recent advancements, Si seems to be a potential candidate for the use in a solar powered water splitting system.

However, regardless of the photoelectrolysis cell configuration, the existence of different junctions in these devices means that minimizing the electrical loss and sustaining the necessary photovoltages for driving the water splitting reactions present a significant challenge. Losses due to the presence of any potential barrier towards charge carrier transport across the system, electrical resistances within the materials and the reflection or scattering of photons at multiple semiconductor layers within the cell will decrease the overall system performance. As the search for the appropriate semiconductor materials and configurations for photoelectrolysis continues, efficient characterization tools and techniques are required to understand the junction properties and electrical behavior of these systems.

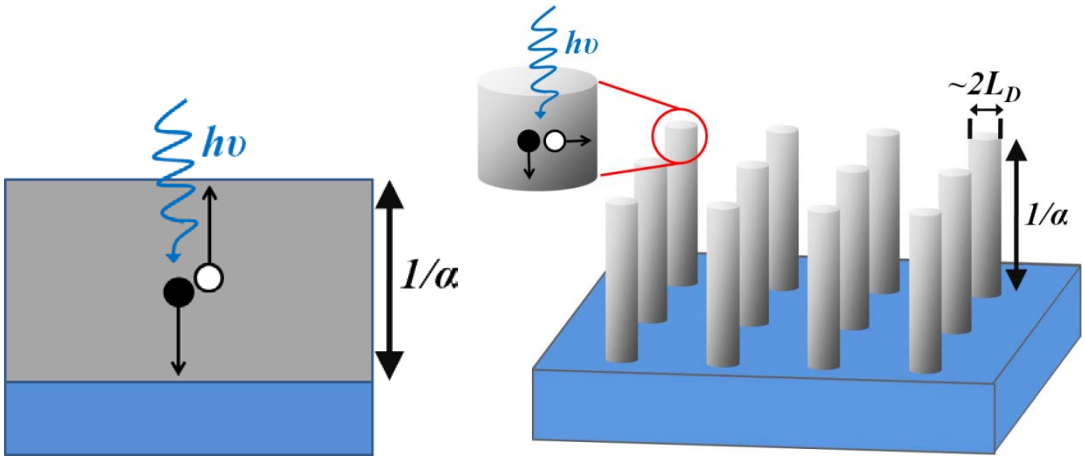

(a) **(b)**

Figure 2.3: Photogenerated carriers (white and black circles) in a planar system (a) travel the entire thickness of the device, *1/α*, before collection, while in a microstructured device, such as a microwire array assembly (b) with appropriate dimensions, carriers must only reach the microwire surface before recombination. In this schematic diagram, α is the absorption coefficient and L_D is the diffusion length of the photogenerated minority carriers (white circles). Multiple reflections of incident photons between the microwires will ultimately lead to complete absorption in the microwire array structures at almost all incident angles.

2.1.2 Photoelectrolysis Cells with Micro- and Nano-Scale Photoelectrodes

Planar and large scale electrodes have been used in the photovoltaic applications and photoelectrolysis cells, however much recent interest has been directed toward the utilization of micro- and nanostructured electrodes in these systems [61-67].

The minority carrier diffusion length (L_D), the distance that a minority carrier can diffuse before recombination, is defined as [68,69]:

$$L_D = \sqrt{D\tau} \qquad (2.1)$$

where τ is the minority carrier lifetime and D is the minority carrier diffusion coefficient. The Einstein relation relates the diffusion coefficient to the minority carrier mobility, μ (in $m^2\ V^{-1}\ s^{-1}$), by the following equation [68,69]:

$$D = \frac{\mu k_B T}{q} \qquad (2.2)$$

To satisfy the constraints for efficient carrier collection in a planar photovoltaic device, L_D should ideally be greater than $1/\alpha$, where α is the absorption coefficient of the semiconductor near the bandgap energy. These devices should be typically made of high purity semiconductors with lowest possible defect concentrations to reduce the number of recombination sites. Employing a non-planar configuration of the light absorber semiconductor electrodes permits the diffusion length requirement to be decoupled from the absorption length. One example of this configuration is micro- and nano-scale semiconductor rod arrays (Fig. 2.3b).

It has been shown [70,71] that high surface area semiconductor micro- and nanowire arrays reduce the minority carrier traveling distance (across the diameter of the wires), and hence enable near-unity collection efficiencies. The amount of the semiconductor material used to fabricate these structures could also be reduced by re-using the same substrates to fabricate new structure. In one approach, the arrays of Si wires are sequentially grown and then embedded in a polymer. The polymer-embedded microwires are then mechanically separated from the substrate. This will preserve the array structure in the film, leaving behind the growth substrate for the next array growth [72].

Despite their advantages, micro- and nanostructures have been shown to reduce the V_{OC} by increasing the junction area of the semiconductor photoelectrode ($\geq$ 60 mV per

order of magnitude increase in junction area [70,71]) as the reverse saturation current, I_0, is directly proportional to the junction area and V_{OC} has an inverse relationship with I_0. Within the junction the photogenerated charge carriers are now distributed over larger junction area leading to smaller charge densities. In turn, the splitting of the quasi-Fermi levels at the solution-semiconductor interface is reduced [73-76]. This is valid even in the ideal case of negligible surface recombination. The reduction of V_{OC} sets a limit on the dimensions of the rods for the use as photoelectrodes in the semiconductor array. In order to achieve the highest performance, the light collection area should be enhanced enough to collect all the photogenerated charge carriers (i.e. L_D = radius of the rod) [71]. Any further increase in the area is undesirable since it will cause an unwanted decrease in the V_{OC}.

On the other hand, different configurations of semiconductor rod arrays could also be examined in order to find geometries that significantly enhance light absorption at a wide range of incident angles, thereby offsetting the loss from charge-carrier dilution over larger surface areas. Recent reports on this subject stress the fact that minor changes in the array configuration (e.g. different tiling patterns) could modify the absorption character of the rod arrays. It is shown that in arrays having less than 5% areal fraction of wires, up to 96% peak absorption is achievable. These arrays are capable of harvesting up to 85% of day-integrated, above-bandgap direct sunlight [77].

This thesis presents a study on the suitability of micro-scale semiconductor rods of this kind, from an electrical resistance perspective, for the use in a proposed solar fuel generation device.

2.2 CCI Collaborative Project: Device Overview

Fabrication of a dual bandgap solar water splitting system is a collaborative project [78] which aims to develop the components, and ultimately a proof-of-principle demonstration of a fuel generating system that is easily manufacturable and uses earth-abundant sources (e.g. water and sunlight). The term artificial photosynthesis is alternately used for this water splitting system since both processes collect and store solar energy in chemical bonds, photosynthesis by converting CO_2 into organic compounds, especially sugars [13], and water splitting cells by breaking water molecules into H_2 and O_2 and storing the hydrogen as a form of fuel.

An idealized artificial photosynthesis system would utilize sunlight and water as the inputs and produce H_2 and O_2 as the outputs. The O_2 would be vented to the atmosphere or stored for other applications and the H_2 transferred to the fuel storage system.

A membrane-bridged structure encompassing high aspect ratio microstructured semiconductor photoelectrodes made from earth abundant materials (Fig. 2.4a) has been proposed as a reasonable approach to the production of hydrogen using sunlight [5,56,79-83]. In principle, this combination of two semiconductor photoelectrodes (photoanodes and photocathodes), with appropriate bandgaps and properly aligned band edges (i.e. dual bandgap photoelectrolysis configuration), would provide the necessary photovoltage (>1.23 V) to split water into H_2(g) and O_2(g). Fig. 2.4b shows the experimental model of a single functional unit of the device demonstrated in Fig. 2.4a (details in section 3.2.2). The photo-induced redox reactions are essential in separating water molecules as they release hydrogen and oxygen ions. However, external photocatalysts are required to increase the speed of reaction at low overpotentials [5,82,84,85].

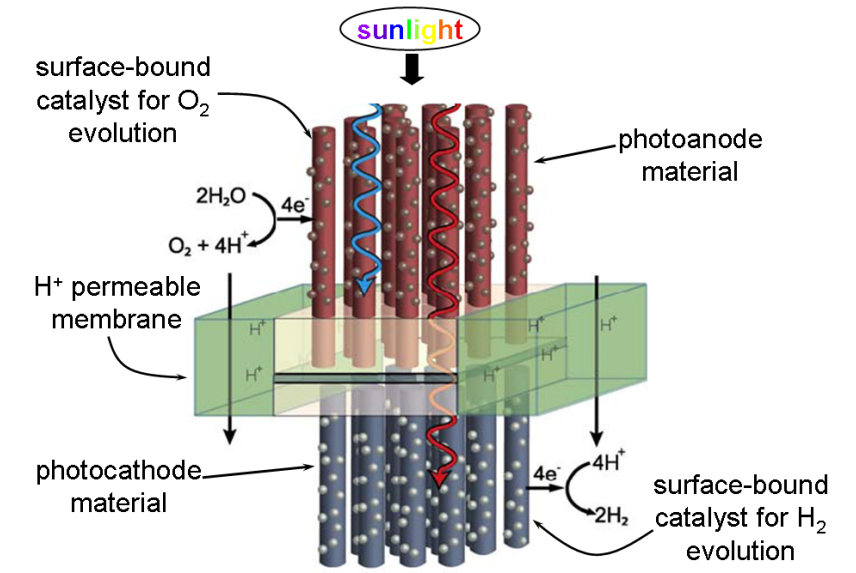

(a)

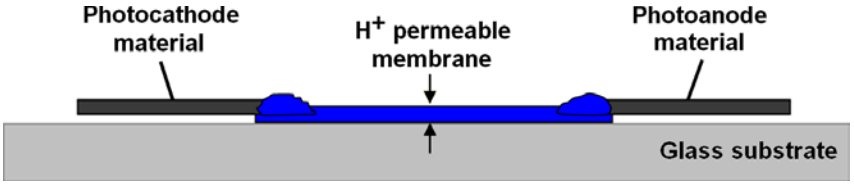

(b)

Figure 2.4: (a) Schematic diagram of the proposed artificial photosynthesis system. The system is a dual bandgap p/n photoelectrolysis structure, for which the approximate energy band diagrams were demonstrated in Fig. 2.1b. Adapted with permission from [79]. Copyright (2009) Macmillan Publishers Ltd: Nature Chemistry. (b) Suggested model representing a single functional unit of (a). Different variations of this model were used in this thesis to investigate the electrical properties of a unit cell of the water splitting system (details in section 3.2.2).

Microstructured semiconductor surfaces used as the photoelectrodes in this system to absorb the sunlight also have the potential to reduce electrocatalysis losses in the form of overpotentials, because of the lower current density at the electrode due to lower

photogenerated charge carrier densities in the larger areas as discussed in section 2.1.4. Lower electrocatalysis losses in the form of overpotentials might allow for earth-abundant catalysts, with lower activities[*], to be uniformly deposited onto the structured electrodes, to replace highly active precious metal catalysts [5].

As another key element, the separating membrane in this structure would support and incorporate the two semiconductor materials and permit ion and electron transport to complete the circuit while separating the evolution of H_2(g) and O_2(g) [84,85,87]. As explained in section 2.1, OER will occur at the photoanode, causing a buildup of positive hydrogen ions in the oxidation half-cell (the cell containing the photoanode array). These excess ions will move through the membrane to the reduction half-cell where the hydrogen evolving reactions (HER) occur. On the other hand, a low loss ohmic contact will be desired between each photoelectrode and the separating membrane in order to facilitate the passage of unused photogenerated charge carriers across the system to maintain the charge neutrality in the system and to keep the water splitting reactions running. Anticipating that optimization of the material parameters will gain desirable efficiencies in the final device, a detailed knowledge about the electrical conduction mechanism in the system is of great importance. This is especially true at the electrical junctions between the photoelectrode microwires and candidate materials for the use as separating membrane [80,88-91].

During the course of this international collaboration, electrochemistry research projects conducted in parallel were aimed at realizing a final system. The idea is to

[*] The catalyst activity of a given material can be quantified (in the dark) by the current density that can be passed in the system including this catalyst at a given voltage applied to the electrode relative to the redox potential of the relevant couple. The noble metals Pt and Pd demonstrate high activity and Ni is the most active non-precious metal [86].

separately develop and optimize the three distinct and critical device components before assembly into a complete water-splitting system. A brief overview of essential elements of the proposed system, excluding the photocatalysts, is presented in the following sections.

2.2.1 Candidate Membrane Systems

Considering the limited energy resources available in the solar water splitting systems, the candidate material for use as the separating membrane must address three major sources of loss in the proposed system: losses due to the unwanted light absorption, recombination of the water splitting gas products and, finally, electronic and ionic losses. Since the energy required for driving HER and OER is directly harvested from sunlight, the membrane needs to be sufficiently transparent for light to reach the light absorbing semiconducting photoelectrodes. Furthermore, the membrane should act as a barrier towards gas diffusion in order to avoid recombination of water splitting products, $H_2(g)$ and $O_2(g)$, which would diminish the efficiency of the system. Finally, the excess photogenerated charge carriers need to freely move across the system to maintain the overall charge neutrality. Also the hydrogen ions generated during OER need to be transferred to the reduction half-cell, the cell containing the photocathode array, for participating in HER. As a result, the membrane should also be of sufficient and desirable equal electronic and ionic conductivity [87,92].

Considering the available current densities from the sun (~20 $mAcm^{-2}$, see Appendix A for details) and assuming that one charge carrier traverses the membrane for every two incident photons absorbed by the photoelectrodes) and, assuming an acceptable IR loss of less than 1% (1% of 1.23V, ~10mV) across the membrane in an ideal solar water splitting

system, the membrane must encompass conductivities of approximately 0.2 $mScm^{-1}$ per one micrometer thickness of membrane (Appendix A). Finally, it is also possible for the membrane to experience large pH gradients with H^+ and OH^- being generated at the two sides of the device so the final candidate should be able to withstand the extreme pH gradients [93].

To summarize the material requirements, in addition to transporting charge carriers and ions with minimal resistance, the candidate membrane material for the use in the proposed solar water splitting system must be water insoluble, mechanically stable, homogeneous on the nano-scale, adherent to a wide range of semiconductors to provide mechanical support, impermeable to gases, stable in the presence of redox intermediates and various pH conditions, optically transparent or have low optical absorption. Furthermore, its electronic and ionic conduction should be tunable to the desired values.

Although there is currently no single material capable of satisfying all the mentioned requirements, recent reports [87,94] suggest that Nafion, a fluorocarbon (CF) based polymer with multiple strong C–F bonds (Fig. 2.5) [94], could be a promising candidate for the use as the separating membrane due to its excellent ionic conductivity (~80 $mScm^{-1}$ [95,96]), transparency and also chemical and mechanically stability (a good barrier towards gas diffusion).

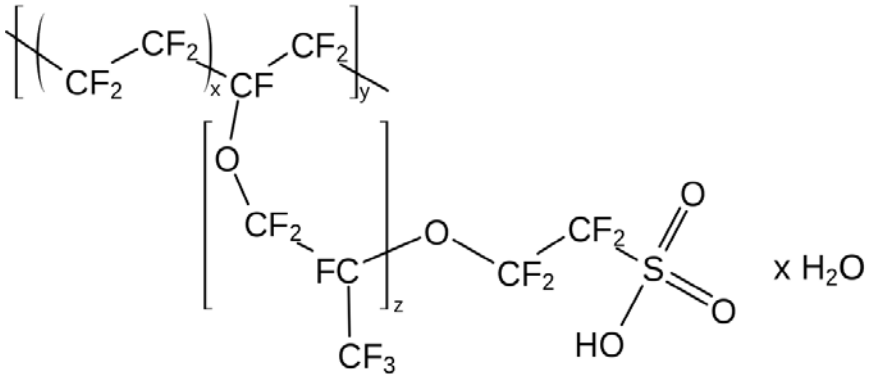

Figure 2.5: Chemical structure of Nafion [94], a fluorocarbon (CF) based polymer with multiple strong C–F bonds.

Nafion is the first of a class of synthetic polymers which are called ionomers [94]. An ionomer is a polymer that comprises repeat units of both electrically neutral repeating units and a fraction of ionized units [97]. Nafion is commercially available, transparent at visible wavelengths, and is easily processed as it comes in different water- and alcohol-based solutions. However, Nafion is an electronic insulator and, as a result, cannot serve as the separating membrane without modification or combination with other materials.

Another interesting class of candidate materials is conducting polymers, which are organic electronic conductors that are important components in emerging technologies ranging from organic light emitting diodes to polymer-based electronics [98-102]. The biggest advantage of conducting polymers is their ease of processing and the ability to tune their chemical and morphological structure [102]. Similar to inorganic semiconductor materials, the electronic conductivity of conducting polymers can also be tuned through a series of oxidation (p-type doping) or reduction (n-type doping) reactions [102]. In addition, this class of material contains a high concentration of ions, improving ionic conductivity. There is an extensive literature on the different classes of organic

conducting polymers such as poly(acetylene)s [103,104], poly(pyrrole)s [105,106], poly(thiophene)s [107,108], and poly(aniline)s [109,110]. In the artificial photosynthesis system, a conducting polymer could be used as a separating membrane as well as a conductive path for both electrons and protons. The choice/design of the polymer is crucial in order to balance electronic and ionic conductivity as the candidate membrane should conduct equal electronic and ionic current densities.

Poly(3,4-ethylenedioxythiophene) or PEDOT is a conducting polymer based on 3,4-ethylenedioxylthiophene or EDOT monomer [111,112]. Fig. 2.6 shows the chemical structure of PEDOT. Some of the advantages of this polymer include a low optical absorption in its conducting state, a high stability, a moderate bandgap (E_g = 1.6 ~ 1.7 eV [112-114]) and a low redox potential.

These characteristics make PEDOT a good candidate for use as the separating membrane in the artificial photosynthesis system. However, poor solubility of PEDOT in water (or in a range of solvents) [111,112] makes its processing harder. This is important as the polymer must be spin-coated (or drop cast) in the form of a solution with different concentrations onto the target substrates to control the conductivity of the films.

By choosing the proper ratio and length of the flexible polymer segments and PEDOT segments [98,102], the electronic conductivity of PEDOT may be adjusted between 0.1 to 300 $S.cm^{-1}$ [112]. However, the low ionic conductivity of PEDOT presents a challenge as the final membrane material should conduct all the charge carriers (electrons and hydrogen ions) equally [87].

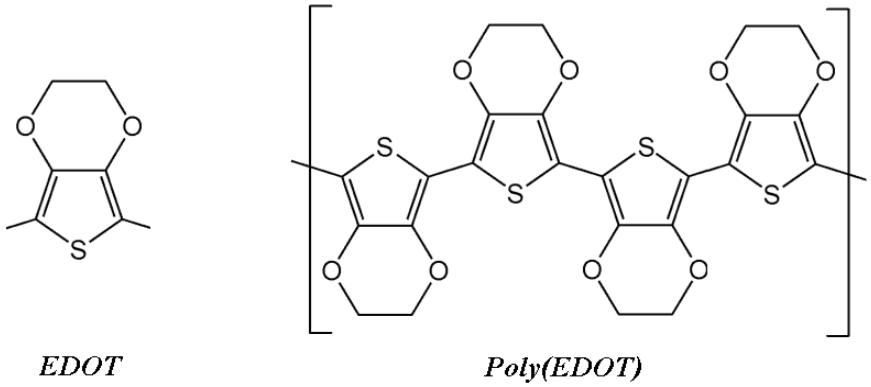

Figure 2.6: Chemical structure of: (a) EDOT (3,4-ethylenedioxythiophene) monomer [112] and (b) Poly(EDOT) or PEDOT conducting polymer.

The ionic conductivity can be improved by controlling the porosity of the membranes through the use of porogens* during the polymerization process [115] or by combining different elements with high ionic conductivity and making composite materials [102]. Both of these issues with PEDOT might be partly circumvented by adding phosphomolybdic acid (PMA), $H_3PMo_{12}O_{40}$, to PEDOT and making a composite polymer known as PEDOT:PMA [116]. Alone, PMA has already demonstrated electron (~1 Scm^{-1}) and ion (~ 24 μScm^{-1} at 1.6 pH) conducting characteristics. PMA is also a strong oxidizing agent, making PEDOT:PMA polymer a p-type semiconductor, which is also important in forming stable PMA-oxidized films with PEDOT [116]. PEDOT:PMA shows a relatively low but constant conductivity over wide pH range [93], although its mechanical properties are sub-optimal for this application. To date, there is no report on

* A material, usually added during the polymerization process to manipulate morphology and porosity of the polymer film. Removal of the porogen after the polymerization will leave behind a porous form of the polymer material. In the mentioned example, ionic conductivity of PPy:PMA films is reported to increase by introduction of sodium sulfate as a porogens during the polymerization process [115] .

production of free-standing PEDOT:PMA composite membranes and the films are also hard to process in comparison to commercially available compounds.

Poly(styrene sulfonic acid) or PSS is another element which, in combination with PEDOT, can improve both electronic (>10 Scm^{-1} [102,112]) and ionic conductivity (~8.1 $mScm^{-1}$ [117]) and also the stability over a wide pH range [87,118]. Furthermore, PEDOT:PSS is commercially available as a water-soluble polyelectrolyte system, making film processing much easier than the PEDOT:PMA composite. Despite its good film forming properties, and excellent stability [119], the mechanical stability is still an issue with PEDOT:PSS as the composite structure is not strong enough to produce free-standing membranes. Furthermore, PEDOT:PSS films (dark blue colored) have relatively high light absorption, which is detrimental for the efficiency of the ultimate water splitting cell.

In one promising approach, composite materials built by combining Nafion with conducting polymers have been reported to show desirable properties for the use in the proposed system [87]. Specifically, it has been shown recently that free-standing, electrically conducting membranes of Nafion could be produced by adding sufficient PEDOT:PSS to the structure.

Initial investigations on PEDOT:PSS:Nafion have shown that it is possible to produce free-standing membranes which are flexible and mechanically stable as shown in Fig. 2.7. Introducing higher amounts of PEDOT:PSS into the Nafion structure enhances the electrical conductivity while reducing the film transparency due to high absorption of PEDOT:PSS in the visible region. It has been determined that 12 wt% of PEDOT:PSS is enough to meet the minimum requirements for the conductivity of the films discussed

earlier in this section while maintaining approximately 95% transparency in 400 to 700 nm region [87].

In this thesis, microwire-polymer junction investigations have been undertaken using both PEDOT:PMA and PEDOT:PSS:Nafion compounds to examine the possibility of each compound for being used in the final device.

2.2.2 Si Microwire Arrays Grown using Vapor-Liquid-Solid Technique

A membrane-supported assembly that captures sunlight and efficiently creates separated electrons and holes having sufficient chemical potential to drive the water-splitting reactions is an important part of the artificial photosynthesis system. As discussed in section 2.1.4, in order to achieve high cell efficiencies, photovoltaic devices must have optically thick absorber layers, while allowing efficient collection of low diffusion length charge carriers.

Figure 2.7: A free-standing PEDOT:PSS:Nafion membrane. Photograph courtesy of S. L. McFarlane (Freund Group, Department of Chemistry, University of Manitoba).

Microstructured configurations of light absorbers have the potential to achieve these goals [120]. More specifically, it has been suggested that an array of vertically aligned semiconducting microwires to enable carrier collection in the wires' radial direction, a distance that is short relative to their optical thickness, the length of the microwires [5,71]. Such structures have been previously produced using lithographic patterning followed by anisotropic etching, however, such methods demand large areas of high-quality substrate materials [121]. Microwires of various materials have also been grown by a 'bottom up' growth technique known as the vapor-liquid-solid (VLS) process [122-124]. Control of the size and position of VLS-grown wires has been demonstrated [125], particularly in the case of Si by examining different surface oxide patterns [126,127]. This is particularly interesting as it provides the opportunity to examine different configurations of microwires within the array in order to optimize the light absorption properties of the arrays [77].

Silicon microwires are currently used in a wide range of applications from solar cells [128-131] to organic [132], liquid junction [65,133], and inorganic solid-state [129] devices. More recently, they have been employed as photocathodes in photosynthetic H_2 production from water [134,135]. This makes Si microwires a promising candidate for the use as light absorbers in the proposed water splitting system.

2.3 Electrical Characterization of Microwire/Polymer Assembly

The design illustrated in Fig. 2.4a, consisting of semiconducting microwires supported in a conducting polymer film, has been suggested in order to eliminate external wiring from

the photoelectrolysis cell as well as minimizing the electrical losses within the resulting membrane-supported assembly. The ultimate system will be a chemically complex structure with critical features on the micrometer scale.

A variety of different electrical parameters such as the Si microwire resistivity, the doping distribution and the total series resistances in the microwire/conducting polymer system, will have to be optimized to produce acceptable overall device performance. The nature of the electrical junctions between doped Si microwires and different candidate conducting polymers will be an important factor in the proper function of the final water-splitting device [5,91,92]. Inorganic semiconductor/conducting polymer junctions and more specifically Si/conducting polymer junctions are also interesting from a fundamental viewpoint for different organic electronic applications.

2.3.1 Current-Voltage Properties of Si/Conducting Polymer Junctions

Contacts between planar Si and conducting polymers have been studied in a number of reports. Polyacetylenes, polypyrroles, and polythiophenes are some of the materials that have been used as contacts [136]. Contacts between inorganic semiconductors and conducting polymers are interesting as they provide the chemical control over the behavior of the contacts. This is due to the fact that the Fermi level of conducting polymers can be manipulated through redox reactions (chemical doping process), leading to a range of different electronic behavior at the inorganic semiconductor /conducting polymer contact.

In general, oxidatively doped (p-type), high work function polymers have been reported to yield rectifying contacts to n-type Si with effective barrier heights of 0.7 to 0.8 V [98]. Rectifying contacts between n-Si and oxidatively doped polyacetylene, with reverse saturation current densities (J_0) of approximately 10^{-6} to 10^{-8} Acm^{-2}, are good examples of this class of contacts [98,137]. Similar behavior has been reported for contacts between n-Si and other high work function polymers, such as polypyrrole [137,138]. In contrast, low work function polymers, such as potassium (K)-doped polyacetylene, yield ohmic contacts to n-Si [136].

Junctions between p-Si and high work function polymers (e.g. polypyrrole) generally exhibit ohmic behavior [139]. Rectifying behavior has been reported in contacts between p-Si and polyisothianapthene [140] as the Fermi level of polyisothianapthene is much more negative than that of polypyrrole. It is difficult to draw a general conclusion from the limited number of investigations performed on these types of junctions. Nevertheless, it is known that when thermionic emission of electrons over the interface energy barrier is the dominant conduction mechanism, the transport properties at semiconductor/conducting polymer junctions can be treated approximately similar to that of semiconductor/metal contacts, with the forward current-voltage properties modeled as [68,69]:

$$J = J_0 \left[exp\left(-\frac{qV}{\eta k_B T}\right) - 1 \right] \qquad (2.3)$$

where J is the total current density at the junction, q is the charge of an electron, V is the applied voltage, η is the ideality factor of the diode (normally ~ 1.0) and k_B and T are the Boltzmann constant and absolute temperature, respectively. Similar to the

semiconductor/metal contacts, the relationship between J_0 and barrier height (Φ_b) for a semiconductor/conducting polymer junction can also be obtained from thermionic emission/diffusion theory and assuming that all the voltage drops at the interface [141]:

$$J_0 = \alpha A^{**} T^2 \left[exp\left(-\frac{q\Phi_b}{k_B T} \right) \right] \qquad (2.4)$$

where A^{**} is the Richardson constant and α is a coefficient that represents the fraction of majority carriers successfully injected into the polymer phase. Values of A^{**} are known for most semiconductor/metal junctions, so relating the barrier height (Φ_b) to the electrical properties of the junction is straightforward for semiconductor/metal contacts.

Previous reports suggest values of 10^{-2} to 10^{-3} for α, based on carrier concentration estimations in conducting polymers [98], although there are qualitative indications that this is not always the case. As an example, in the case of contacts between p-Si and PTCDA (3,4,9,l0-perylenetetracarboxylic dianhydride), a quantitative comparison between *J-V* and *C-V* data implies a value of $\alpha = 10^{-4}$ [142]. In related work, the junction between oxidatively doped polyacetylene coated onto n-type Si demonstrated $\alpha = 1.0$ [143]. This example provides another qualitative indication that the transport properties at semiconductor/polymer junctions might be different from those at semiconductor/metal barriers. Although the smaller effective contact area between semiconductors and polymers (e.g. due to wetting and/or adhesion issues) may have also contributed to the small values of α, it still implies that application of equation (2.4) to calculate Φ_b for semiconductor/polymer junctions is uncertain without independent information regarding the value of α.

In general, the exact values of α are not known for most semiconductor/conducting polymer junctions and more information is required in order to obtain a complete description of semiconductor/polymer contacts, making it more challenging to predict the behavior of these junctions specially in the case of new structures with novel polymer composites.

2.3.2 Ohmic Contact Formation to Si Microstructures

With semiconductor/conducting polymer contacts [98] gaining more attention especially in solar cells, photosynthetic and hydrogen evolution applications, more research is devoted to application of such junctions. However, the research is mostly focused on planar thin film devices [136,144,145] rather than characterizing photoelectrical properties of individual semiconductor micro- and nanowires [131,146-148] despite their growing application in this field.

For the specific case of water splitting systems based on microstructured semiconductor arrays, characterization and reliable bulk measurement [90,128,129,149-152] similar to the case of planar devices becomes more challenging (difficulties in forming reliable ohmic contacts due to the size issues, identification of each factor playing a role in forming the overall behavior, etc). Bulk measurements may give an understanding about the overall function of the system, however a more accurate understanding at the single cell level (Fig. 2.8) is required in order to accurately characterize the system and, if necessary, modify and improve each element. A shown in Fig. 2.8, various DC series resistances contribute to the total resistance of the system.

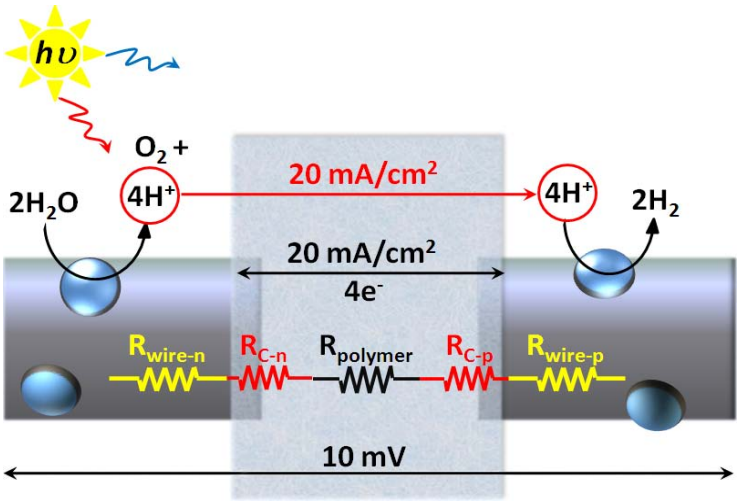

Figure 2.8: Schematic diagram of a single cell of the proposed water splitting device. Each cell will ideally include two semiconductors with enough energy levels to provide the necessary photovoltage for water splitting, with redox electrocatalysts deposited onto their surface. Semiconductor light absorbers (in this case Si microwires) are embedded into an electronic and ionic conducting membrane. Reprinted with permission from [92]. Copyright (2011) American Chemical Society.

The resistances R_{wire} and $R_{polymer}$ represent the microwire and polymer resistances, respectively. The resistances $R_{C\text{-}n}$ and $R_{C\text{-}p}$ are the junction resistances of the n-Si and p-Si microwire/polymer contacts, respectively.

Forming ohmic contacts to Si and Si micro- and nanostructures have been discussed and/or demonstrated in many previous articles [131,146,148,149,153-155]. Thermal evaporation of contact metals is probably the most common approach, typically comprising a single-lithographic step followed by a lift-off* process [146].

Although this method will yield low resistance contacts, it is only applicable to a certain range of microwire diameters. Lithographic processes and, more specifically, the

* A micro-fabrication processes in which a sacrificial material, such as photoresist, is first deposited and patterned on the target substrate. The material of interest is then deposited and the sacrificial material is subsequently removed, leaving behind only the material deposited directly onto the target substrate. Lift-off process is useful for patterning materials that cannot be etched without affecting underlying materials and the target substrate.

image resolution of an optical mask aligner to image small size structures, puts a lower limit on the diameter of wires that can be imaged for mask alignment. On the other hand, metal films that are too thick for lift-off processes are usually required to ensure reliable ohmic contact to microwires with diameters larger than 1.5 μm [146]. Furthermore, conventional contact formation approaches are not compatible with many microwire/polymer structures due to the interactions between polymers, photoresists, and the etchant solutions as well as high temperatures used during lithographic processes. Micro-fabrication using alternate lithography and/or deposition approaches such as electron beam lithography (EBL) [156,157], X-ray beam lithography [156,157], and focused ion beam (FIB) [156,158] direct fabrication was not available on-site. However, in the case of microwire/polymer structures these more expensive techniques share similar issues with conventional contact formation approaches.

Characterization techniques based on scanning probe microscopy (SPM) such as Kelvin probe force microscopy (KPFM) and scanning photocurrent microscopy (SPCM) have been used for characterizing a variety of different parameters such as: doping distribution in nanowires [153,154], defects in carbon nanotube devices [155], studying contacts in nanowire and carbon nanotube devices [147,159,160], transport in thin-film organic semiconductors [161,162], and quantitative determination of electron and hole mobility-lifetime in cadmium sulfide (CdS) nanowires [163]. The high spatial resolution of these techniques makes them well suited for applications mainly in nanometer scales which are small compared to the solar water splitting cell dimensions.

New, reliable and straightforward approaches were needed in order to make reproducible ohmic contact to microwires and efficiently characterize solar water

splitting systems. In this work, new approaches to forming and characterizing model microwire/polymer junctions for photosynthetic systems were developed.

Chapter 3

Experimental Methods

In order to investigate the photo-physical properties of the microwire/membrane system, single microwires need to be isolated and electrical connections between them and the candidate polymer membrane must be formed. In this chapter, the experimental methods that were used to characterize individual solar water splitting cells, including sample preparation, isolation of the microwires, conducting polymer film preparation and microwire/polymer junction formation are explained in detail.

3.1 Si Microwires

Silicon microwires (Fig. 3.1) were grown by collaborators in the Lewis group at California Institute of Technology (Caltech) using VLS chemical vapor deposition (CVD) from Si (111) wafers patterned with copper (Cu) catalyst. The samples were doped with boron (B) or phosphorus (P) up to different doping concentration levels of 10^{15} to 10^{18} cm^{-3} [90,120,122,133]. Grown in a square arrangement with a 7 μm pitch, the single crystalline Si microwires were 90 ± 15 μm in length and ~1.5 to 1.7 μm in diameter.

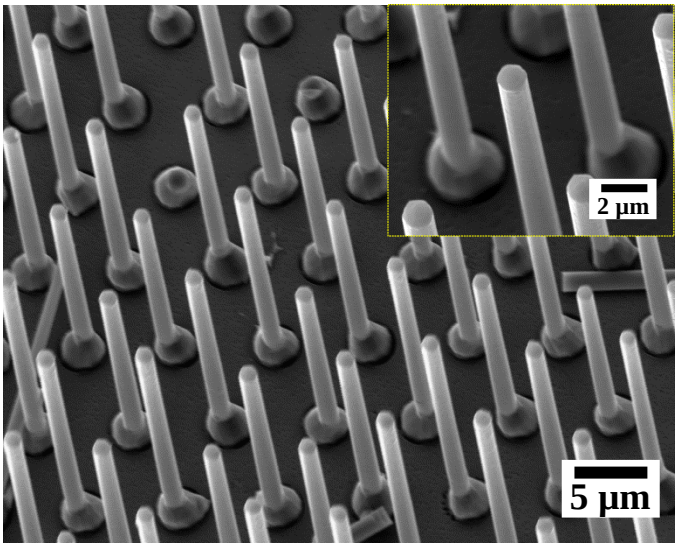

(a)

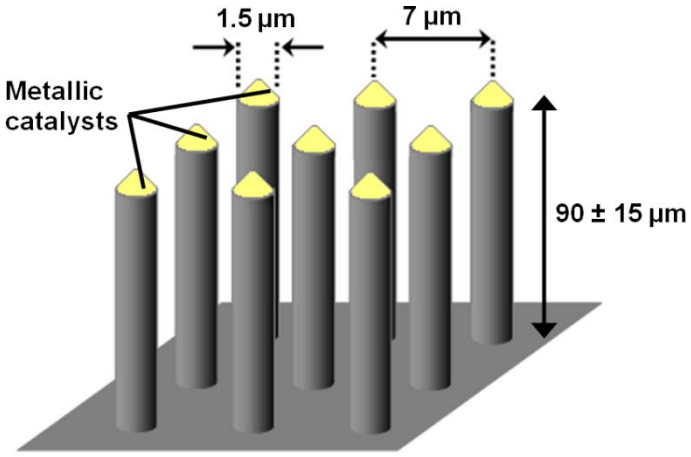

(b)

Figure 3.1: (a) Scanning electron microscope (SEM) image of Cu-based Si microwire arrays grown using the VLS technique [90,120,122,133]. The metallic catalyst has been removed from the tip of the microwires (figure inset) in this sample. (b) Schematic diagram of the microwire arrays. The average diameter of the microwires is 1.5 to 1.7 µm and the array pitch is approximately 7 µm. The average length of the microwires is 90 ± 15 µm. The metallic caps are shown in yellow.

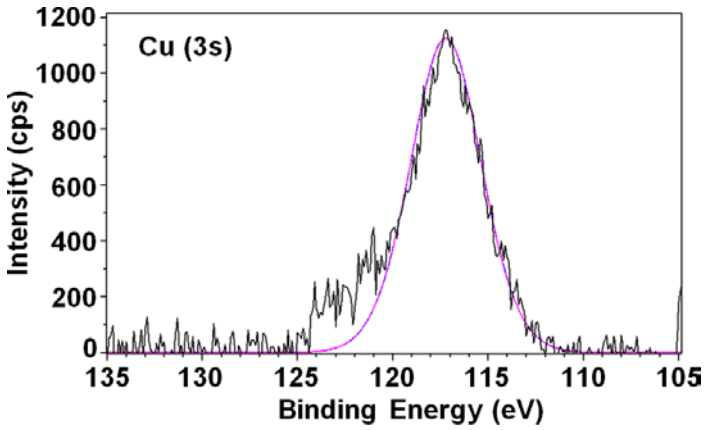

(a)

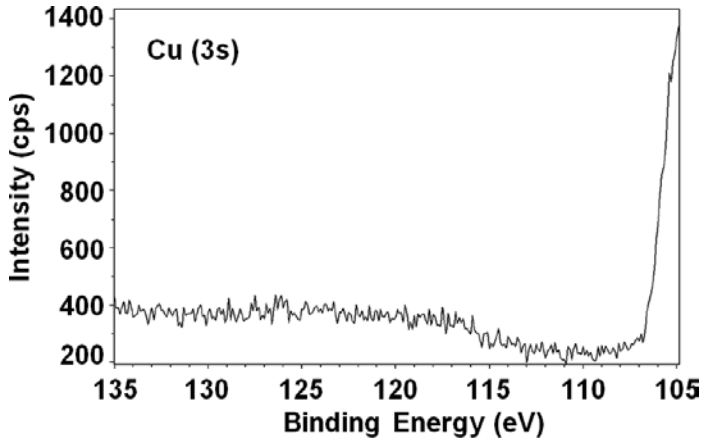

(b)

Figure 3.2: XPS data (a) before and (b) after the catalyst removal procedure to confirm the removal of Cu from Si microwires grown from a Cu VLS catalyst. After the etch procedure, no feature was observed at ~117 eV, confirming the complete removal of Cu catalyst from the microwire samples. The peak starting at ~105 eV in both cases is the onset of Si oxide peak. Reprinted with permission from [92]. Copyright (2011) American Chemical Society.

Any residual metallic growth catalyst at the top of each microwire (and some small amounts on the sides) from the VLS growth process was removed using a two-step etching procedure (Appendix B). Analysis using XPS confirmed that the growth catalyst had been eliminated (Fig. 3.2).

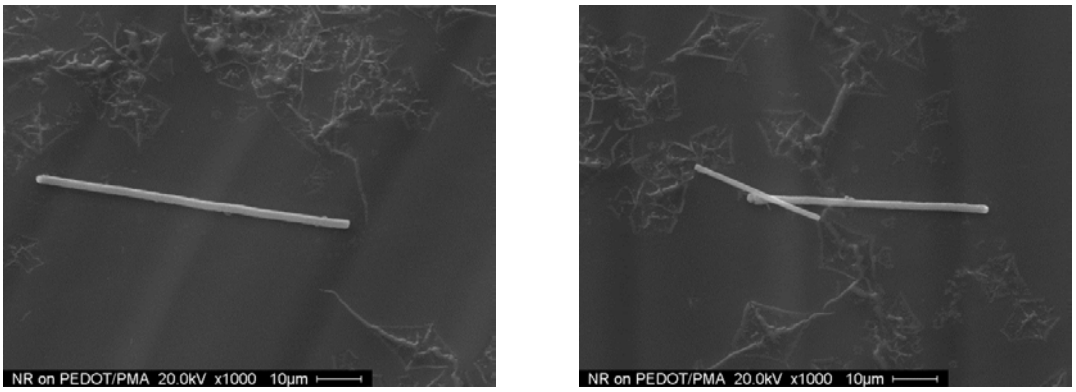

Figure 3.3: SEM micrographs of microwires isolated on the surface of PEDOT:PSS:Nafion membrane. As these microwires were broken during the separation from the growth substrate, they are shorter than the average microwire length.

3.1.1 Isolation of Individual Microwires

Following removal of the metallic catalyst (Fig. 3.2), and native oxide removal process (Appendix B) a suspension of microwires was prepared for coating on the target substrates. The microwires were removed from the growth substrate either by sonication [146] or scraping a corner of the substrate using a razor blade and removing a smaller portion of the microwires in isopropanol or acetonitrile. The latter is a particularly desirable approach for single microwire measurements as the final solution was more dilute and, when coated on the substrate, resulted in completely isolated microwires (Fig. 3.3).

Using a micropipette, approximately 10 μL of the microwire suspension was deposited on the desired substrates for individual microwire measurements. Since the suspended microwires tend to aggregate and deposit at the bottom of the vials, it was found helpful to sonicate these suspensions for 10-15 s, immediately prior to drop casting on the target substrates.

The main characterizations on individual microwires and microwire/polymer junctions were performed on glass substrates in order to eliminate unwanted conduction paths into the substrate. The native oxide, as well as any oxide that may have formed during the growth catalyst removal process, was removed by etching the Si microwires in buffered HF(aq.) prior to each set of measurements, replacing oxygen bonds at the surface with hydrogen bonds, creating H-terminated microwire samples. In these studies, the time interval between the native oxide removal process and the measurements was kept as short as possible (typically <15 min). In experiments detailed in chapter 4, a methylation process was used to replace the hydrogen termination at the wire surface in order to investigate the long-term oxidative stability of the microwire surface.

3.1.2 Ohmic Contact Formation to Individual Si Microwires

There are many means to form ohmic contacts to semiconductor microstructures. For Si microwires, the most frequently utilized one is the thermal evaporation of metal contact elements onto the wires. This approach has inherent applicability issues mostly related to the limitations of micro-fabrication processes [146]. The time and complexity associated with micro-fabrication processes required as an initial step for characterization also became an issue, considering the number of samples that needed to be examined and the alignment of the microwires with the polymer. This greatly limited the flexibility of the characterization process, thus limiting the ability to explore new combinations with every new polymeric system and/or configuration. In addition, a great amount of effort would have been required to make sure that the relatively complicated micro-fabrication processes required for the characterization do not affect different elements within the system. Furthermore, due to the sensitivity of the composite polymer elements to the high

temperatures used during the thermal evaporation processes, characterization of the system without compromising the basic electrical properties of the polymer would have been extremely challenging.

Seeking a direct, non-lithographic contact formation approach, bonding Al wires to Au/Pd pads and to the microwires was initially investigated. However, the small dimensions of the microwires made it difficult to properly align the contact wire for contact formation. In addition, positioning of the microwires relative to the polymer and ensuring proper adhesion of the contact wires to the Au/Pd pads and to the microwires presented another issue. Consequently, this method was abandoned as being impractical.

An alternate direct contact formation and testing instrument available in the lab was a standard probe station. This approach was particularly desirable as it provided more mechanical control compared to the wire-bonding through the use of tungsten (W) probes. Unlike the wire bonding approach, accurate electrical measurements are also possible at the time of contact formation using a parameter analyzer connected to the probe station. Employing W probes as a direct contact formation approach has the potential to eliminate complicated micro-fabrication processes required for contact formation and is a relatively inexpensive measurement compared to micro-fabrication based techniques.

Direct access to the microwires was immediately possible. Initially, thermal fusion of Al wires attached to the W probes in contact with the microwires was examined, to mimic the thermal evaporation of metal contacts. To perform this, sufficient electrical current (typically > 10 $kA.cm^{-2}$ [146]) must be passed through the system to increase the temperature in the immediate contact area, above that of the Al-Si eutectic point (577 ºC).

However, it was found to be difficult to apply controllable current levels through the initially non-conducting contacts. The mechanical flexibility, when handling Al wires to form contact to the microwires, was also found to be challenging. Furthermore, a non-destructive approach was more desirable as it provided the ability to repeat the measurements on an individual microwire under different conditions. As will be shown later, this proved to be very useful during the microwire characterization.

In the next step, direct interactions between W probes and microwires was investigated as the W probes could directly contact and mechanically manipulate the microwires. This investigation ultimately led to development of a novel ohmic contact formation approach to both p- and n-type Si microwires. This technique provided a simple, fast and more flexible path for characterizing complex systems such as the solar water splitting system in this case.

It was shown that direct and reliable ohmic contacts to the Si microwires could be made using W probes with the application of sufficient local mechanical pressure [91] as the resistivity and electronic structure of Si has been reported to vary as a function of pressure [164,165]. More specifically, the application of ~11 GPa, i.e. ~11 $mN\mu m^{-2}$, to planar Si samples has been reported to change the contact character from a Schottky contact to an ohmic contact due to transition from a semiconducting to metallic phase [166,167]. Consequently, the basic electrical properties of single Si microwires and of Si microwire/polymer junctions may be extracted using a standard probe station without the need for thermal evaporation of metallic contacts or basically any other micro-fabrication process involved [91,92].

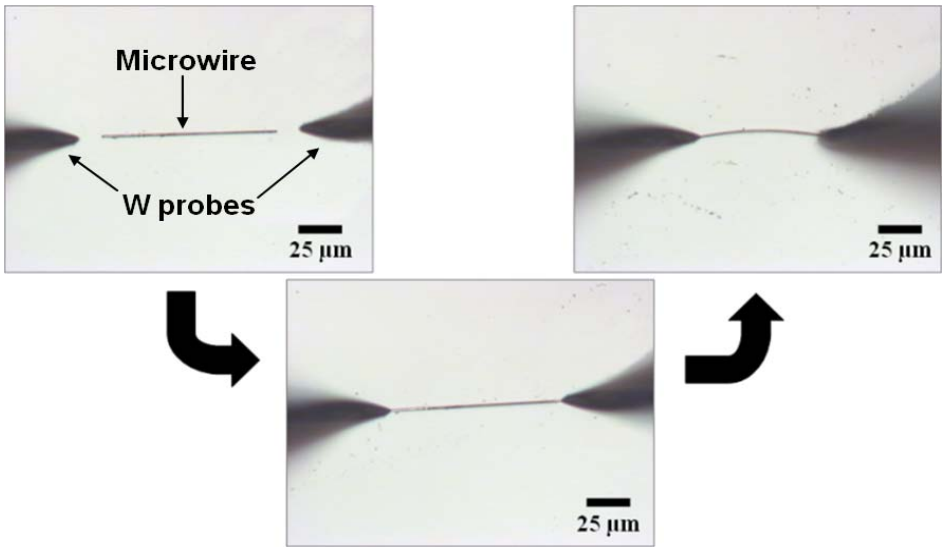

Figure 3.4: Optical micrograph of an individual Si microwire on glass substrate. Tungsten probes, approaching from the above, were used to mechanically manipulate the microwire. Using the W probes, it is possible to move microwire across the substrate and exert mechanical force (~37 mN, details below) directly to the individual microwires. However, the force required to bend a microwire, as shown in this micrograph, greatly exceeds the force applied during the electrical measurements. Reprinted with permission from [92]. Copyright (2011) American Chemical Society.

Furthermore, the W probes allowed for mechanical manipulation of the microwires (Fig. 3.4). During the initial measurements, the use of the conventional, electrically conductive, fluid indium/gallium (In/Ga) metal eutectic as an interfacial metallic phase [168] was also examined.

To estimate the pressure applied by the probe to the Si microwire during the measurements, the force of the probe holder setup was measured using a balance. Placing the probe holder on a labjack adjacent to a tared balance (Fig. 3.5), the probe was lowered until the balance recorded a weight greater than zero. The probe was then retracted until the balance returned to zero. This was taken as just touching the balance.

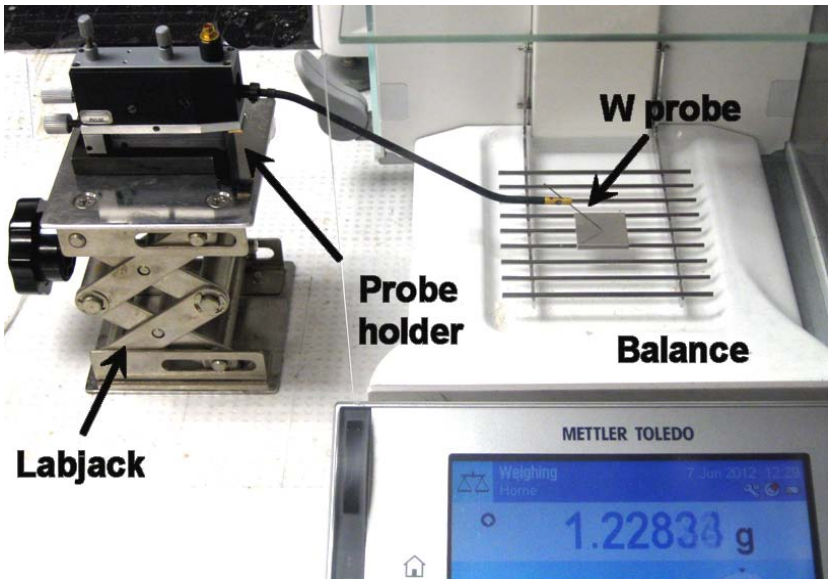

Figure 3.5: Setup used to measure the maximum mechanical force applied form the W probes. In these measurements, the probe holder was placed on a labjack adjacent to a tared balance. The probe was then lowered until the balance recorded a weight.

From this point the probe was lowered a number of turns until the recorded weight was saturated and a constant weight was achieved. The force exerted on the microwires by the W probes was measured to stabilize at a maximum value of ~37.3 mN (equal to approximately 3.80 g). Assuming a maximum circular contact diameter of 2 μm based on the maximum diameter of the microwires, the local mechanical pressure at the point of contact was thus > 12 $mN\mu m^{-2}$ which is enough to pass the reported metallic transition threshold (~11 $mN\mu m^{-2}$) [166]. The overestimated contact area yields the minimum amount of pressure attainable in this system and the actual pressure applied to the microwires is anticipated to be larger than the estimated value. By alternately increasing and decreasing the pressure on the microwires, the transition in electronic character of the contact as a function of pressure was observed. Fig. 3.6 shows the measured current-voltage (*I*-*V*) response for individual p- and n-type microwires.

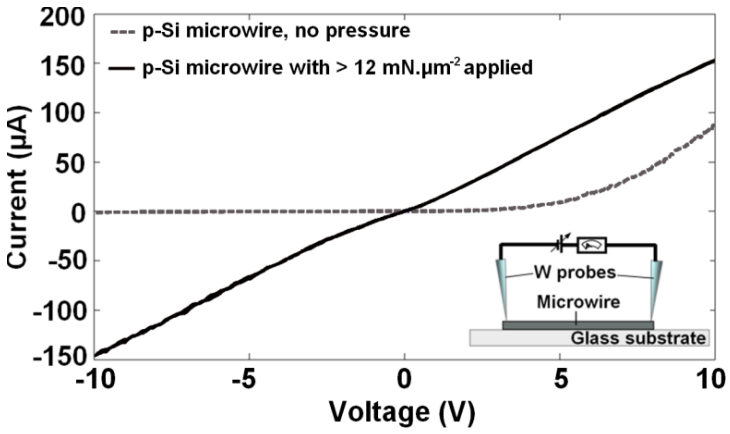

(a)

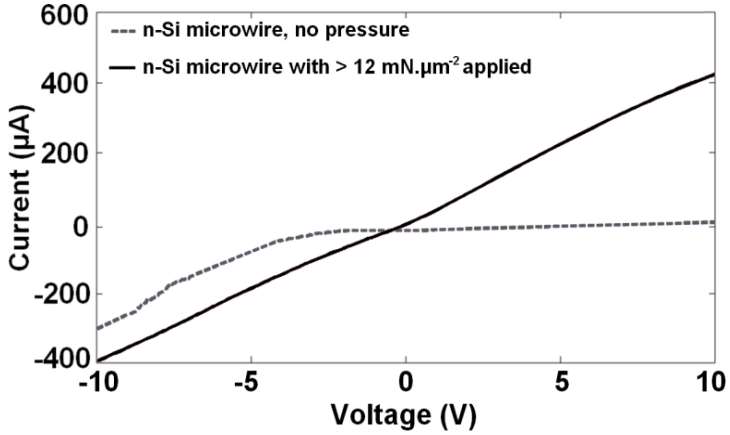

(b)

Figure 3.6: Local phase transition in the measured *I-V* profile of a 100 μm long (a) p-Si microwire and (b) n-Si microwire, in response to mechanical pressure at the contact areas. During these measurements, the first W probe was held at one end of the microwire with >12 mNμm^{-2} of local pressure applied, while the second probe touched the other end with: almost no applied force (dashed line) or the same amount of force applied (solid line). As the pressure increased, the phase transition occurred, changing the nonlinear *I-V* behavior to that expected for an ohmic contact. In these measurements, the fixed probe with a constant applied pressure of >12 mNμm^{-2} was connected to the "Common"/"Frame Ground" terminal of the parameter analyzer. Reprinted with permission from [92]. Copyright (2011) American Chemical Society.

The dashed line in Fig. 3.6 shows the *I-V* response for individual p- and n-type microwires when > 12 $mN\mu m^{-2}$ of mechanical pressure was applied to the contact between one probe that was fixed at one end of the microwire while the second probe was loosely connected to the other end of the microwire with no additional force.

The solid line in Fig. 3.6 shows the transition in the *I-V* profile as a result of the application of >12 $mN\mu m^{-2}$ of mechanical pressure via the second probe. This observation was reversible for both types of microwires, and could be readily reproduced by increasing or decreasing the force applied to the probes. The measured DC resistance of the microwires in these measurements was consistent with the calculated values based on the known doping concentration (details in section 4.2.2).

This technique was used as the main approach in determining the basic electrical properties of individual Si microwires as well as many different combinations of Si microwires and polymer systems. Standard W probes (with a diameter of ~2 μm), used in the *I-V* measurements, were etched for ~30 s in 2.0M KOH(aq.) immediately before the experiments, to remove the W native oxide and to improve the quality of the contacts [169,170].

3.2 Microwire/Polymer Assembly

3.2.1 Polymer Film Preparation

To investigate the behavior of the electrical junction between the polymers and Si microwires, solutions of two candidate conducting polymers, polyethylenedioxythiophene: phosphomolybdic acid (PEDOT:PMA) [116] and

polyehtylenedioxythiophene:polystyrene sulfonate:Nafion (PEDOT:PSS:Nafion) [87] with 12 wt.% PEDOT:PSS, were prepared according to established procedures (Appendix C).

The membrane with 12 wt.% PEDOT:PSS reaches an optimized state in terms of electronic and ionic conductivity as well as optical transmission. A 40 μm thick film of PEDOT:PSS:Nafion that contains 12 wt.% PEDOT:PSS would yield a conductivity of 7.4 $mScm^{-1}$ [87], close to the minimum required conductivity of 8 $mScm^{-1}$ (Appendix A), discussed in section 2.2.1. The ionic conductivity of these films is also similar to its electronic conductivity with 12 wt.% PEDOT:PSS.

Both types of polymer samples were prepared directly from wet processing (Appendix C) and then spin coated or drop cast on target substrates, e.g. PEDOT:PSS:Nafion was prepared by mixing adequate volume of PEDOT:PSS and Nafion, then spin coating the solution onto the target substrates (Fig. 3.7).

Each procedure includes the polymer solution preparation and spin coating the solution on the target substrates. The solution could be coated at different speeds to achieve desired film thickness. Normally, coating at 2000 rpm for 20 seconds will lead to film thicknesses of approximately 150 to 200 nm as independently verified by optical profilometry and Alpha-Step measurements. The film preparation for each polymer was followed by a rinsing process to remove residual PSS or PMA.

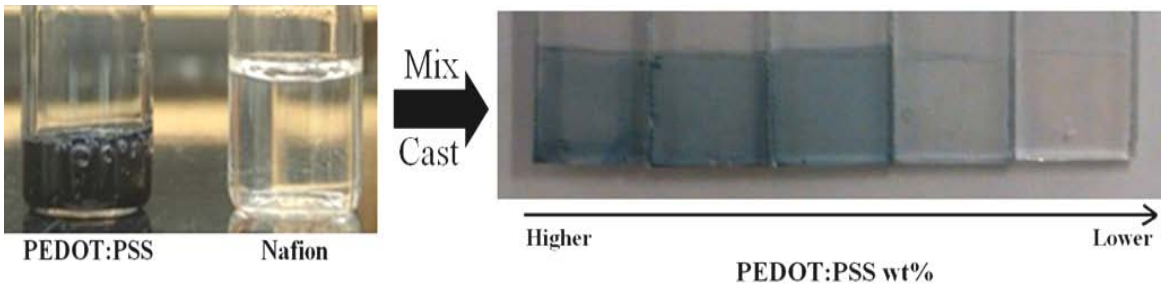

Figure 3.7: PEDOT:PSS:Nafion is prepared by mixing adequate volume of PEDOT:PSS and Nafion solutions (left) then spin coating the solution onto the glass substrates (right). The transparency of the films is tunable by changing the concentration of PEDOT:PSS, reaching an optimized state at 12 wt.% of PEDOT:PSS.

Ohmic contacts to the conducting polymer films were then formed by sputtering 32 nm thick pads of gold-palladium (Au/Pd) directly onto the polymer (Fig. 3.8). An aluminum shadow mask with 3-4 circular patterns (5 mm diameter, 9 mm center to center spacing) was used to pattern the Au/Pd contacts on the polymer surface. The polymer films used for measurements described in this thesis were all prepared in the same manner and onto different substrates.

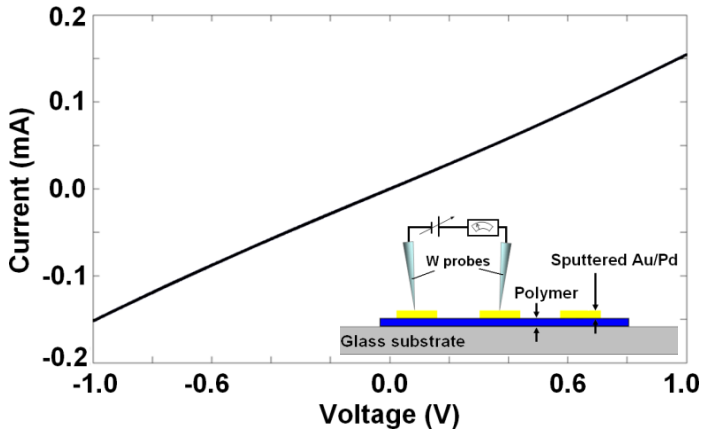

Figure 3.8: *I-V* response of the ohmic contacts between 32 nm thick Au/Pd pads on PEDOT:PSS:Nafion conducting polymer films, coated on glass substrate. The diameter of the sputtered Au/Pd pads was 5 mm and the center to center spacing was 9mm.

3.2.2 Microwire/Polymer Junction Formation

In order to form microwire/polymer assemblies, conducting polymer films (thickness: 150 to 200 nm) were deposited by spin-coating a solution of polymer onto a glass substrate that contained prepositioned Parafilm masks either on one side (providing single side coverage for measurements with one microwire, Fig. 3.9a) or on the left and right sides of one surface of the substrate (for complete cell measurements with one microwire on each side, Fig. 3.9b). Following the removal of the Parafilm mask, p-type and/or n-type Si microwires were deposited onto the exposed glass substrate. Single microwires were then positioned perpendicular to the border between the conducting polymer and the glass substrate using W probes. Approximately 2-5 μm of the microwire length in contact with polymer was covered with a small amount (<5 μL) of polymer to ensure good electrical contact.

Even though the eventual embedding depth of the microwires in the polymer membrane has not been finalized, this configuration more closely resembled the eventual envisioned device structure (Fig. 2.4a) than any other configuration in which a microwire was physically on top of a planar polymer film layer. Microwires were aligned before the polymer rinsing process in all of the cases. The p-Si microwire/polymer/n-Si microwire assembly (Fig. 3.9b) was used as a model for a single unit of the proposed solar water splitting microwire array cell (Fig. 2.8).

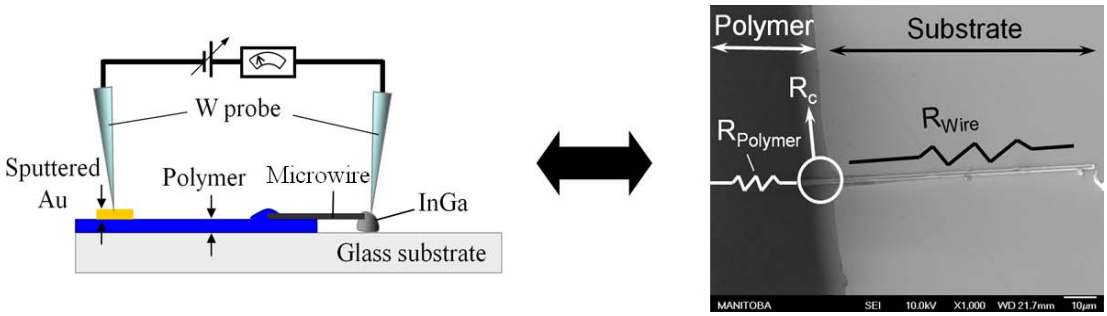

(a)

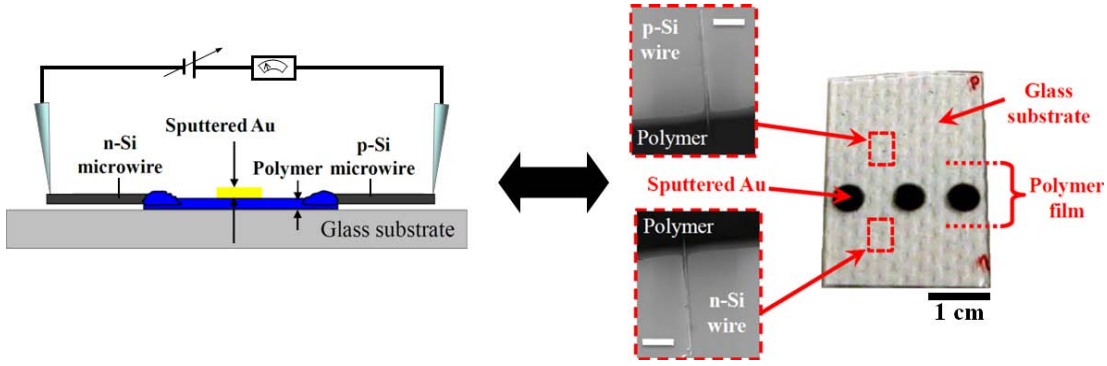

(b)

Figure 3.9: (a) Schematic diagram for single microwire/polymer junction measurements (left) along with SEM micrograph of a microwire aligned at the polymer border with important resistances marked (right). (b) Schematic diagram of the complete photoelectrolysis cell measurement system (left) and photograph of the test structure along with SEM micrographs of the microwires aligned at each side. All SEM images were taken on an Au-coated slide to alleviate charging issues. The scale bars in the bottom SEM images are 20 μm. Adapted with permission from [92]. Copyright (2011) American Chemical Society.

Auger electron spectroscopy (AES) and SEM imaging indicated an intimate contact between the polymer and microwires, as well as a sharp border between the polymer and substrate (Fig. 3.10). Unlike the samples used for electrical characterization, a drop-cast film of PEDOT:PSS:Nafion was prepared on a Au-coated slide, to minimize charging issues for the SEM and AES analysis.

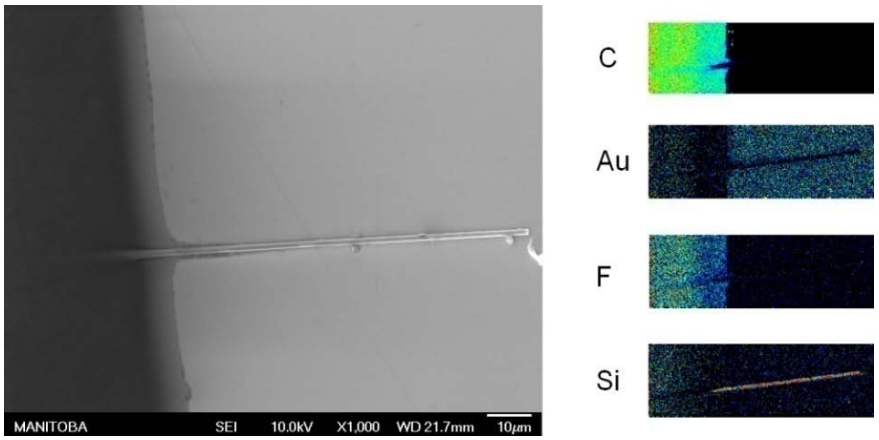

Figure 3.10: SEM image of a Si microwire embedded in to a PEDOT:PSS:Nafion (left). The polymer film was drop casted on a Au coated substrate to alleviate charging issues. SEM image shows a sharp polymer/Au border, however, Auger elemental analysis (right) was also performed to verify the localization of the polymer. C and F were traced on the left side indicating the polymer as well as the microwire (Si) extending toward the right side. Reprinted with permission from [91]. Copyright (2011) American Chemical Society.

Analysis using AES indicated that both C and F were localized in the polymer, with a decrease in intensity observed where the microwire entered the polymer. Examining the image for Si, the microwire was clearly present both inside the polymer as well as over the Au substrate. The Au image also showed a void region where the microwire covered the Au substrate.

Auger analysis also confirmed that there was minimal polymer wicking (due to capillary motion) beneath the microwire in this configuration. Considering the average resistance per unit length of the microwires (sections 4.2.1 and 4.2.2) and the average resistance of the polymer films (sections 4.3.1 and 4.3.2), the minimal wicking beneath the microwire is anticipated to be a negligible contribution to the total measured resistance in the system.

3.2.3 Electrical Properties of the Microwire/Polymer Systems: Requirements

One important factor that needs to be considered is the amount of current that is expected to flow through each microwire. Assuming that the microwires fill the substrate plane, the maximum short circuit photo-generated current from an array of 100 μm long microwires, based on the maximum reported values for a single crystalline Si solar cell, is J_{sc} ~ 43 $mAcm^{-2}$ [171]. Considering the average dimensions of the microwires (Fig. 3.1b), there are approximately 2×10^{6} cm^{-2} microwires in the array structure. Therefore, the capture of all photons falling on the membrane area would result in a current of ~21 nA in each (existing) microwire.

The current project roadmap requires a maximum voltage drop of ~10mV across the microwire-membrane system and, assuming the same amount of current (21 nA) flowing through the junction to the polymer film, the total resistance in the microwire-polymer system should be less than 480 kΩ. Quantifying the upper limit of the resistance of the microwire and characterizing the microwire-polymer junction behaviour are critical steps to achieving these goals.

3.3 Apparatus for Individual Si Microwire and Si Microwire/Polymer System Characterizations

Following the preparation of polymer membranes, an *Edwards s150b* sputter coater was used to sputter Au/Pd pads onto the polymer surface. A *Fogale Photomap 3D* optical profilometer and a *KLA Tencore AS-500* Alpha-Step were used for the polymer film

thickness measurements. A *Kratos Axis Ultra DLD* instrument was employed to perform XPS analyses on the microwire samples. A field emission Auger microscope, model *JAMP-9500F* from *JEOL*, was used for AES analysis on the microwire/polymer samples. An *Agilent 4155c* semiconductor parameter analyzer in a *Suss MicroTec* standard semiconductor probe station (Fig. 3.11) was used for *I-V* measurements. A *Newport* model *96000* full spectrum solar source (Fig. 3.12a) with global air mass (AM) 1.5G filter was used to simulate standard solar spectrum (see Appendix D for output power calibration procedure).

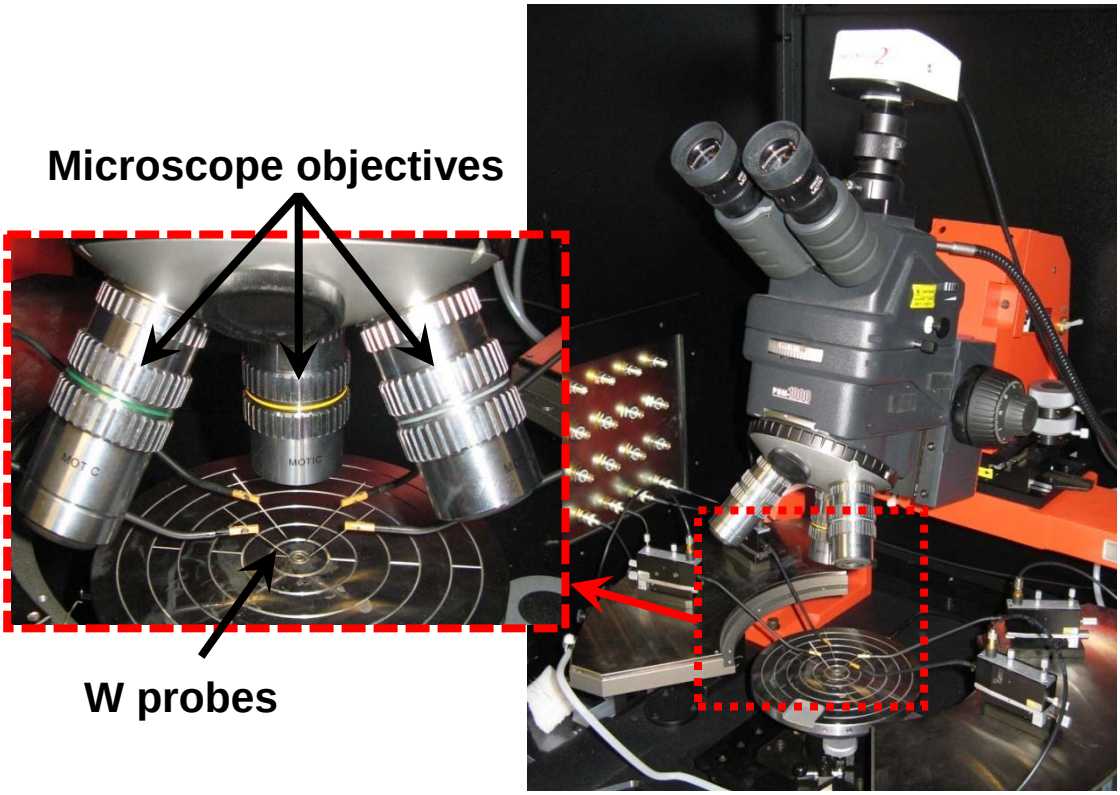

Figure 3.11: *I-V* measurements were performed using an *Agilent 4155c* semiconductor parameter analyzer in a standard probe station. The stage, four W probe holders and the microscope are shown in the right side image. W probes can be seen in the magnified image on the left.

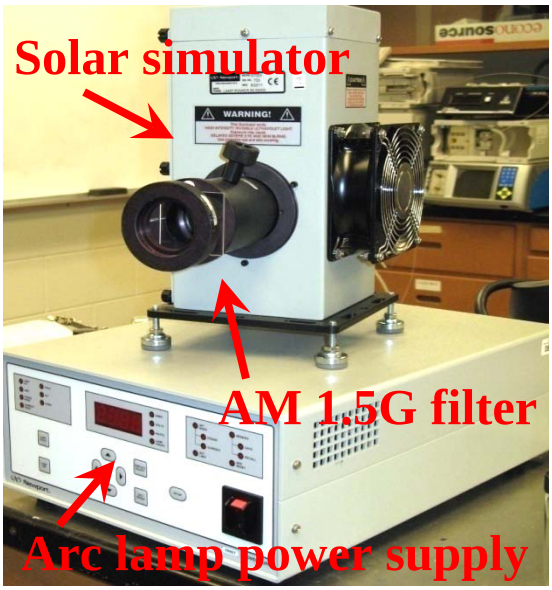

(a)

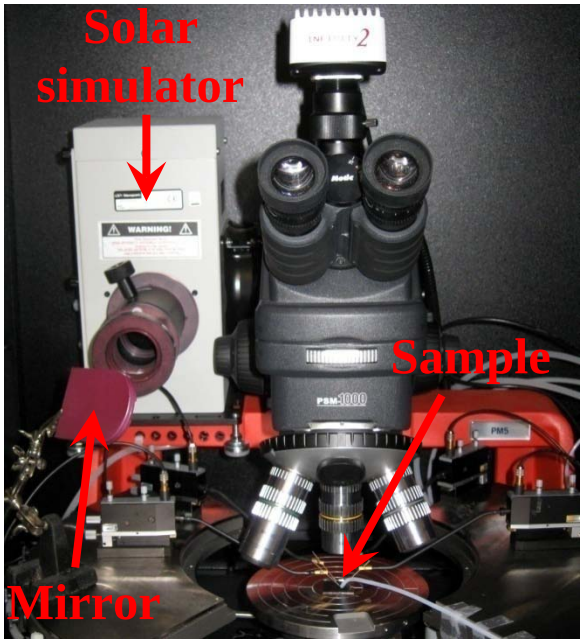

(b)

Figure 3.12: (a) A *Newport* model *96000* full spectrum solar source with global air mass (AM) 1.5G filter and a universal arc lamp power supply was used to simulate standard solar spectrum. (b) Typical measurement setup with solar simulator inside the probe station chamber. A mirror was used to direct light beam onto the sample.

The solar source was mounted inside the probe station and a mirror was used to direct the light beam onto the sample (Fig. 3.12b). The power loss due to the mirror was considered during the calibration procedure in order to extract the exact amount of power reaching the samples (Appendix D).

Tungsten probes from *American Probes & Technologies* model *72T-G3/10* (with a diameter of ~2 μm) were used in the *I-V* measurements. Probes were etched for ~30 s in 2.0 M KOH(aq.) immediately before the experiments to remove the W native oxide and to improve the quality of the contacts [169,170].

Chapter 4

Results and Discussion

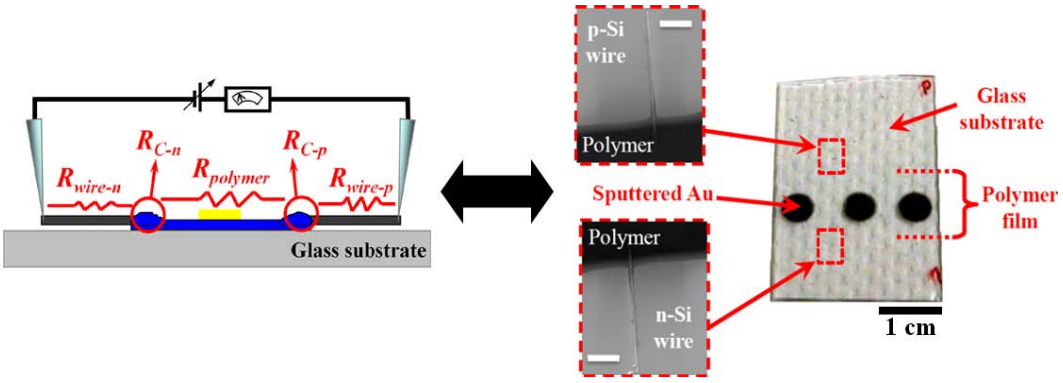

Characterizing the single microwires, the microwire/polymer junctions and quantifying the voltage drops at each point of the structure will guarantee the appropriate function of the final device and acceptable energy conversion efficiency. These measurements will determine the acceptable wire resistivity (doping concentration) as well as the required electronic conductivity of the polymers, in turn allowing selection of the wire-polymer structure for the use in the final device.

Using the soft contact formation approach, introduced in chapter 3, these parameters can be individually extracted for a single cell of the proposed artificial photosynthesis system. The outcome of these measurements will be used in optimizing electrical properties of different elements to be used as building blocks of the ultimate water splitting device. Specifically, the soft contact formation process enabled individual

microwire/polymer junction properties to be extracted. This chapter presents the measurement results on single Si microwires as well as microwire/polymer junctions and describes the modifications that were made in order to improve the electrical characteristics of the system.

4.1 Soft Contact Formation to Individual Si Microwires

Doped Si microwires are an important component in the proposed artificial photosynthesis device. These microwires play two critical roles: absorbing sunlight and conducting the electrons between the two sides of water-splitting reaction. Characterization of the microwires is of great importance as it defines the critical limits for different electrical parameters (e.g. resistivity, doping concentration). In the first stage of the measurements and, following the methodology described in section 3.1.2, contacts to individual microwires were formed using W probes in a standard probe station (Fig. 3.11).

During these measurements, microwires were typically placed onto the glass substrate. The W probes were then moved down to the microwire until they made contact. The probes were placed on both ends of the microwire and the current passing through the microwire was measured for a range of applied voltages using an *Agilent 4155c* semiconductor parameter analyzer. Ohmic behavior was observed as the applied force from the probes was gradually increased to the threshold force level, as was described in section 3.1.2. Reproducible results were obtained when an identical amount of force was applied from both probes.

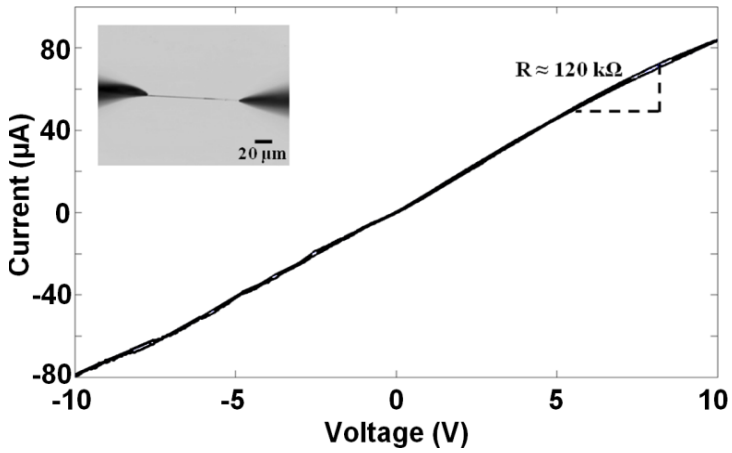

Figure 4.1: Measured I-V profile for a 100 µm long p-Si microwire with a diameter of ~1 µm. The probes were placed on the microwire close to the ends. The measured resistance was approximately 120 kΩ.

Fig. 4.1 shows an example of the initial *I-V* measurement results, including an optical micrograph of a 100 µm long wire with 1 µm diameter on glass (Fig. 4.1 inset).

4.2 Probe Spacing Measurements

4.2.1 Controlling the Probe Spacing

When compared to conventional lithographic contact formation approaches, the proposed soft contact formation technique brings a high level of flexibility in making contact with an arbitrary location of the sample under investigation. Using W probes provided not only the ability to mechanically manipulate the microwires (Fig. 3.4), but also the possibility to form a contact to each and every point along the length of the wires (Fig. 4.2) or any other position in the system without the need for lithographic procedures.

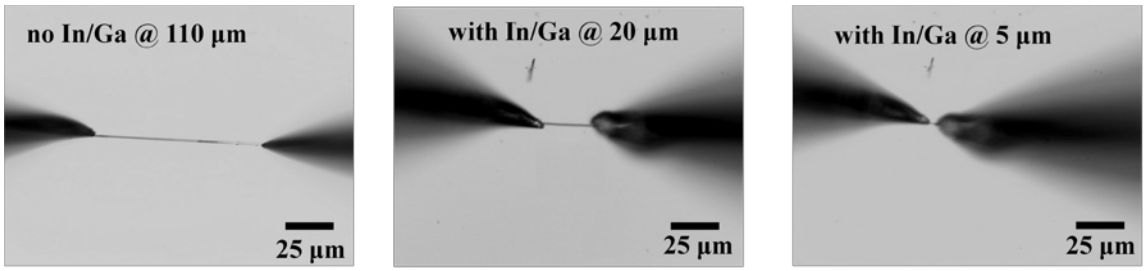

Figure 4.2: Forming direct electrical contact to arbitrary positions across the microwires with or without In/Ga.

As shown in Fig. 4.2, it is possible to freely move the W probes (with or without In/Ga) across the length of the microwires and make *I-V* measurements versus different probe separations. These measurements were performed on different microwires of different characters with three main goals: 1) to show that the *I-V* measurement was unaffected by variation in the positions of the probes along the microwires; 2) to determine the value of contact resistance between the probes and the different microwires; and 3) to investigate the uniformity of the doping concentration along the length of the microwires. Sections 4.2.2 - 4.2.4 present the results of these investigations.

In all the measurements described in these sections, each data point is the average of seven independent measurements in which the probe was completely disconnected from the microwire before the contact for the next measurement was made. The data thus demonstrate the reliability and reproducibility of the contacts to different microwires, regardless of their doping type or concentration.

4.2.2 Microwires' Resistance and Doping Concentration

Fig. 4.3 depicts the resistance versus probe separation data obtained for p-type and n-type Si microwires, doped with B and P, respectively (section 3.1). Contacts were

reproducibly formed to microwires with different types of doping. The resistance per unit length was constant for all of the measurements, at values of 0.50 $k\Omega\mu m^{-1}$ for the p-type and 0.18 $k\Omega\mu m^{-1}$ for the n-type Si microwires. The contact resistance between W probes and microwires was calculated by performing a linear fit to the resistance versus probe separation data, in conjunction with evaluation of the intercept of such a plot (Fig. 4.3).

The calculated contact resistance values, ~2.4 kΩ (i.e. 4.8 kΩ / 2) for the contact between p-Si microwire and W probe, and ~1.8 kΩ (i.e. 3.5 kΩ / 2) for n-Si microwire/W probe contact, were reasonably similar for both types of Si microwires. This is consistent with expectations based on previous reports describing pressure-induced transition from Schottky to fully ohmic contacts [164,166].

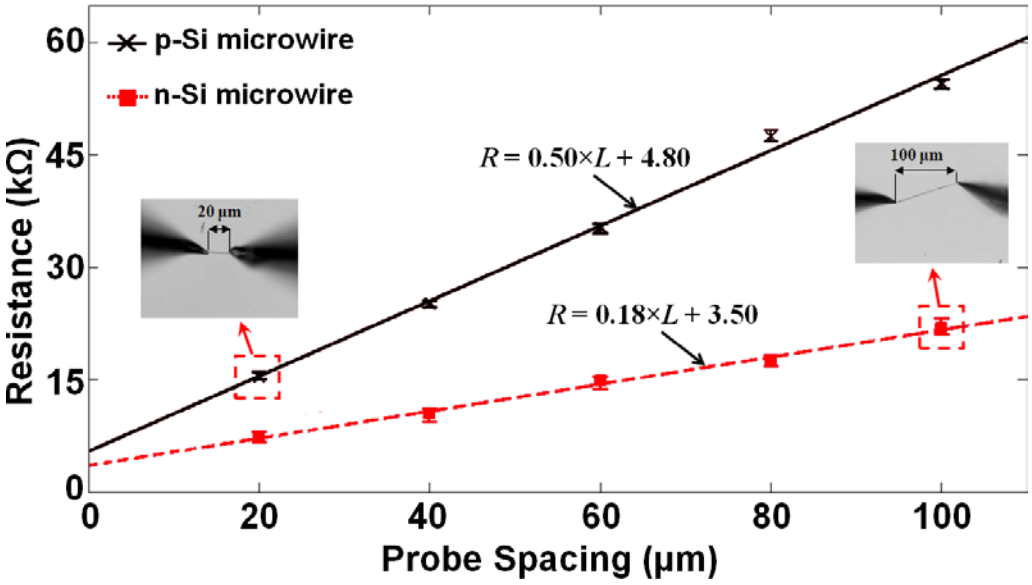

Figure 4.3: Contact resistance measurements for p- and n-type Si microwires with ~1.5 μm diameter. Each data point includes seven independent measurements and the error bar represents the standard deviation from the mean value. The results shown here represent one pair of microwires and were verified by repeating the experiment with other microwires of different doping type/concentration and originating from different fabrication batches. Reprinted with permission from [92]. Copyright (2011) American Chemical Society.

The calculations based on data such as that presented in Fig. 4.3 verified that the contact resistance was a negligible contribution to the total measured resistances (e.g. microwire resistance). However, the contact resistance was subtracted from the total measured resistance prior to calculating the resistivity and, in turn, prior to estimation of the doping concentration of the microwires.

The resistivity of each individual microwire with known dimensions can be extracted from the measured resistance values and assuming a uniform flow of electric current:

$$\rho = R\,\frac{A}{L} \tag{4.1}$$

where ρ is the resistivity, R is the measured resistance, A is the cross-sectional area of the microwire and L is the length of the microwire. Extraction of the doping concentration of individual microwires from the resistivity values is straightforward knowing that the resistivity and doping concentration are related as:

$$\rho = \frac{1}{q(\mu_n n + \mu_p p)} \tag{4.2}$$

where q is the charge on an electron, n is the electron density in the conduction band, p is the hole density in the valence band, μ_n is the mobility of electrons ($\leq$ 1400 $cm^2\ V^{-1}\ s^{-1}$) and μ_p is the mobility of holes ($\leq$ 450 $cm^2\ V^{-1}\ s^{-1}$). In the special case of n-type semiconductors (n >> p), (4.2) can be simplified to $\rho = \frac{1}{q\mu_n n}$. In a similar manner, it can be re-arranged as $\rho = \frac{1}{q\mu_p p}$ for p-type semiconductors (p >> n).

The doping concentration of the microwires, calculated from these bulk resistivity values, was estimated to be 10^{17} ~ 10^{18} cm^{-3}. This is well within the expected range of

doping concentrations based on the conditions used to grow the Si microwires [120,172]. Furthermore, it was concluded that the p- and n-type doping concentration is uniformly distributed over the length scales considered as no detectable variation in the resistance measurements was observed between different regions of the microwires.

The measurement results demonstrated in Fig. 4.3 were obtained from an individual microwire. However, measurements on microwires with similar doping concentrations but taken from different fabrication batches (Fig. 4.4), showed negligible variation from the results taken from an individual microwire, confirming the uniformity of bulk electronic properties from batch to batch. Fig. 4.4 depicts the resistance versus probe separation data obtained for p-type microwires, doped with B up to doping levels of 10^{17} ~ 10^{18} cm^{-3}, selected from 5 fabrication batches.

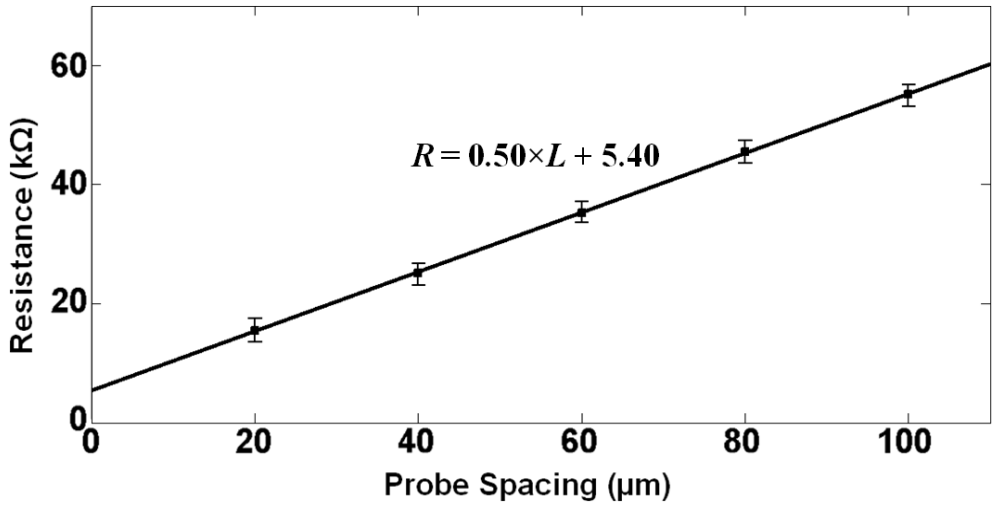

Figure 4.4: Contact resistance versus W probe separation data for p -type Si microwires with ~1.5 μm diameter. Each data point includes five independent measurements performed on five microwires taken from different fabrication batches and the error bar represents the minimum to maximum measured values.

It is worth mentioning that no noticeable change was observed in the measurement results by repeating these measurements over the course of 14 to 21 days; a period of time that was long enough to conclude that the Si native oxide had re-grown on the microwires' exterior and achieved equilibrium coverage. This suggests that, as a result of local mechanical force, the Si native oxide is by-passed by the W probes. However, unless otherwise stated, the microwires were etched using buffered HF before the measurements to minimize any unwanted effect arising from surface SiO_2.

4.2.3 Microwires with Different Levels of Doping and Effect of In/Ga

Silicon microwires with two different levels of p-type doping concentrations were investigated in order to study the effect of doping concentration level on the electrical contact behavior and also to verify the ability of the technique to account for such difference within the samples. The expected active doping concentration (based on VLS growth conditions) for the first set of microwires was approximately $10^{15} \sim 10^{16}$ cm^{-3} and for the second set was $10^{17} \sim 10^{18}$ cm^{-3}, identified in the rest of this section respectively as low doped and highly doped microwires. As discussed in section 3.1.2, it is conventional to use the electrically conductive fluid metal eutectic, In/Ga (25% In and 75% Ga by weight, 15.5 °C melting point [173]), as an interface metal to make ohmic contacts in different semiconductor applications. In order to investigate the effect of the In/Ga metal eutectic on the quality of contacts between the W probes and Si microwires, comparative resistance versus probe spacing measurements between the low doped and

highly doped microwire samples were performed, both with and without In/Ga as the interface metal.

In the case of measurements with In/Ga, a small amount of In/Ga (<< 1mL) was placed onto the glass substrate and the W probes (pre-cleaned using KOH) were dipped into the In/Ga prior to the measurements. Fig. 4.5 shows the measurement results for both highly doped and low doped microwires. The diameter of the selected microwires was ~1.5 μm.

The resistance per unit length (~0.5 kΩ μm^{-1} for the highly doped and ~14.2 kΩ μm^{-1} for low doped microwires) was consistent between all of the measurements with or without In/Ga. Other than a slight decrease in the value of the contact resistance, this behavior verified that the nature of the contacts was unaffected by the presence or absence of In/Ga.

The doping concentration of 10^{17} ~ 10^{18} cm^{-3}, calculated based on the measured resistivity of the microwire in Fig. 4.5a, was in agreement with previously reported values [90,120,133,172]. Similar measurements performed on the low doped microwires (Fig. 4.5b) verified that their doping concentration was in the range 10^{15} ~ 10^{16} cm^{-3}. In Table 4.1 the measured values for both types of Si microwires using the soft contact approach, with and without In/Ga eutectic are summarized.

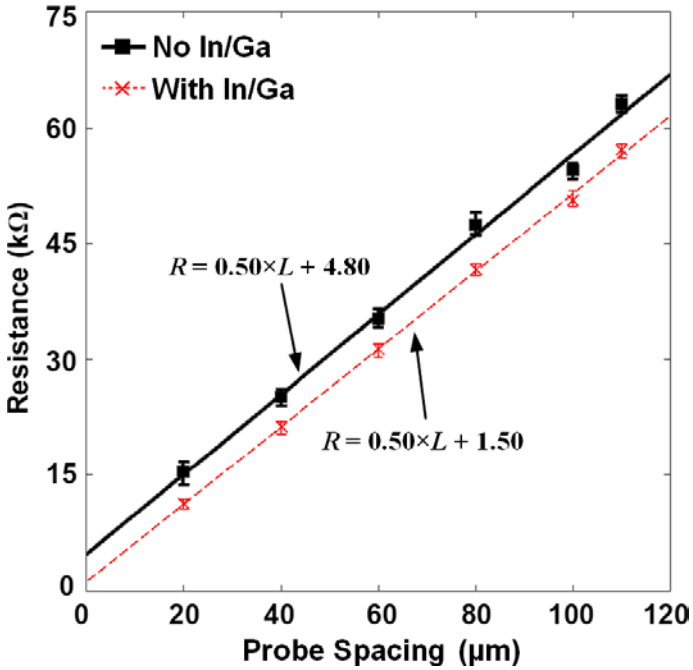

(a)

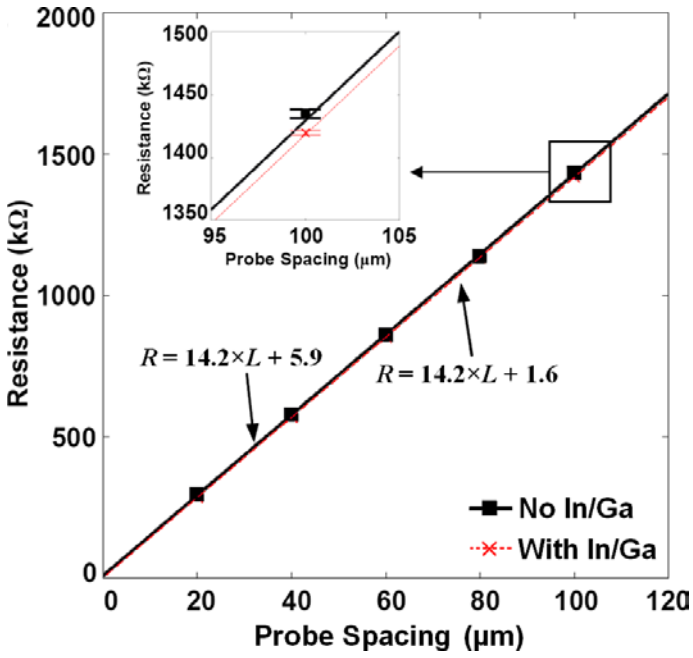

(b)

Figure 4.5: Contact resistance measurements for ~1.5 μm microwires (a) highly doped and (b) low doped Si microwires both with and without In/Ga. Reprinted with permission from [91]. Copyright (2011) American Chemical Society.

Table 4.1: Measured resistance values (±1%) for 100 μm long, highly doped and low doped Si microwires with an average diameter of 1.5 μm. R_L is the microwire resistance per unit length, $R_{Contact}$ is the calculated contact resistance between the W probe and the microwire. The microwires were 100 μm long and 1.5 μm in diameter.

	R_{wire} (kΩ)	R_L (kΩ μm^{-1})	$R_{Contact}$ (kΩ)	Doping (cm^{-3})
No InGa	50	0.50	2.40	10^{17}~10^{18}
With InGa	50	0.50	0.75	10^{17}~10^{18}
No InGa	1420	14.20	2.95	10^{15}~10^{16}
With InGa	1420	14.20	0.80	10^{15}~10^{16}

Since the change in the W probe/microwire contact resistance value is negligible compared to the magnitude of the microwire resistance, In/Ga was omitted in the future measurements. The omission was mainly due to the issues associated with the application of In/Ga, such as unwanted attachment of microwires to the W probes and also In/Ga residues on the microwires that could potentially affect the microwire/polymer junction measurements. As a result, it was easier to reliably move the microwires and form a contact without In/Ga and this outweighed any benefit associated with the lower contact resistance value.

4.2.4 Methyl-Terminated versus H-Terminated Si Microwires

In the final set of measurements, the soft contact formation approach using W probes was applied to methyl-terminated Si microwire samples. Methylation of the microwires (detail in section 4.3.4) was employed in the final samples to avoid the formation of native oxides on the Si microwires. All microwire samples, obtained from the collaborators in the Lewis group at Caltech, were prepared in a similar manner using VLS growth technique. These microwires were investigated using soft contact formation approach in order to verify their DC resistance and doping concentration.

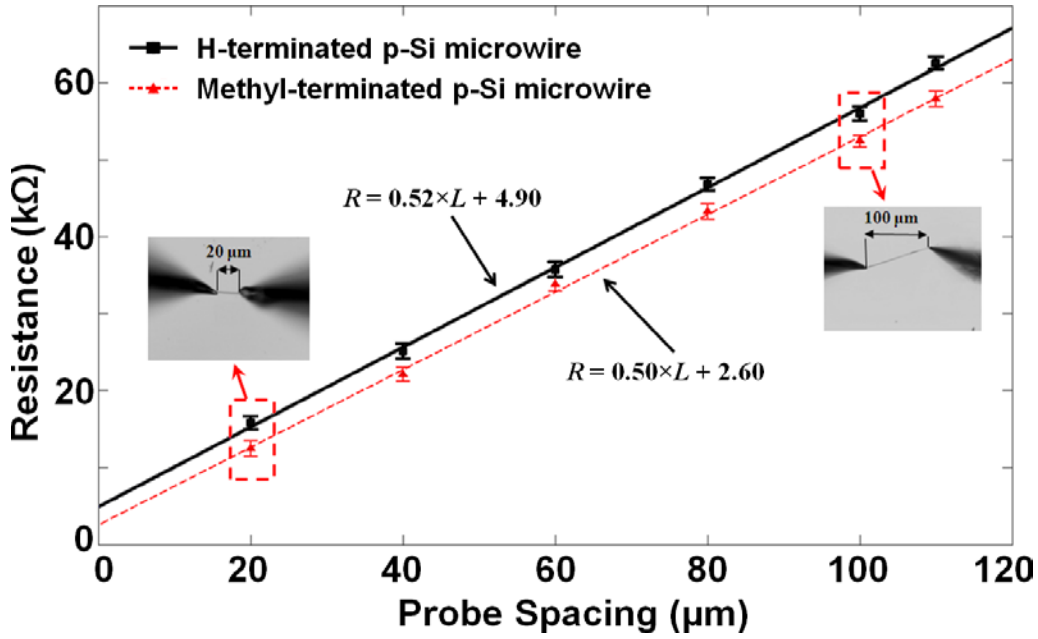

Figure 4.6: Resistance versus probe separation data obtained for methyl-terminated p-type as compared to H-terminated p-type microwires.

To give a direct comparison between methyl-terminated and H-terminated samples with the same type of doping, in Fig. 4.6 the resistance versus probe separation data obtained for methyl-terminated p-type is compared to the H-terminated p-type microwires.

Fig. 4.7 depicts the resistance versus probe separation data obtained for methyl-terminated p-type and n-type Si microwires. The resistance per unit length of the methyl-terminated microwires was approximately 0.50 kΩ μm^{-1} and 0.18 kΩ μm^{-1} for the p-type and n-type Si microwires respectively. As expected, these values are similar to those calculated for H-terminated Si microwires (Fig. 4.6).

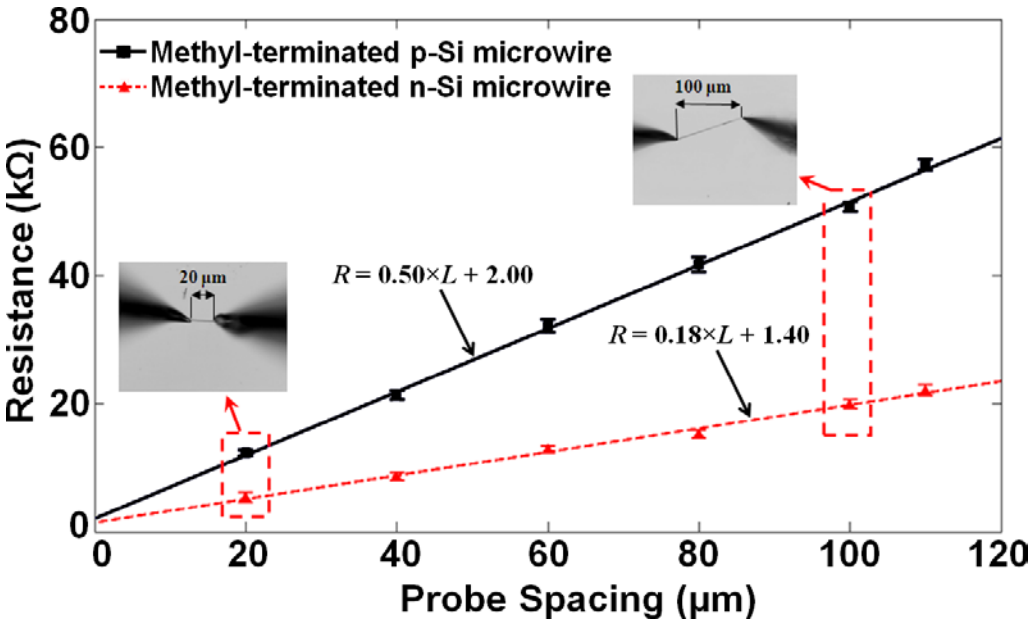

Figure 4.7: Contact resistance measurements for methyl-terminated (or methylated) p- and n-type Si microwires with ~1.5 μm diameter. These results were verified by repeating the experiment with other microwires of different doping type, different doping concentration, and originating from different fabrication batches.

The contact resistance between the W probes and the microwires was also calculated and verified to be a negligible contribution to the total measured resistance for the system (< 1 kΩ). The doping concentration of the microwires was found to be uniform over the length scales considered (Fig. 4.6 and 4.7) and estimated to be 10^{17} to 10^{18} cm^{-3}, within the expected range of doping concentrations based on the growth conditions [90,120,133,172].

4.3 Microwire/Polymer Junction Characterization

In the previous section, it was verified that the soft contact formation method had the ability to form reliable contacts to single microwires. Basic electrical properties of the microwires including DC resistance and doping concentration as well as uniformity of the

doping across the length of the microwire were investigated for different microwires. Also, microwires with different doping concentrations as well as different types of dopants were studied. The reliable application of the technique was also demonstrated on the microwires functionalized with methyl (CH_3) groups.

This section presents the investigation of the photoelectrical properties of individual solar water splitting devices based on different microwire/polymer combinations. The candidate conducting polymers, PEDOT:PMA and PEDOT:PSS:Nafion with 12 wt.% PEDOT:PSS, were investigated. Candidate conducting polymer films were prepared according to the procedures described in section 3.2.1 and Appendix C. As demonstrated schematically in Fig. 3.9, three main junctions were present for each single microwire/polymer combination in the final measurement system: the sputtered Au/Pd/polymer junction; the W probe/microwire junction; and the microwire/polymer junction. The sputtered Au/Pd junction with both conducting polymers has well defined ohmic characteristic (Fig. 3.8). The contact resistance associated with the junction between W probe/microwire was also investigated in previous section and quantified.

To investigate the Si microwire/polymer junction, one W probe was held in contact with the microwire while the second probe was in contact with the Au/Pd pad, as illustrated in Fig. 3.8a. The current passing through the system for different applied voltages was then recorded using an *Agilent 4155c* semiconductor parameter analyzer in a standard probe station (Fig. 3.11). The results of these measurements for different microwire/polymer combinations will be presented in the following sections.

In each case, the total series resistance, R_{total}, included contributions from the conducting polymer resistance, $R_{polymer}$, the microwire/polymer contact resistance, R_C

(denoted as $R_{C\text{-}p}$ for p-type and $R_{C\text{-}n}$ for n-type microwires), and the microwire resistance, R_{wire} (denoted as $R_{p\text{-}wire}$ for p-type and $R_{n\text{-}wire}$ for n-type microwires) as shown in Fig. 2.8. The microwire/polymer contact resistance (R_C) was then calculated from the expression:

$$R_{total} = R_{polymer} + R_{wire} + R_C \qquad (4.3)$$

where, R_{total} is the total measured resistance of the microwire/polymer system. The $R_{polymer}$ value was calculated from four-point probe measurements. The $R_{C\text{-}p}$ and $R_{C\text{-}n}$ values were extracted from these independent measurements, and the total series resistance across a single unit of the membrane-bridged device was then approximated by adding these values to the values of $R_{p\text{-}wire}$, $R_{n\text{-}wire}$ and $R_{polymer}$.

4.3.1 PEDOT:PMA in Combination with H-terminated Si Microwires

The measurement process started with an investigation on the electrical behavior of PEDOT:PMA/Si microwire system. More specifically, H-terminated p-Si microwires were studied in this case, as these wires are anticipated to form ohmic contact to p-type PEDOT:PMA conducting polymer [136]. The *I-V* data for an approximately 100 μm long p-Si microwire with a diameter of 1.5 μm and low doping levels (i.e. 10^{15} to 10^{16} cm^{-3}), aligned at the PEDOT:PMA/glass border are shown in Fig. 4.8.

At low bias voltages, the *I-V* behavior of the junction between the microwires and polymer films was non-linear (Fig. 4.8), likely due to tunneling through an oxide layer on the surface of the microwires, which is in agreement with prior measurements on oxide-coated Si microwire devices [174,175].

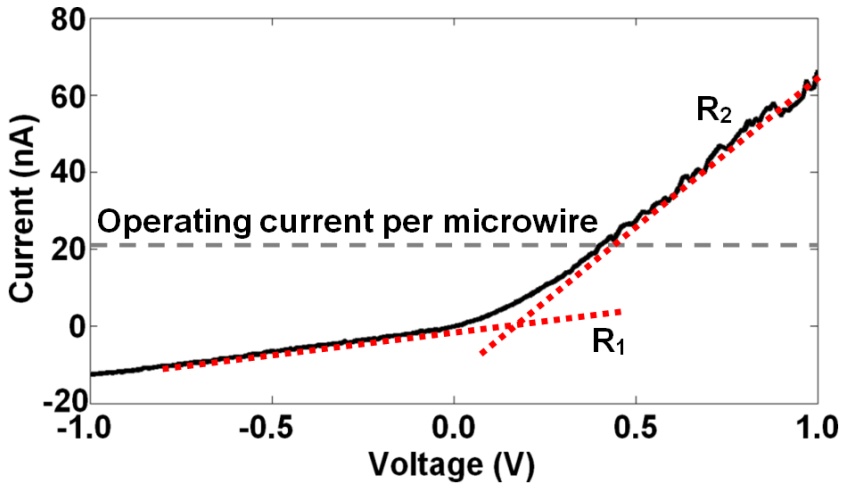

Figure 4.8: The *I-V* data for an approximately 100 µm long p-Si microwire with a diameter of 1 µm, with low doing levels (i.e. 10^{15} to 10^{16} cm^{-3}), aligned at the PEDOT:PMA/glass border. The measured DC resistance in the near zero-bias region (R_1) was approximated to be 100 MΩ that decreased to $R_2 \approx 13$ MΩ for higher bias voltages. The current level of 21 nA that is anticipated to flow through microwires at maximum light absorption (section 3.2.3) is also marked for reference.

Although the Si microwires were etched immediately prior to the measurements, a thin layer of native oxide was presumed to form on the surface of the Si, because the alignment of the microwires at the polymer/glass interface was conducted in air. At higher bias voltages this nonlinear behavior was not dominant and the *I-V* profile appeared purely resistive. Therefore, in addition to the measurements at small-bias, which is closer to the expected working regime of the solar water splitting device, the total resistance values for the system were also measured at higher bias voltages (±10 V). The large-bias measurements in the following section establish a lower bound for the DC resistance of the candidate systems.

It is also more likely to form an optimal electrical contact between microwires and conducting polymer membranes when the polymer film is still wet (i.e. the solvent is not

completely evaporated), a phenomenon observed during initial measurements. For this reason, effort was made to keep the time interval between the film preparation and alignment of the microwires, as short as possible, most favorably within 5 to 10 minutes or less.

The average total series resistance, R_{total}, measured for the junctions between low doped p-Si microwires and PEDOT:PMA at large bias voltages is approximately 13 MΩ (R_2 in Fig. 4.8). This value was reduced to approximately 2 MΩ for the case of microwires with higher level of doping concentration (i.e. 10^{17} to 10^{18} cm^{-3}). The contact resistances involved in the system (e.g. W probe/microwire and Au/Pd/polymer contact resistance) were significantly smaller than these resistances. Considering the calculated value of the polymer film resistance based on 4-point probe measurements (~ 1MΩ) [116], and the values of microwire resistance calculated in section 4.2.4 for different levels of doping concentration (~1.42 MΩ and ~50 kΩ respectively for low doped and highly doped, 100 μm long microwire), average $R_{C\text{-}p}$ values of ~9.8 MΩ and ~0.3 MΩ were calculated from (4.3), for the low doped and highly doped microwires/polymer junctions, respectively. Table 4.2 summarizes the values measured for the H-terminated p-Si microwire/PEDOT:PMA system.

Table 4.2: Measured resistance values (±1%) for 100 μm long p-Si microwires with an average diameter of 1.5 μm, in contact with PEDOT:PMA. R_{PMA} is the resistance of PEDOT:PMA film and $R_{C\text{-}p}$ is the calculated resistance of the junction between low doped (1st row) and highly doped (2nd row) H-terminated p-Si microwires and the films.

	R_{wire} (MΩ)	R_{PMA} (MΩ)	$R_{C\text{-}p}$ (MΩ)
With low doped microwires	1.42	1.32	9.75
With highly doped microwires	0.05	1.32	0.30

Based on the maximum acceptable DC resistance value of ~ 480 kΩ (section 3.2.3) for the complete water splitting cell (including both p-type and n-type semiconductor microwires), the DC resistance associated with only a half-cell of the ultimate system including low-doped p-Si-microwires is far above the minimum requirements.

The resistance of the PEDOT:PMA in combination with highly doped p-Si microwires is also greater than, but closer to, the critical value. Also, as mentioned earlier, these values were calculated at large bias voltages (±10 V). At bias voltages close to the actual expected working conditions (±10 mV), higher resistances were observed, further indicating the fact that PEDOT:PMA/Si microwire system is not a suitable candidate in terms of electrical properties.

Due in part to the large resistances observed in these systems, no further investigation was performed on PEDOT:PMA based systems.

4.3.2 PEDOT:PSS:Nafion in Combination with H-terminated Si Microwires

PEDOT:PSS:Nafion with 12 wt.% PEDOT:PSS is the other candidate composite that was investigated for the use as supportive membrane in the proposed photosynthetic device. The measurement process started with an investigation on the H-terminated p-Si microwires junctions with this polymer similar to the case of PEDOT:PMA conducting polymer. Similar to the case discussed in section 4.3.1, junctions between this polymer and both highly doped and low doped microwires were investigated.

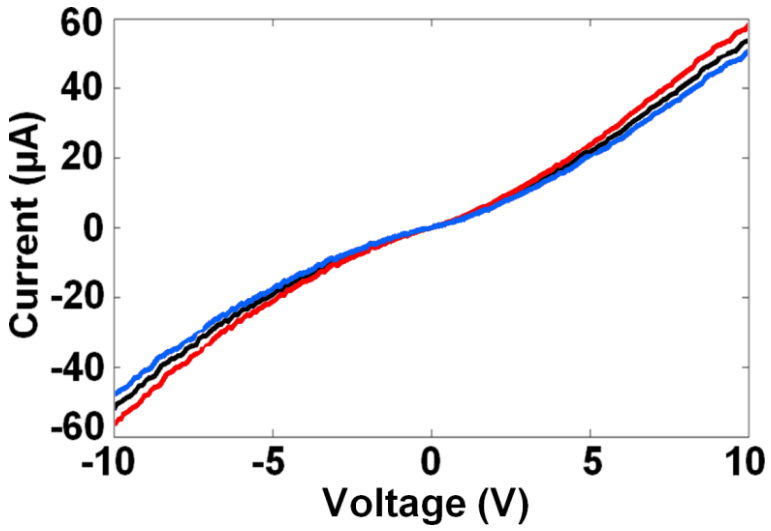

Figure 4.9: The *I-V* data for three, approximately 100 μm long p-Si microwires with a diameter of 1.5 μm and high doping levels (i.e. 10^{17} to 10^{18} cm^{-3}), aligned at the PEDOT:PSS:Nafion/glass border of the same sample. The variation in observed junction to junction resistance was ~5%.

The *I-V* data for approximately 100 μm long p-Si microwires with a diameter of 1.5 μm and high doping levels (i.e. 10^{17} to 10^{18} cm^{-3}), aligned at the PEDOT:PSS:Nafion/glass border are shown in Fig. 4.9. The data taken from three microwire/polymer junctions showed a negligible junction to junction resistance variation of approximately 5%, for the resistance values calculated at 8-10 V bias region.

The average total series resistance, R_{total}, is approximately 3 MΩ for the junctions between low doped p-Si microwires and PEDOT:PSS:Nafion composite conducting polymer (at large bias voltages), and 160 kΩ for the case of microwires with higher level of doping concentration, both significantly lower than the case of PEDOT:PMA. This is partially due to the higher electronic conductivity of PEDOT:PSS:Nafion composite ($R_{polymer}$ ~8kΩ) compared to PEDOT:PMA ($R_{polymer}$ ~1.32 MΩ). Using a similar measurement approach reported in section 4.3.1, the contact resistance values ($R_{C\text{-}p}$) of

~1.5 MΩ and ~100 kΩ were extracted for the low doped and highly doped samples respectively.

The calculated $R_{C\text{-}p}$ values for low doped p-Si microwire/PEDOT:PSS:Nafion system also exceeded the maximum acceptable DC resistance value of ~ 480 kΩ (section 3.2.3), for the complete water splitting cell (which would include both p-type and n-type semiconductor microwires). This ruled out the possibility of using these low-doped wires as part of the envisioned solar water splitting system.

The PEDOT:PSS:Nafion junctions with highly doped Si microwires, however, did meet the minimum conductance requirements. However, as mentioned earlier, these values were calculated at large bias voltages (±10 V).

To provide a more realistic measurement scenario, freshly HF-etched (H-terminated) p- and n-Si microwires with high doping levels (10^{17} to 10^{18} cm^{-3}) were aligned at the border between PEDOT:PSS:Nafion and glass substrate as described in section 3.2.2 (Fig. 3.9b). The R_{total} values were then measured for different ranges of applied bias voltage, ±10 V and ±1 V to give an estimation of the maximum attainable conductance (at a large bias) and the real conductance in the working region (at a small bias).

As an example of these measurements, Fig 4.10 demonstrates *I-V* data measured for 100 μm long H-terminated p-type Si microwire (Fig. 4.10a) and H-terminated n-type Si microwire (Fig. 4.10b); both with diameters of ~1.5 μm aligned at the PEDOT:PSS:Nafion/glass border (figure insets) in the ±1 V bias region.

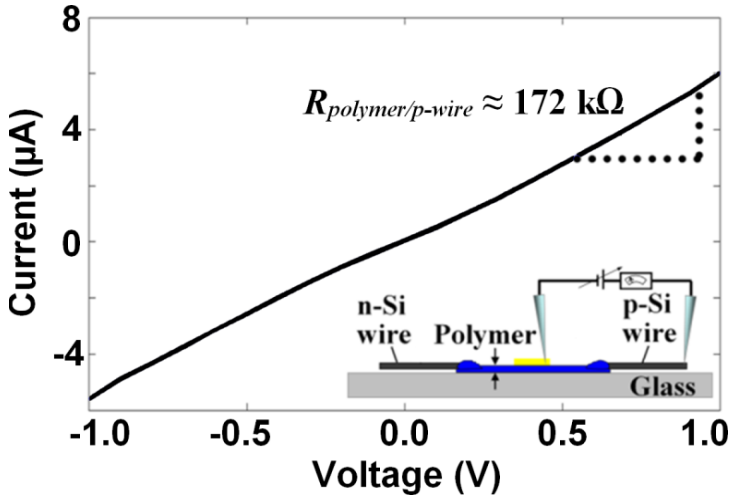

(a)

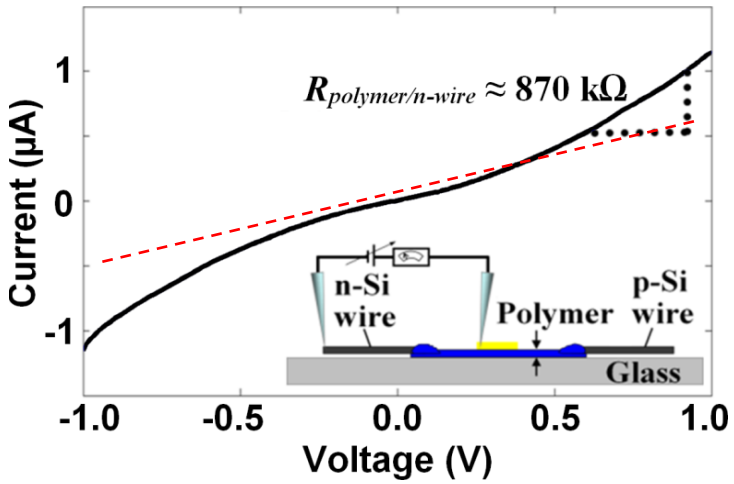

(b)

Figure 4.10: *I-V* data measured for 100 μm long H-terminated (a) p-type Si microwire and (b) n-type Si microwire; both with diameters of ~1.5 μm aligned at the PEDOT:PSS:Nafion/glass border (figure insets) in the ±1 V bias region. The total series resistance of the system in each case (displayed in the figures) was used to extract the value of junction resistances, $R_{C\text{-}p}$ and $R_{C\text{-}n}$. In the case of n-type microwires, the I-V profile demonstrates a slight bend at small bias voltages, leading to larger DC resistance values in these regions as demonstrated by fitting an asymptote to the zero bias point of the curve (dashed red line). Adapted with permission from [92]. Copyright (2011) American Chemical Society.

In each case, the total measured resistance, R_{total} (displayed in the figures), was used to extract the value of junction resistances, $R_{C\text{-}p}$ and $R_{C\text{-}n}$ by incorporating the known values (R_{wire}, $R_{polymer}$). In the case of n-type microwires, the I-V profile demonstrates a slight bend at small bias voltages, leading to total resistance values approaching 1MΩ, in these regions as demonstrated by the asymptote at the zero bias point (dashed red line in Fig. 4.10b).

The results of these calculations for individual microwire/polymer junctions were also compared to the results of a measurement on a complete structure (Fig. 4.11) in which one W probe was placed on the n-type microwire while the second probe contacted the p-type wire, and a test current was passed through the entire structure.

Measured R_{total} in this case included contributions from the conducting polymer ($R_{polymer}$), the microwire/polymer contacts ($R_{C\text{-}p}$ for p-type microwires and $R_{C\text{-}n}$ for n-type microwires), and the microwire (denoted as $R_{wire\text{-}p}$ for p-type and $R_{wire\text{-}n}$ for n-type microwires). The microwire/polymer contact resistances, $R_{C\text{-}p}$ and $R_{C\text{-}n}$, calculated by incorporating the known values, are in agreement with the calculations on the individually measured contacts (Fig. 4.10).

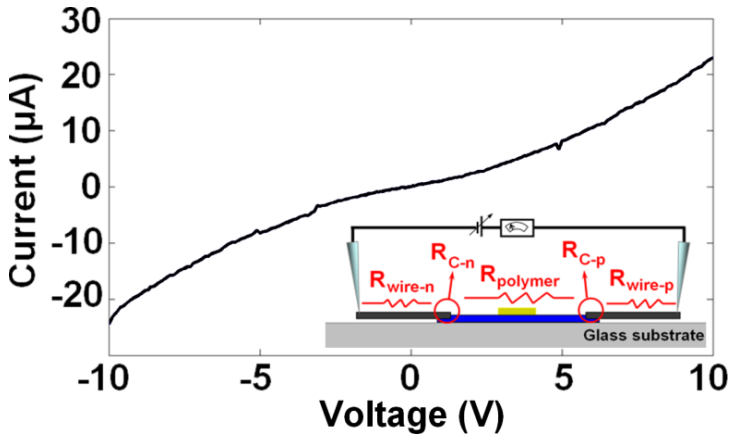

(a)

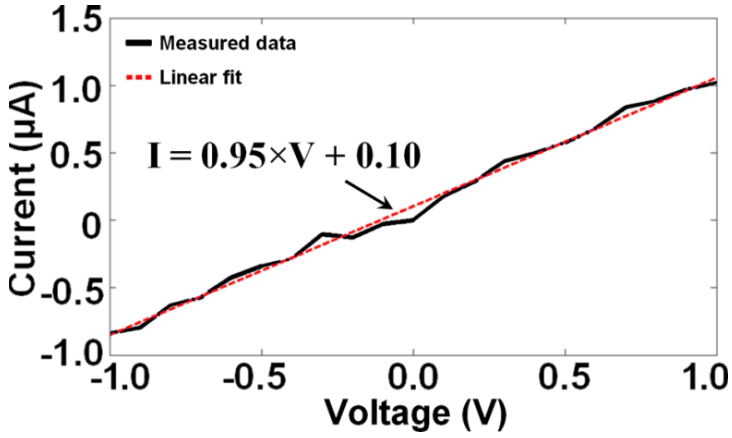

(b)

Figure 4.11: A complete unit of the proposed solar fuel generation device, including two 100 μm long n-type and p-type Si microwires with diameters of ~1.5 μm, aligned at the PEDOT:PSS:Nafion/glass border (figure inset). *I-V* data measured for different ranges of applied bias voltages, (a) large-bias regime: -10 V to +10 V and (b) small-bias regime: -1 V to +1 V. The total series resistance of the system in the large-bias regime was ~250 kΩ, and increased to ~1 MΩ in the small-bias regime. Reprinted with permission from [92]. Copyright (2011) American Chemical Society.

In Table 4.3 the measured resistances for both small- and large-bias regimes is summarized where it is shown that the measured value of $R_{C\text{-}p}$ in the small-bias regime was ~20 kΩ larger than the value recorded at large-bias. This behavior was ascribed to the presence of a thin native oxide layer on the microwire. However, the more than 8× increase in the value of $R_{C\text{-}n}$ in the small-bias regime reflected both the presence of native oxide layer on the microwires and the Fermi level mismatch between the n-type microwires and PEDOT:PSS:Nafion film (with p-type characteristics) [98,102]. The other resistance results from both small- and large-bias measurement were in reasonable agreement (Table 4.3).

In all cases, at bias voltages close to the expected working conditions (±10 mV), higher resistances were observed, indicating the importance of the microwire surface treatment (e.g. native oxide removal, etc) on the electrical properties of the Si/polymer junctions. While the PEDOT:PSS:Nafion junction with highly doped Si microwires was less resistive, improvements in IR losses at these low current levels are required to meet the minimum requirements for a final device.

Table 4.3: Measured and calculated resistances in kΩ (±1%) for highly doped Si-microwire/PEDOT:PSS:Nafion system. The microwires were 100 μm long and 1.5 μm in diameter. $R_{polymer}$ is the resistance of the PEDOT:PSS:Nafion film.

	$R_{wire\text{-}p}$	$R_{wire\text{-}n}$	$R_{C\text{-}p}$	$R_{C\text{-}n}$	$R_{polymer}$	R_{total}
Large-bias	50	18	100	93	2	263
Small-bias	50	18	120	850	2	1040

4.3.3 Temporal Changes in the Electrical Properties of Polymer/H-Terminated Si Microwire System

A candidate conducting polymer/microwire system with appropriate electrical properties must also meet another, equally important, requirement in order to be considered for the use in a solar fuels generation device. Similar to the case of thin film solar cells [176,177], long-term electrical stability of these systems may also be a key feature in reducing the total implementation cost. Long-term electrical stability of these systems is the subject of investigation in this section.

Since this research was focused on investigating the electrical properties of different semiconductor microwire/polymer combinations for the use in a solar water splitting cell, the temporal change in the microwire/polymer junction properties was also considered as a measure of the stability of these combinations. In a sequence of measurements, the individual p-Si microwire/polymer/n-Si microwire structures were investigated over a period of 30 days. As described in section 4.3.2, highly doped microwires in combination with PEDO:PSS:Nafion were used in these investigations.

All the microwires were etched in HF (forming H-terminated surfaces) prior to the initial measurements at day 1. Although the H-terminated Si microwires have relatively low surface recombination velocities, the formation of native oxide as a consequence of exposure to air leads to increased total recombination, reflecting the greater availability of electrically active trap sites within the oxide layer [178]. The growth of native oxide on the microwires in the proposed solar water splitting system would be enhanced by the aqueous environment and high level of exposure to oxygen. Given these environmental factors, oxide formation within the Si microwire/conducting polymer membrane junction

was predicted to significantly increase the junction resistance, resulting in more electrical loss in the system. Such losses could compromise the functionality of the device, considering the limited amount of photogenerated voltage available to drive the water splitting reactions [5,88,89,151,152].

The *I-V* data for H-terminated p- and n-type microwires aligned at the PEDOT:PSS:Nafion/glass border (Fig. 4.10) suggests ohmic behavior at the junction between H-terminated p-Si microwires and polymer and a non-ohmic behavior between H-terminated n-Si microwires and polymer. More importantly, the characteristics of the n-type microwire/polymer junction was ascribed to the Fermi level mismatch between the n-type microwires and PEDOT:PSS:Nafion film, which has p-type characteristics.

Although the H-terminated Si microwires were etched immediately prior to the measurements, a thin layer of native oxide is presumed to have formed on the surface of the Si because the alignment of the microwires at the polymer/glass interface was conducted in air. As a result, quantum tunneling through the native oxide is expected to contribute to the junction resistance, causing a more visible non-linear behavior in the small bias region.

These microwire/polymer structures were kept under the lab conditions for a period of 30 days, when a new set of *I-V* measurements revealed a more than 20× increase in the junction resistance (Fig. 4.12) and in some cases loss of electrical conduction at the junction. The likely source of this change in behavior is increased native oxide formation on the surface of the microwires at the polymer interface progressively degrading the contact.

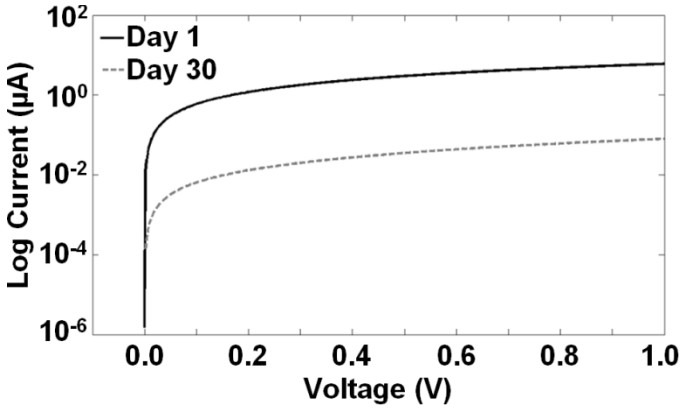

(a)

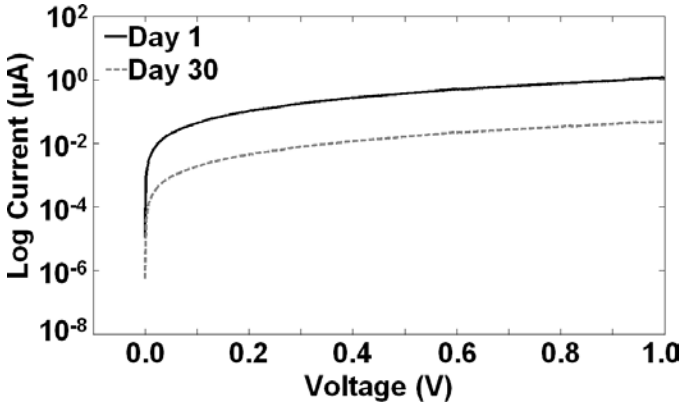

(b)

Figure 4.12: *I-V* data measured for 100 μm long H-terminated (a) p-type Si microwire and (b) n-type Si microwire; both with diameters of ~1.5 μm aligned at the PEDOT:PSS:Nafion/glass border. The measured data (with current in logarithmic scale) taken on the first day and after a period of 30 days are shown together for comparison. A noticeable increase in the total measured resistance was observed compared to the measurements with freshly etched microwires.

In order to exclude the potential aging effect associated with the polymer membrane, aged microwire samples were also used to form contacts with freshly prepared polymer films. The results of these measurements were more or less similar to the case depicted in Fig. 4.12, with almost no conduction at the contact in most of the cases.

Repeating the measurements after a 30-day period of time, considering the working conditions envisioned for the ultimate solar water splitting devices, was a clear indication of the need to effectively address the issues related to native oxide formation at the microwire surface. In response to this need, the following section describes the investigation of new microwire samples with functionalized surface to limit further formation of native oxide.

4.3.4 PEDOT:PSS:Nafion Combination with Methyl-Terminated Si Microwires

In the case of junctions between conducting polymer composite and H-terminated samples (section 4.3.3) the observed increase in the junction resistance over time was attributed to Si native oxide formation at the microwire/polymer interface. To address this issue, methyl-terminated microwires were used, and the stability of the electrical properties of the microwire/polymer system was investigated over a similar length of time, following a similar measurement procedure described in section 4.3.3.

In the case of H-terminated microwires, the native oxide, as well as any oxide that may have formed during the growth catalyst removal process, is removed by etching the Si microwires in buffered HF(aq.) (section 3.1.1), replacing oxygen bonds at the surface with hydrogen bonds. Considering the fact that formation of native oxide at the Si surface begins with replacement of unstable Si-H bonds, one promising approach to surface functionalization is to replace unstable Si-H surface bonds with more kinetically stable Si-C bonds [179-181].

Numerous articles in the existing literature have reported successful alkylation of the H-terminated Si samples using different techniques such as alkylmagnesium reagents [182,183], radical halogenation [184], chemical free-radical activation [185,186], irradiation with ultraviolet light [187-191], thermal activation [186,192-194], and hydrosilylation [195-197], for both the Si(100) [193,198] and the Si(111) surfaces [178,180,199] as well as porous Si [200].

Enhanced oxidative stability and decreased surface recombination velocities as a result of Si surface passivation with alkyl groups have been reported for planar samples [181], suggesting that functionalization of the Si microwire surface may also provide protection against further oxidation by air and/or water, prevent photogenerated charge-carrier recombination and decrease electrical loss at the junction between microwires and conducting polymer membranes.

For a new series of measurements, microwire structures doped with B and P up to $10^{17} \sim 10^{18}$ cm^{-3}, that grown and functionalized in the collaborating laboratory at Caltech, were studied using the standard soft contact formation approach with W probes. The microwire samples were grown using the VLS technique and functionalized following a two-step chlorination-alkylation process that has been reported for planar Si and is known to produce electrically and chemically stable surfaces with negligible native oxide growth over time [178,180,181,199]. The functionalization process involved an initial etching in 10% HF(aq.) to remove the native oxide from the wire surface. Samples were then placed into a nitrogen-purged flushbox and, using a saturated solution of PCl_5 in chlorobenzene, chlorinated at 90 °C for 45 minutes. The microwires were then rinsed of the reagents and

solvents and placed in a 1M methyl Grignard solution (CH_3MgBr) for time periods that were varied systematically between 1 hour and 1 day at 60 °C [178,180,181,199].

A comparison between the electrical properties of these microwires and the H-terminated samples was performed. In order to eliminate any variation in the results due to the microwire growth process parameters, two samples were taken from the same growth substrates, the first batch etched in HF(aq.) to remove native oxide and form H-terminated wires while the second batch was functionalized with methyl groups to study the effect of surface passivation on the electrical properties of the microwires.

I-V measurements, similar to those described in sections 4.3.2 and 4.3.3, were performed on these H-terminated microwire samples. These measurements confirmed an increase in the microwire/polymer junction resistance, consistent with the results discussed in sections 4.3.2 and 4.3.3. The characterization of the methyl-terminated microwires started with individual microwire characterization, described in section 4.2.4. The resistance per unit length of the methyl-terminated microwires was extracted and the consistency of doping concentration along the methyl-terminated microwires was also confirmed using resistance versus probe spacing measurements (Fig. 4.6 and 4.7).

The *I-V* measurements described in sections 4.3.1 through 4.3.3 were all performed in dark conditions. In this section, measurements on methyl-terminated microwires/polymer junctions were performed both in dark and under AM 1.5G (100 $mWcm^{-2}$) illumination using a Newport model *96000* full spectrum solar source with a global air mass (AM) 1.5 filter (see Appendix D for the output power measurements).

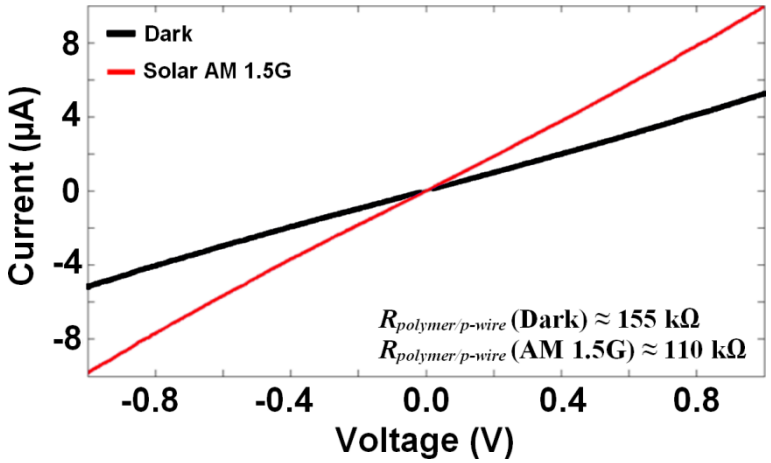

Figure 4.13: *I-V* data for a 100 μm long methyl-terminated p-Si microwire with diameters of ~1.5 μm aligned at the PEDOT:PSS:Nafion/glass border, in dark and under solar AM 1.5G. As expected, ohmic behavior was observed at p-Si microwire/polymer contact. The average measured resistance in dark was ~180 kΩ and decreased to ~120 kΩ under illumination.

The methyl-terminated microwires were used to form individual solar water splitting devices as shown in Fig 3.9b. Methyl-terminated p-Si microwires aligned at the PEDOT:PSS:Nafion/glass border demonstrate ohmic character (Fig. 4.13), in agreement with prior measurements on planar methyl-terminated p-Si and PEDOT [151]. The total measured resistance in dark was ~180 kΩ and decreased to ~120 kΩ under 1 sun illumination.

As shown in Fig. 3.9, the microwires were oriented parallel to the substrate and were illuminated from above so the illuminated photoactive area was ~1.5 μm × 100 μm. Under AM 1.5G illumination, increased conductivity was observed in the microwires which now behaved as a photoresistor, leading to slightly lower R_{total} values as indicated in Fig. 4.13. Assuming a relaxation time of 10 μs between the currents in the dark and under illumination, approximated through a set of *I-V-t* measurements, a photogenerated charge density of ~10^8 cm^{-3} may be approximated, knowing the total photogenerated

charge is equal to $\int_0^{10\mu s} I.dt$ with I being the average difference in the amount of electrical current between dark and illuminated states [68,201]. However, this does not agree with the observed change in the resistance when compared to the bulk doping concentration of ~10^{17} cm^{-3}. This behavior could potentially be due to the changes in the surface states under illumination.

This experiment was repeated following the storage of the samples in ambient conditions for 30 days; at which time the calculated junction resistance was found to be within 10% of the original value (180 kΩ in Fig. 4.13). One explanation for the increase in the junction resistance in the case of methyl-terminated microwires is oxidation at the base of the microwires where they had been cut off from the growth substrate. In some designs for the final water-splitting device design [88,150,151], despite the harsh aqueous environment, such exposure will not exist in the eventual device.

Compared to the H-terminated microwires, the methyl-terminated n-Si microwires also show better oxidative stability. This was further confirmed by XPS analyses (Appendix E) that suggested a smaller amount of oxide grown over time for the methyl-terminated microwires. The XPS analysis results on the H-terminated and methyl-terminated n-Si microwire samples are shown in Fig. 4.14. In order to perform this test, a large amount of microwires were scraped from ~1 cm^2 of the growth substrate (equal to ~760 µg of microwires) and piled on an Au-coated glass substrate. This sample was then mounted into the XPS vacuum chamber for analysis. The XPS measurement parameters are presented in Appendix E. The escape depth of XPS beam in these measurements is estimated to be 6-15 nm. As a result, the XPS data could be reliably attributed to the surface region of the microwires.

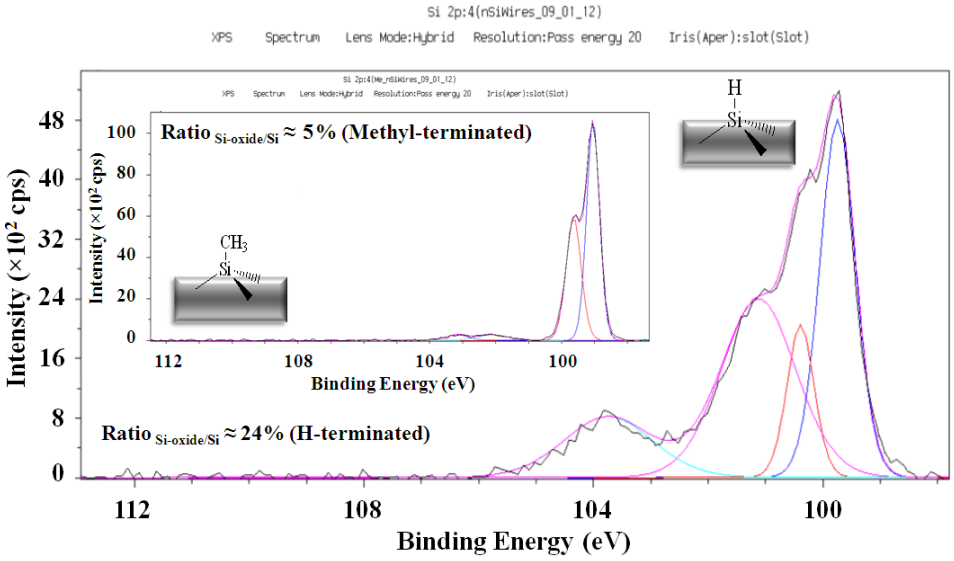

(a)

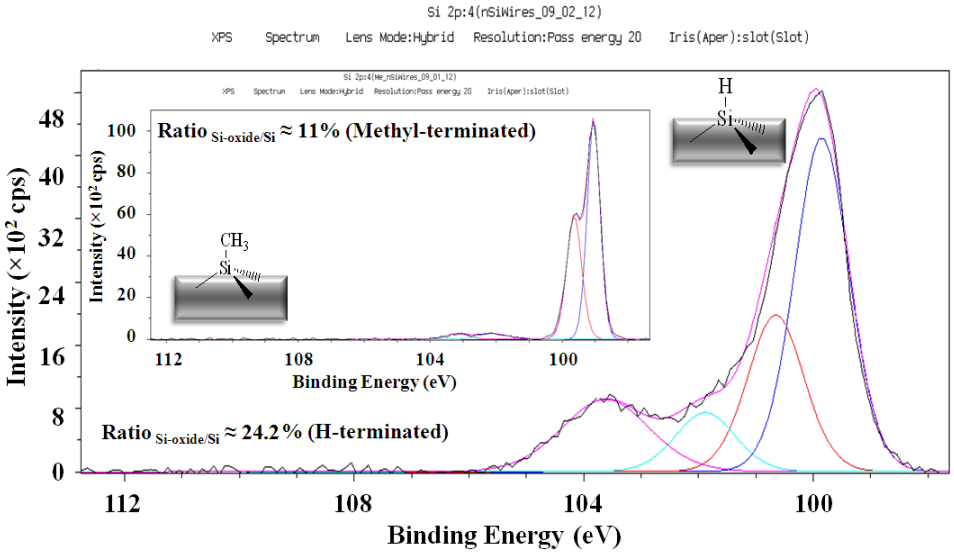

(b)

Figure 4.14: Results from XPS analysis on H-terminated and methyl-terminated n-Si microwire samples, featuring the Si-2p region; (a) at day 1 and (b) after one month. The escape depth of the XPS beam in these measurements is estimated to be 6-15 nm. As a result, the XPS data could be reliably attributed to the surface of the microwires. Larger amounts of oxide were observed in the case of H-terminated samples compared to the methyl-terminated samples. The oxide observed in the case of methyl-terminated samples was attributed to the base of the microwires, where they had been cut off from the growth substrate.

H-terminated n-type Si microwires were freshly etched at the time of first XPS analysis (day 1). Methyl-terminated n-Si microwires were also taken from a recently methylated batch. Both samples were then kept under the lab conditions for one month prior to the analysis being repeated.

From the Si XPS analysis results (Appendix E), the ratio of the feature at ~103 eV, attributed to oxidized Si, to neutral Si 2p peak at ~99eV was chosen as a measure of oxide ratio in each case. Although the H-terminated wires were etched before the measurements, the time interval between the etch and mounting the samples into the XPS chamber was long enough for the native oxide to form. A large intermediate oxide (hemi-oxide) peak was observed around 101 eV in the 'Day 1' results. The feature at 101 eV was excluded in the calculation of the oxide ratio given in the inset of Fig. 4.14a and 4.14b and only the peak at 103 eV was considered. Inclusion of this feature leads to even larger oxide ratios (>40%) in the case of H-terminated microwire samples.

The oxide ratio for the case of H-terminated microwires remained roughly constant over the course of a month indicating the presence of a saturated native oxide layer. The unchanged ratio for H-terminated samples (~24%) following a one-month period contrasts greatly with the changed ratio recorded for the methyl-terminated samples (from ~5% initially to ~11% after one month). This clearly indicated that methylation improved oxidative stability.

The oxide observed in the case of methyl-terminated samples was attributed to the base of the microwires, where they had been cut off from the growth substrate. This area was exposed to ambient conditions and having no methylation, oxidation could initiate here. However, as observed in the XPS curves, Fig. 4.14, a smaller amount of oxide was

formed on the methyl-terminated samples as compared to the H-terminated microwires. This was attributed to the added protection provided by the passivation layer.

Unlike the H-terminated n-Si microwire/polymer junctions which exhibit a non-rectifying character (Fig. 4.10b), the methyl-terminated n-Si microwire/polymer junctions demonstrate strong rectifying behavior (Fig. 4.15), leading to a larger effective polymer/microwire junction resistance. Methylation of Si has been reported to shift the Si band edges by creation of negative dipoles at the surface [5,180,181]. The behavior observed in this case could be attributed to this effect which in combination with the initial Fermi level mismatch between n-Si microwires and p-type polymer could result in a strong rectifying character. Dark *I-V* data analysis indicated that approximately 630 mV is required to achieve ~21 nA of current (anticipated maximum current per microwire at complete light absorption, see section 3.2.3) in these junctions.

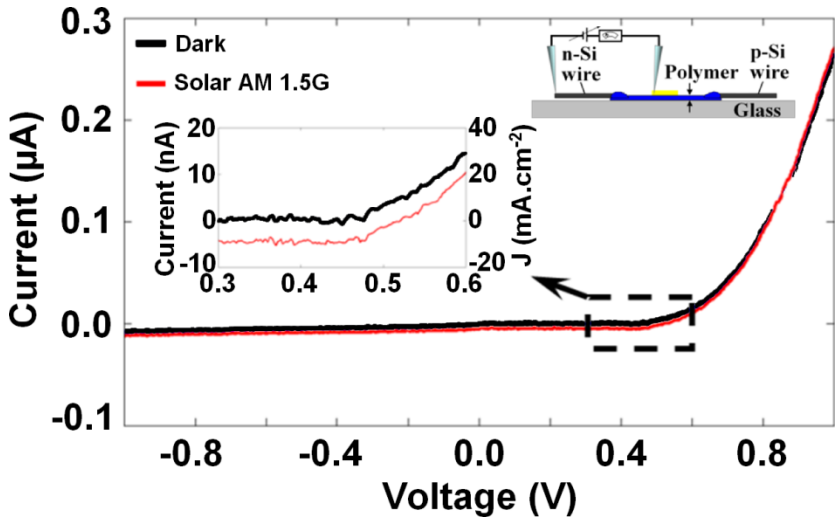

Figure 4.15: *I-V* data for a 100 μm long methyl-terminated n-Si microwire with a diameter of ~1.5 μm aligned at the PEDOT:PSS:Nafion/glass border, in dark and under solar AM 1.5G. A strong rectifying behavior, attributed to the shift in the Si band edges induced by methylation, was observed at methyl-terminated n-Si microwire/polymer junction. Approximately 630 mV is required to achieve ~21 nA of current in these junctions

The electrical character of the water splitting cell under test, formed using the combination of methyl-terminated n-Si and p-Si microwires, was dominated by the rectifying behavior at the n-type microwire/polymer junction (Fig. 4.16). Under illumination, ~5 nA of short circuit current was measured for this rectifying junction. In the 0.8-1 V bias region, the dark and illuminated DC resistance values were almost the same.

The anticipated maximum current per microwire at complete light absorption (21 nA) was measured at ~650 mV in these junctions under illumination. This demonstrates the detrimental effect of the large junction resistance at small bias levels. The results of comparative measurements on both H-terminated and methyl-terminated samples at day 1 are summarized in Table 4.4.

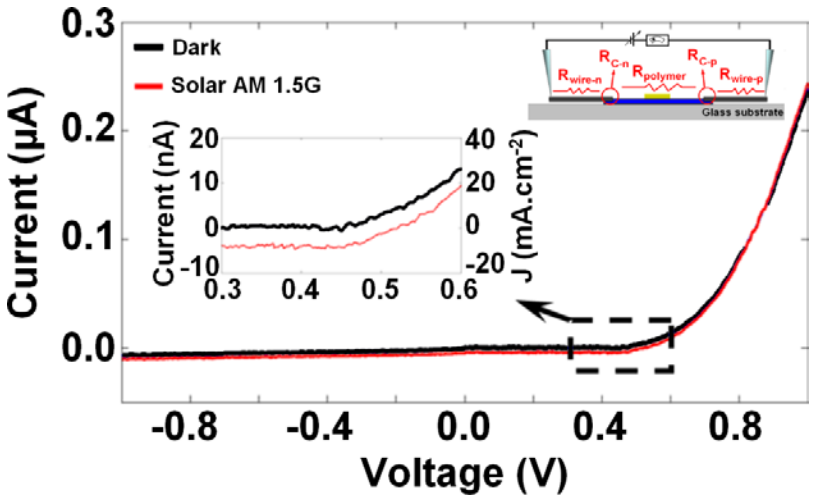

Figure 4.16: Measured *I-V* for complete photoelectrolysis cell with ~100 μm long methyl-terminated p-Si and n-Si microwires with diameters of ~1.5 μm. The electrical character of the cell is dominated by the rectifying behavior at the methyl-terminated n-type microwire/polymer junction (Fig. 4.15). Anticipated maximum current per microwire at complete light absorption (21 nA) was measured at ~650 mV in these junctions under illumination.

Table 4.4: Measured resistances in kΩ (±1%) for both H-terminated and methyl-terminated Si microwire/polymer systems at day 1. The microwire length and diameters were ~100 μm and ~1.5 μm respectively. In the case of rectifying junctions (Fig. 4.15), the measured DC resistance represents the series resistance in turn-on region.

	$R_{wire\text{-}p}$	$R_{wire\text{-}n}$	$R_{C\text{-}p}$	$R_{C\text{-}n}$	$R_{PEDOT:Naf.}$	Expected R_{total}
H-terminated (dark)	50	18	120	850	2	1040
Methyl-terminated (dark)	50	18	100	900	2	1070
Methyl-terminated (AM 1.5G)	30	10	90	850	2	982

Although passivation of the Si surfaces added to the stability of the electrical properties of the microwire/polymer junctions, the overall resistance measured for the system is still higher than the maximum acceptable resistance values (~480 kΩ for the individual water splitting cell). Also, further energy must be invested to achieve desirable current levels in the rectifying junction between the methyl-terminated n-Si microwires and polymer membrane which, considering the limited amount of photovoltage generated from sunlight, presents another challenge towards the optimized function of the system.

4.4 Application of Methyl-terminated Si Microwires with Modified Base

As shown in section 4.3.4, the electrical character of the junction between methyl-terminated p-Si microwires and PEDOT:PSS:Nafion demonstrates a desirable stability over time. This also was the case for methyl-terminated n-Si microwire/polymer junctions however, the rectifying behavior of these junctions presents a challenge toward

the optimal function of the system. Fully ohmic behavior is a desirable property for all of these junctions to form a working dual bandgap solar water splitting system as demonstrated in Fig. 2.1b.

Ohmic behavior in such a case could be achieved by combining two separate conducting polymers, one that makes ohmic contact to each electrode or, by modification of the n-type microwire base (in contact with membrane) either by addition of a metallic interfacial layer or increased doping levels to narrow down the depletion region and facilitate quantum mechanical tunneling of charge carriers [69].

Combining two separate conducting polymers will likely be challenging as the first issue is to find another conducting polymer compound with desired characteristics (section 2.2.1). Furthermore, it is reasonable to anticipate that such a polymer compound, one that forms an ohmic junction to the methyl-terminated n-Si microwires, will likely form a rectifying contact with the first conducting polymer, PEDOT:PSS:Nafion. As a result, this approach might only shift the position of the rectifying junction further inside the layered polymer membrane. Introducing a metallic interface seems to be more realistic. However, it also requires a search for appropriate interfacial metallic element as well as potentially further fabrication issues associated with the deposition of such an element in a chemically and spatially complex structure.

Modification of the n-type microwire base by increased doping seems to be the most practical approach as it neither requires additional material to be matched into the system nor demands major changes into the design or fabrication procedures of the solar water splitting cell. In addition, the VLS growth procedure for Si microwire fabrication is well studied [90,120,122,133] and as a result, introducing an increased amount of doping into

a region of Si microwires seems to be a plausible approach to resolve the unwanted rectification issue at the methyl-terminated n-Si microwire/polymer junctions.

A local increase in the doping concentration at the base of the microwires may be possible by thermally-induced diffusion of dopants from degenerately doped growth substrate. This would cause the dopants to diffuse from the substrate into the base of the wires (Fig. 4.17).

It is well known [202] that during high temperature processing, impurity profiles are redistributed through a diffusion process. There are different forms of impurity atom diffusion that may occur: vacancy diffusion, when a substitutional atom exchanges lattice positions with a vacancy; interstitial diffusion, when an interstitial atom jumps to another interstitial position; or a combination of these mechanisms, known as interstitialcy diffusion (Fig. 4.18) [69,203]. Since dopant atoms such as P, occupy substitutional positions once activated, dopant diffusion is closely linked to and controlled by the presence of vacancy and interstitial point defects.

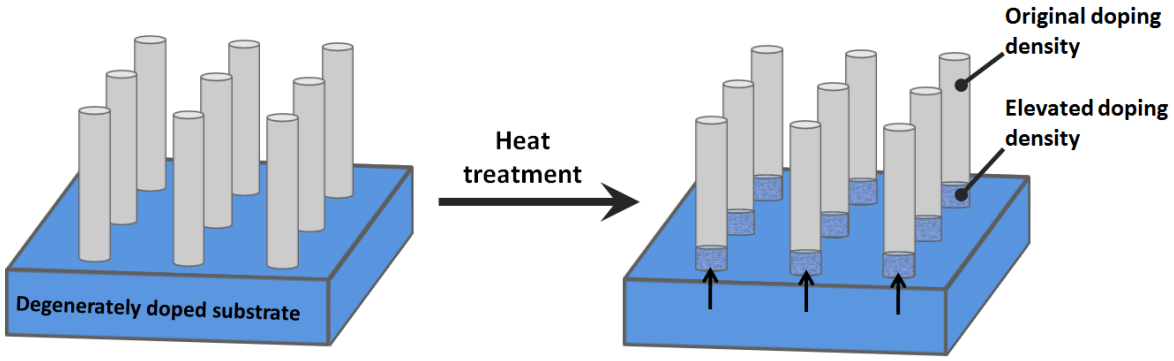

Figure 4.17: A local increase in the doping concentration at the base of the microwires may be possible by performing a thermal annealing. The dopants will diffuse from the degenerately doped growth substrate towards the base of the wires, leading to an elevated doping density in the base area (right-side image).

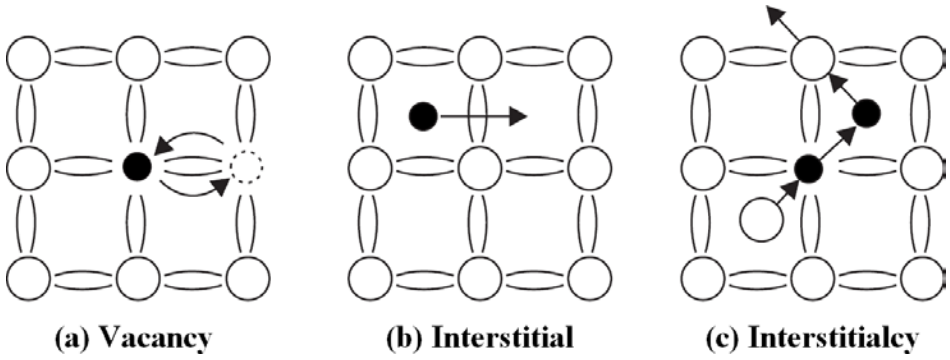

Figure 4.18: (a) Vacancy, (b) interstitial and (c) interstitialcy diffusion mechanisms. The white circles represent the host atoms and the black circles represent the diffusing species.

The diffusion constant, D (in cm^2s^{-1}) derived from Fick's first law, can be expressed as [204,205]:

$$D = \frac{s^2 f}{2} \qquad (4.4)$$

where s is the spacing, and f is the rate at which each atom jumps from one site to the adjacent site for any given temperature.

Whether an impurity atom occupies a substitutional or interstitial position in single crystal Si, the atom is trapped in a periodic potential defined by the lattice, with the probability of an atom jumping from one position to the next, increasing exponentially with increasing temperature. The diffusion process now can be characterized by an activation barrier with an energy, E_a, where E_a is the energy that must be overcome by an atom to jump from one site to the next site [205].

The jumping rate, f, is given by the product of two terms, with the first term being the rate with which the atom collides with the barrier f_0 (approximately 10^{13} to 10^{14} Hz for Si [205]), and the second term being the probability the atom will overcome the barrier during a collision given by the Boltzmann factor, $exp(-E_a/k_BT)$, where k_B is Boltzmann's

constant and T is the absolute temperature in Kelvin. The rate at which atoms jump to a new position is then given by [205]:

$$f = f_0 exp\left(-\frac{E_a}{k_B T}\right) \tag{4.5}$$

Each atom can also move to any adjacent site, so (4.5) should be multiplied by the number of adjacent sites (four for Si). For the interstitial case, equation (4.5) simply becomes:

$$f = 4f_0 exp\left(-\frac{E_a}{k_B T}\right) \tag{4.6}$$

For substitutional atoms (vacancy diffusion), an additional term must also be added to account for the probability of a vacancy or interstitial existing in the adjacent site (vacancies for vacancy diffusion and interstitials for interstitialcy diffusion). Assuming E_d as the activation energy required for producing such point defect formation sites, (4.5) will then be modified to:

$$f = 4f_0 exp\left(-\frac{E_a+E_d}{k_B T}\right) \tag{4.7}$$

Experimentally determined activation energies for interstitial atoms are approximately 0.5 eV and for substitutional atoms are approximately 3 eV [205].

Taking into account that the spacing, s, between atoms can be written as $a/\sqrt{3}$ for a diamond structure [68,69], where a is the lattice constant, the diffusion constant equation (4.4) can be rewritten by substituting equation (4.6) for the interstitial diffusivity:

$$D = \frac{4 f_0 a^2}{6} exp\left(-\frac{E_a}{k_B T}\right) \quad (4.8)$$

Substituting equation (4.7) into equation (4.4), the diffusion coefficient for substitutional atoms is given by:

$$D = \frac{4 f_0 a^2}{6} exp\left(-\frac{E_a + E_d}{k_B T}\right) \quad (4.9)$$

Although implied by equations (4.8) and (4.9), interstitial and substitutional diffusivities are not the same for all the atoms and a variety of different factors such as electric fields, impurity-lattice size mismatch induced strain, and multiple diffusion mechanisms complicate actual diffusion coefficient values [202]. However, the exponential increase as a result of the elevated temperatures is evident. This was used as the basis for one potential approach, in order to induce the doping concentration at the base of the n-type microwires.

The diffusivity of P in Si in high doping concentrations is explained as a vacancy dominated diffusion [203] and is shown in Fig. 4.19 versus different concentrations of P and different temperatures [206,207]. In order to modify the base of the microwires, following an 10% HF(aq.) etch to remove the Si native oxide, n-Si microwire arrays were treated at 1000 ˚C for approximately 10 hours. It is predicted that the n-type dopants (P) will diffuse up to 3 μm upwards from the degenerately doped growth substrate to the base of the microwires, providing n-Si microwires with higher doping concentrations at the base (Fig. 4.17).

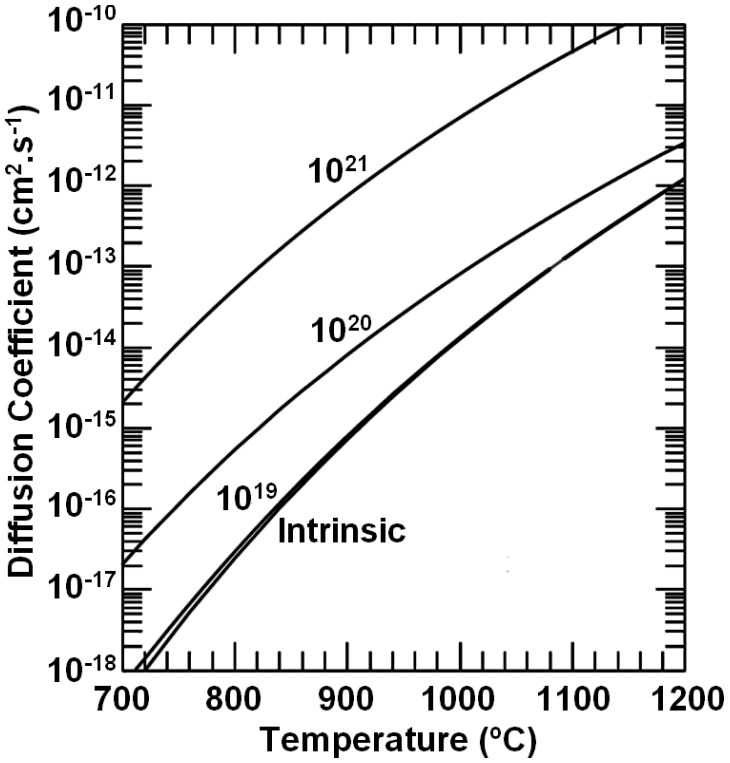

Figure 4.19: Diffusion coefficient of P in Si versus concentration of P (cm^{-3}) and temperature. The diffusivity of P in Si is dominated by vacancy diffusion. Adapted with permission from [207]. Copyright (1981) North-Holland Publishing Company.

The n-Si microwires with elevated doping concentration at their bases were then methylated and used in a new set of microwire/polymer junctions for characterization. It is worth mentioning that SEM imaging on these microwire arrays did not provide any visual evidence of the differential doping at the base area and single microwires/polymer junction measurements were used as the only verification tool.

I-V measurements on the junctions formed between methyl-terminated n-Si microwires (with increased doping level at the base via thermally-enhanced diffusion) and PEDOT:PSS:Nafion (Fig. 4.20a) showed increased conduction in the junction area, potentially due to quantum mechanical tunneling of charge carriers, leading to an improved reverse bias *I-V* with less DC resistance.

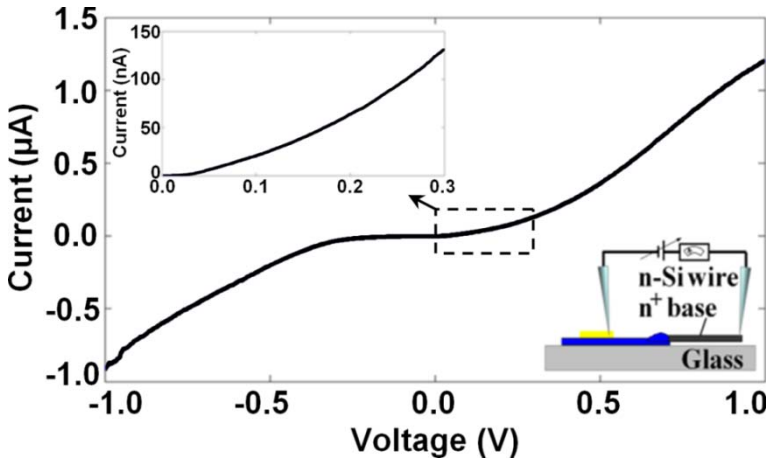

(a)

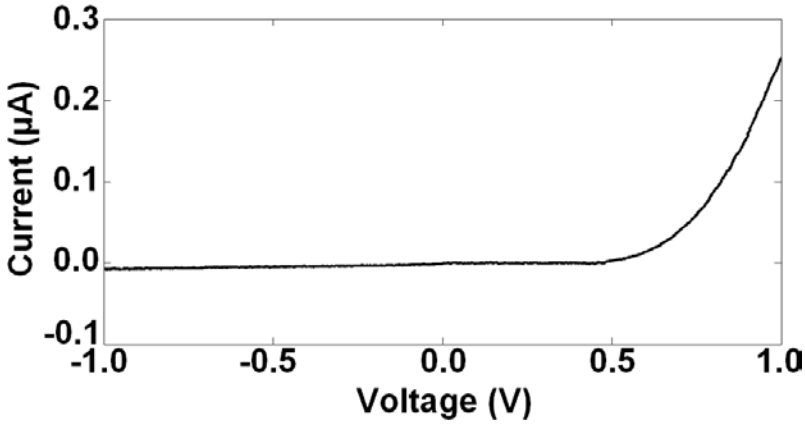

(b)

Figure 4.20: (a) *I-V* measurements on the junctions formed between a methyl-terminated n-Si microwire (with elevated doping at the base via thermally-enhanced diffusion) and PEDOT:PSS:Nafion conducting polymer composite. No rectification similar to the case of Fig. 4.15 was observed in this case and the target current of 21 nA was achieved in these junctions at approximately 100 mV. (b) Measured I-V profile of the same microwire, with the other end of the microwire (with normal doping profile) in contact with the polymer. Rectification behavior was observed, confirming the effect of increased doping density at the base of the microwire.

The effect of increased doping density at the base was further verified by measuring the *I-V* profile of the same microwire, having the tip with normal doping density in contact with the polymer. A rectifying behavior, similar to Fig. 4.15, was observed in this case (Fig. 4.20b).

The measured DC resistance in this set of measurements, varied from approximately 600 to 800 kΩ, between different batches of microwires with modified bases. This is well below the values measured for H-terminated and methyl-terminated n-Si microwire/polymer junctions (Table 4.4). Although, the target current of 21 nA (section 3.2.3) was achieved at approximately 100 mV bias voltage in these junctions due to the elevated DC resistance close to zero-bias, assuming the measured DC resistance at high bias voltage region as an absolute limit, a total loss of ~16 mV may be achievable in a system including these microwires. Further improvement in the junction properties is required to meet the acceptable DC resistance value (~480 kΩ).

4.5 Comparative Summary of the Candidate Systems

A comparative summary of the final measurements is presented in Table 4.5 with the critical parameters that require further improvement being highlighted. Doping the base of the microwires via thermally-induced diffusion process, in combination with the stable methylation process has the potential to address the oxidative stability issues as well as high junction resistances in the photoanode region, leading to a suitable candidate system for the use in the artificial photosynthesis system.

Table 4.5: Measured resistances in kΩ (±1%) for both H-terminated and methyl-terminated (with and without highly doped base) Si microwire/polymer systems. The microwire length and diameters were ~100 μm and ~1.5 μm respectively. The measured DC resistance in all cases represents the series resistance in the 0.8-1.0 V region. In the case of rectifying junctions, higher resistance is expected in the ±30 nA region. Highlighted cells indicate the critical areas where further improvement is required.

	$R_{wire\text{-}p}$	$R_{wire\text{-}n}$	$R_{C\text{-}p}$	$R_{C\text{-}n}$	$R_{PEDOT:Naf.}$	R_{total}
H-terminated (dark)	50	18	120	850	2	1040
H-terminated (dark-after 30 days)	50	18	>10,000	>17,000	2	>27,000
Methyl-terminated (dark)	50	18	100	900	2	1070
Methyl-terminated (AM 1.5G)	30	10	90	850	2	982
Methyl-terminated (dark-after 30 days)	50	18	103	915	2	1088
Methyl-terminated - highly doped base (dark)	50	18	100	580	2	750
Methyl-terminated - highly doped base (AM 1.5G)	30	10	90	550	2	720

Chapter 5

Conclusions and Future Work

5.1 Conclusions

This thesis described research on the electrical characterization of the materials and structures for the use in a proposed artificial photosynthesis system. The contribution made by this work spanned two topics. The first contribution concerned the development of a novel contact formation technique that employed W probes (with or without In/Ga) to make good electrical contacts to Si microwires. The advantage of this technique was that the contacts were formed only by applying mechanical pressure to the probe/microwire junction area. The local pressure in the immediate contact area of the Si microwire resulted in a local phase transition in Si and resulted in the observed, reproducible, ohmic contact. This alleviated the need for lithography and high-temperature process step to form a metal/Si ohmic contact, providing an easy, reliable, fast and extremely flexible contact formation approach. Using this technique, Si microwires with different doping types and concentrations were examined and the measured resistances and calculated doping concentrations were in agreement with the expected doping levels for the microwires [90,120,133,172].

The second contribution concerned the successful application of this technique to characterize the electrical junction between single Si microwires and two conducting polymer films. The electronic character of a functional unit of a proposed photosynthetic water splitting system and each junction within the cell was investigated both in the dark and under simulated AM 1.5G solar spectrum. The flexibility of the developed contact formation technique facilitated the characterization of different combinations of the water splitting cells.

Water splitting cell configurations employing low doped and highly doped Si microwires in combination with two different conducting polymer materials were initially investigated. The results of these initial measurements helped to define the required electrical properties for the individual microwires and for the candidate conducting polymers to be used in a working artificial photosynthesis device. The data indicated that the PEDOT:PSS:Nafion combination with highly doped Si microwire would provide a suitable combination, from an electrical resistance perspective, to be used in a solar fuels generation device.

Both the short term and long term stability of a single artificial photosynthesis cell, comprising the selected microwire/polymer combination was investigated. It was concluded that H-terminated microwire/polymer contacts exhibit poor long-term stability due to native oxide formation. In an attempt to resolve the stability issue, the surface of Si microwires was passivated using kinetically stable Si–C bonds, following a dual-step chlorination–alkylation technique. Long term electrical stability was demonstrated with these samples as compared to their H-terminated counterparts. Furthermore, it was verified that CH_3-terminated n-Si microwire/PEDOT:PSS:Nafion junctions demonstrated

rectifying behavior potentially due to the shift in the energy of the Si band edges at the interface, induced by creation of negative surface dipoles [5,180,181]. This suggested that in order to provide ohmic contacts on both Si/polymer contacts in the finalized device, a modified approach will likely be needed.

Finally, in order to resolve the rectification issue at the CH_3-terminated n-Si microwire/polymer junctions, the base of n-type microwires, in contact with the membrane, was modified by a local increased in the doping concentration. The measurement results on the system comprising these microwires in contact with PEDOT:PSS:Nafion suggest a promising improvement in the reverse bias I-V character at these junctions. In combination with the stable methylation process, this approach has the potential to address the oxidative stability issues as well as high junction resistances in the photoanode region, leading to a potential candidate for the use in the ultimate artificial photosynthesis device.

Measurements on the systems including microwires with doped bases through thermally-enhanced diffusion suggested that the target current of 21 nA (section 3.2.3) may be achieved at less than 100 mV bias voltage due to the elevated DC resistance close to zero-bias, indicating the need to further improvement in the junction properties to meet the acceptable DC resistance value (~480 kΩ). However, assuming the measured DC resistance at high bias voltage region as an absolute limit, a total loss of ~16 mV may be achievable in a system including these microwires.

More generally, the work presented in this report provides not only a further insight in the material-related issues that need to be addressed in order to achieve a complete

artificial photosynthetic device, but also a potential approach for investigating many different microstructures comprising Si microwires.

5.2 Future Work

Several pathways for future work are possible. As the search continues for appropriate photoelectrode materials, a potentially interesting application of this technique is to examine its utility to characterize microwires with different structures such as radial PN junctions [71,131,135,149] or semiconductor materials other than Si [61,208]. Other water splitting structures including layered polymer membranes are also under investigation [151]. Modifications could be made to apply this technique for characterization of these new structures.

The technique described in this thesis provides a tool for investigating random local sites on the polymer membrane. It will be interesting, from a fundamental viewpoint, to develop an accurate characterization tool for investigating electronic homogeneity of these membrane materials in larger scales. For example, considering the present microwire array arrangement (Fig. 3.1), a 100 μm × 100 μm area on the polymer membrane will include more than 200 microwires embedded into the polymer. It is clear that there is a need for a characterization technique with sufficient spatial resolution to investigate the electronic properties of a candidate polymer membrane at these length scales.

One potential approach to this may be found in the development of a dynamic homodyne electrostatic force microscopy (EFM) technique. Separate studies by the present author including the recently reported stable imaging of surface acoustic wave

(SAW) interference patterns at GHz frequencies [209] suggest that the dynamic homodyne EFM technique can be applied to characterize large scale electronic homogeneity of polymer membranes for the use in the artificial photosynthesis system. Independent of the probe cantilever mechanical resonant frequency, this non-contact EFM technique has no theoretical limit in detecting polarization effects at GHz frequencies. Considering the limited number of reports investigating high frequency dielectric properties of polymeric systems such as Nafion [210], this sets the ground for fundamental studies on high frequency dynamic properties of the candidate materials for the use in a wide range of applications including the solar water splitting systems.

Appendix A

Calculation of the Minimum Required Membrane Conductivity

Estimating the current density, J, passing through a membrane, assuming a solar flux of 4×10^{-7} mmol s^{-1} cm^{-2} (taken for a range of ~400 - 700 nm of solar spectrum [87]) and assuming that one charge carrier traverses the membrane for every two incident photons absorbed by the semiconductor photoelectrodes:

Current density (J) = $(4\times10^{-7}$ mmol s^{-1} $cm^{-2}) \times (6.02\times10^{23}$ e $mol^{-1}) \times [(1.602\times10^{-19}$ $e^{-})/2]$

= 0.019 A $cm^{-2} \approx$ 20 $mAcm^{-2}$

Knowing that membrane thickness (L in the resistance formula) is actually the direction of current flow so given a current density of 20 $mAcm^{-2}$ and a maximum allowable voltage loss, ΔV, of 10 mV:

$$R = \rho\frac{L}{A}$$

$$\rho = R \times \frac{A}{L} = \frac{\Delta V}{I} \times \frac{A}{L} = \frac{\Delta V}{J \times A} \times \frac{A}{L} = \frac{\Delta V}{J \times L}$$

$$\sigma = \rho^{-1} = \left[\frac{\Delta V}{J \times L}\right]^{-1} = (2\ \Omega^{-1}\ \mathrm{cm}^{-2}) \times \mathrm{L}$$

Given a membrane thickness of L = 1 μm, then σ = 0.2 $m\Omega^{-1}$ cm^{-1} or 0.2 $mScm^{-1}$. Hence, every 1 μm increase in membrane thickness requires a corresponding increase in membrane conductivity of 0.2 $mScm^{-1}$. For a membrane thickness of 40 μm, the minimum conductivity required to support an IR loss ≤ 1 % would be 8 $mScm^{-1}$.

Appendix B

Metallic Catalyst Removal Procedure

The Si microwires were grown on <111> Si substrates using a chemical-vapor-deposition, vapor–liquid–solid (VLS) growth process by the collaborator lab at Caltech [90,120,133,172]. The VLS catalyst employed was Cu. For most samples the metallic catalyst was removed from the top and sidewalls of the microwires by chemical etching processes discussed below. After growth, a slow cool down procedure was performed so that the metallic catalyst diffused out readily from the Si. The etch procedure for removing the catalyst and for etching off the SiO_2 that resulted from the catalyst removal was as follow:

10 s, 10% HF(aq.)

RCA2 Etch: 20 min, DI water:HCl:H_2O_2 (7:1:1, v/v/v)

10 s, 10% HF(aq.)

RCA2 Etch: 20 min, DI water:HCl:H_2O_2 (7:1:1, v/v/v)

10 s, 10% HF(aq.)

1 min, 30 wt.% KOH(aq.)

10 s, 10% HF(aq.)

After each step, the microwires were rinsed thoroughly with DI water and dried under a stream of N_2. RCA2 etch was used to remove the metallic catalyst. The KOH was used

to remove leftover Cu impurities at the Si surface. Finally, diluted HF was used to remove the native oxide and any oxide formed during the catalyst removal process.

Appendix C

Conducting Polymer Film Preparation

Three different conducting polymer solutions were prepared for the measurements. Each procedure includes the polymer solution preparation and spin coating the solution on the target substrates. The solution was typically coated at 2000 rpm for 20 seconds. The film preparation for each polymers followed by a rinsing process to remove the residual PSS or PMA. Microwires were aligned before the rinsing process in all of the cases.

C.1 PEDOT:PMA

PEDOT:PMA solution was prepared using acetonitrile (CH_3CN) as the solvent. The procedure is as follows:

PMA solution: CH_3CN (1 mL) + PMA (1.9 gr)

EDOT solution: CH_3CN (1 mL) + EDOT (42.6 μL)

These solutions were mixed and spin coated on the target substrates to form the final PEDOT:PMA membranes. For the rinsing process, the films were placed in dichloromethane (CH_2Cl_2) solution with a small amount of acetonitrile (3~4 mL) for ~ 30 min.

C.2 PEDOT:PSS:Nafion

PEDOT:PSS was purchased from *Sigma-Aldrich* (and later on from *Clevios*) as an aqueous solution. Nafion was also purchased form *Sigma-Aldrich* as 10 wt.% dispersion in water. In order to prepare 12 wt.% PEDOT:PSS:Nafion, 1250 mL of Nafion solution was mixed with 750 mL PEDOT:PSS for 2-5 minutes on a vortex mixer. This solution was then spin coated on the glass substrate. For the rinsing process (optional), the films were placed in acetonitrile for ~ 30 min. The films were then allowed to dry for 6–8 hours under the lab conditions and then annealed at 100–150ºC for one hour.

Appendix D

Solar Simulator: Beam Profiling and Output Power Calibration

In order to have an understanding about the exact amount of optical power that reaches the microwire/polymer samples, the output power of the solar simulator was measured and calibrated using a *Thorlabs BP109-UV* slit-scanning optical beam profiler for 200-1100 nm wavelength range (Fig. D.1a) and a *Newport 1918-R* high-performance hand-held optical power meter (Fig. D.1b).

Furthermore, to study the power variation across the diameter of the projected beam, the uniformity of the output power across the beam diameter was also investigated using the optical beam profiler. As the magnitude of solar power is commonly noted in the form of power density (power/area), it was necessary to convert the measured power values into the power density. Knowing the diameter of the sensor aperture, calculation of the power density in Wcm^{-2} will be straightforward for any given amount of optical power. Fig. D.2 demonstrates the general measurement setup. Fig. D.3 shows measured solar power density versus distance between the solar simulator light aperture and power detector surface, for 225 W of input power applied to the solar simulator lamp.

(a)

(b)

Figure D.1: (a) A *Thorlabs BP109-UV* optical beam profiler was used to investigate the optical output power and the uniformity of the power density across the optical beam diameter. With an aperture diameter of 9 mm, *BP109-UV* is able to scan optical beams with diameters ranging from 20 µm to 9 mm. (b) The absolute optical power was measured using a *Newport 1918-R* high-performance hand-held optical power meter. The measured power was then used to calibrate the optical beam profiler readings.

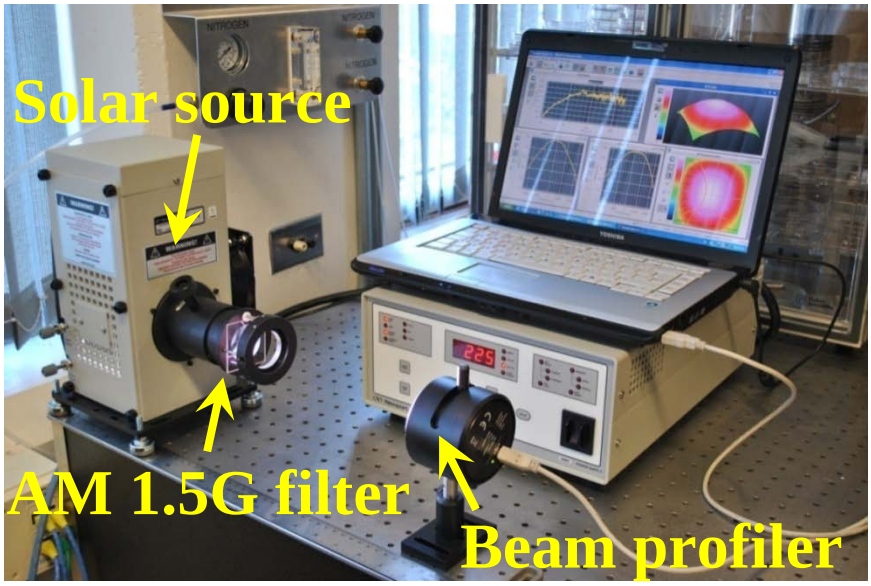

Figure D.2: Calibration of solar simulator. The distance between the light aperture and detector was ~20 cm, close to the distance between the light source and samples during the microwire/polymer characterization. Calibration was performed with and without mirror to investigate the power loss, as a result of reflection from mirror.

Fig. D.4 shows measured solar power density versus different lamp input power. In this case, the distance between the light aperture and detector was 20 cm, close to the distance between the light source and samples during the microwire/polymer characterization. The same mirror used to reflect the beam onto the samples during the measurements, were used during the calibration to account for any power loss and ensure enough power density at the samples. In order to investigate the uniformity of optical power density across the beam diameter, a standard aperture with a diameter of 1 mm was used immediately before the beam profiler and optical power was measured across the sensor diameter of the beam profile (9 mm). Variation of optical power density across the diameter of the sensor was verified to be less than 5%. This guarantees the uniformity of optical power during the characterization of the microwire/polymer test structures.

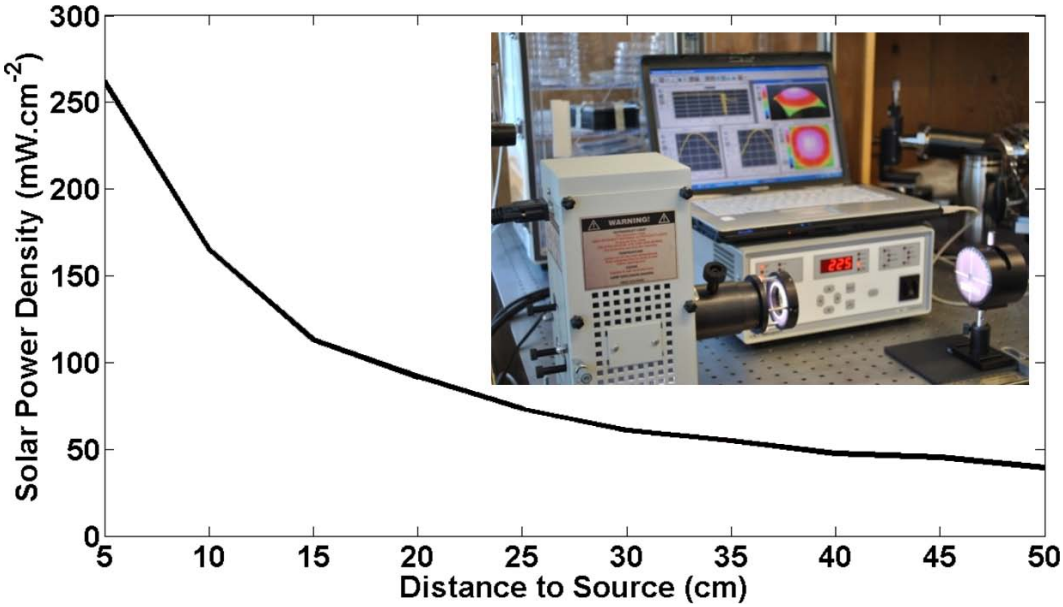

Figure D.3: Measured solar power density in Wcm^{-2} (± 5%) versus distance between the solar simulator light aperture and power detector surface (Fig. inset), for 225 W of input power applied to the solar simulator lamp.

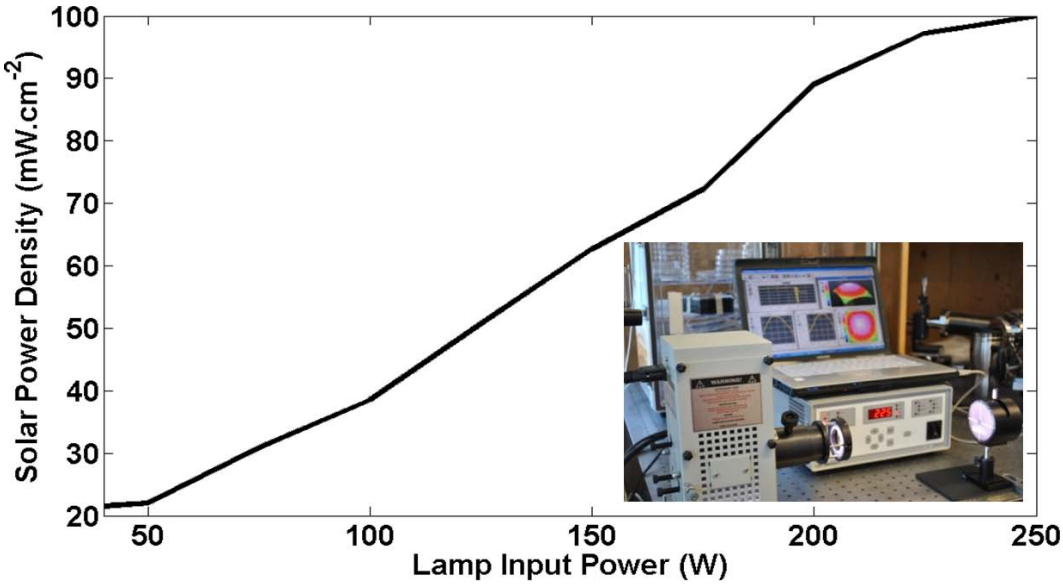

Figure D.4: Measured solar power density in Wcm^{-2} (± 5%) versus different lamp input power. The distance between the light aperture and detector (Fig. inset) was 20 cm.

Appendix E

Si Microwires XPS Analysis Surveys

As discussed in section 4.3.4, XPS analysis was carried out on H-terminated and CH_3-terminated n-Si microwire samples.

XPS spectra were collected on a *Kratos Axis Ultra DLD* spectrometer under ultrahigh vacuum conditions (~1.3×10^{-7} Pa). Monochromatic Al *Kα* radiation at 15 mA emission current and 15 kV anode potential was used for excitation. Elemental scans were acquired with a pass energy of 20 eV. A charge neutralizer was employed to minimize charging and all spectra were calibrated to the C 1s line at 285.0 eV. XPS surveys for each set of measurements are presented in this section.

E.1 Methyl-Terminated n-Si Microwires: Day 1

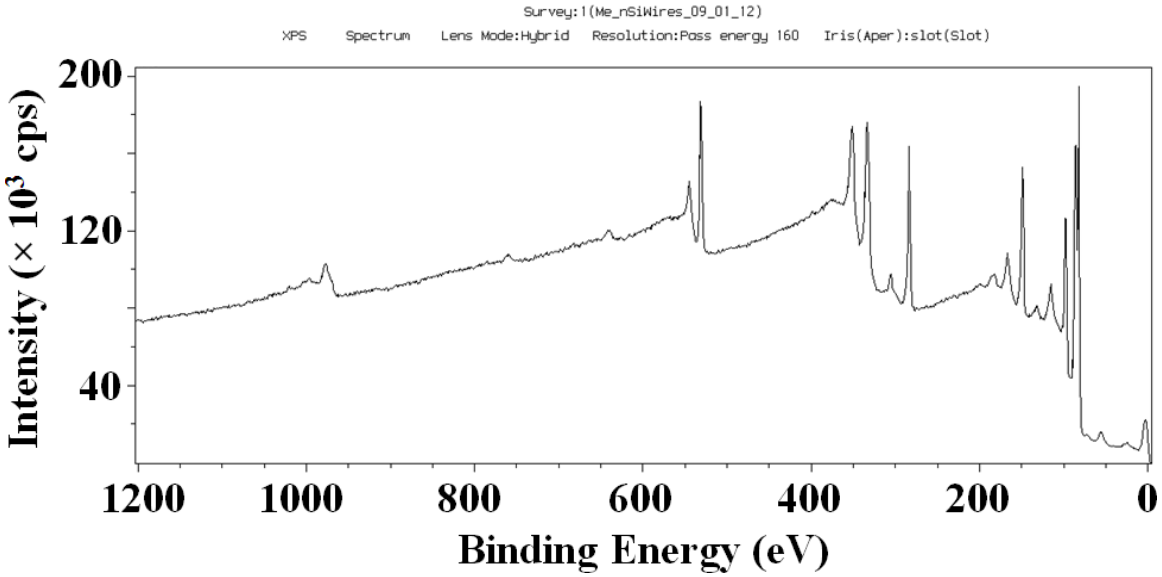

Figure E.1: The XPS survey of a batch of recently methylated n-Si microwires at day 1.

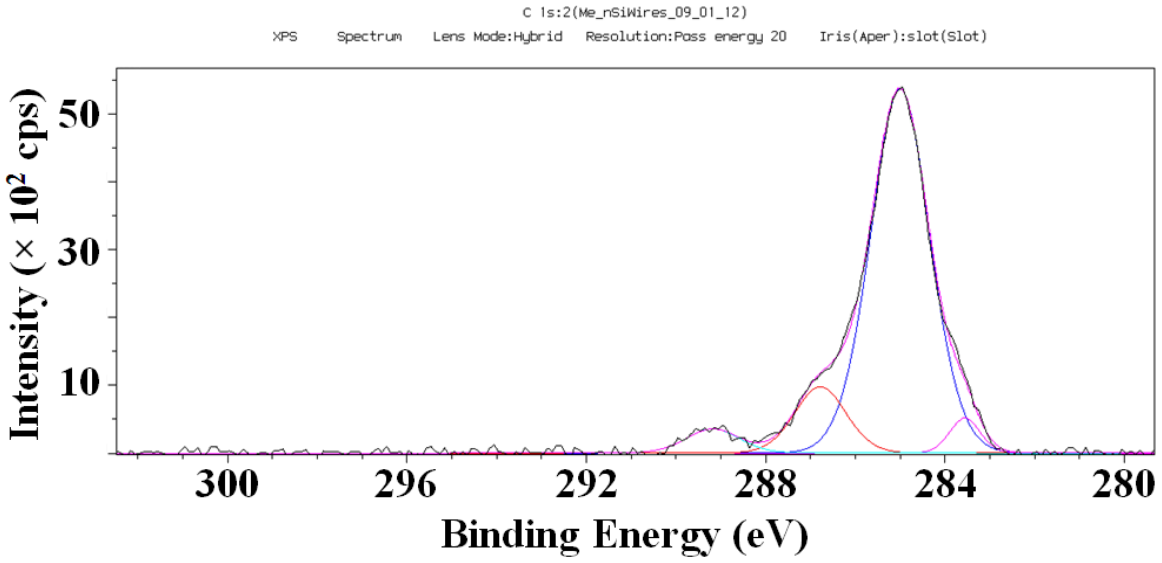

Figure E.2: C1s region of the XPS survey for CH_3-terminated n-Si microwires at day 1.

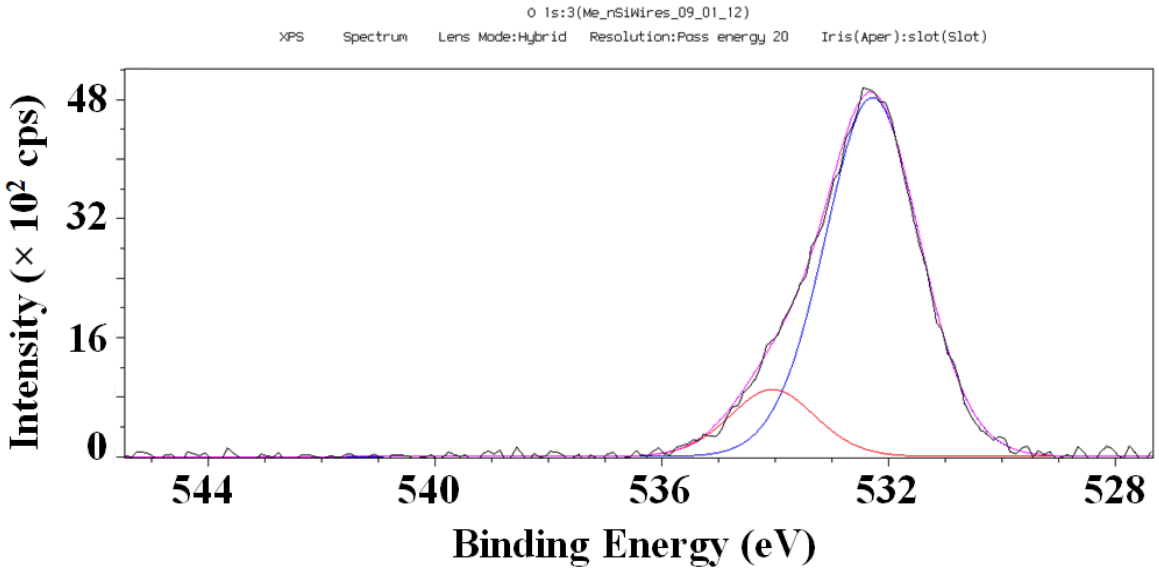

Figure E.3: O1s region of the XPS survey for CH_3-terminated microwires at day 1.

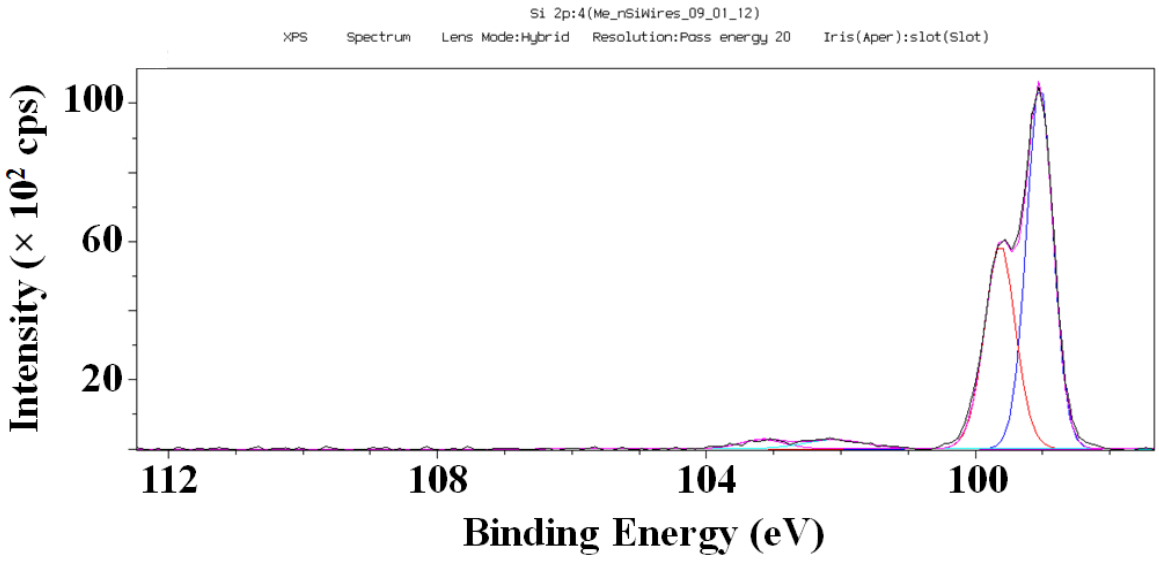

Figure E.4: Si2p region of the XPS survey for CH_3-terminated microwires at day 1.

Table E.1: Details of the XPS analysis results on the freshly methylated n-Si microwires at day 1.

Peak	BE (eV)	FWHM (eV)	Raw Area (cps eV)	RSF	Atomic Mass	Atomic Conc. (%)	Mass Conc. (%)
C 1s	284.952	1.588	11623.2	0.278	12.011	47.1	30.2
O 1s	532.452	2.111	11805.8	0.78	15.999	15	13
Si 2p	99.052	0.947	9606.6	0.328	28.086	37.9	56.9
C 1s a	285	1.42	8456.7	0.278	12.011	34.1	21.9
C 1s b	286.643	1.628	1851.7	0.278	12.011	7.5	4.8
C 1s c	283.605	0.915	762.2	0.278	12.011	3.1	2
C 1s d	289.223	1.39	585.8	0.278	12.011	2.4	1.5
O 1s a	532.306	1.914	10202	0.78	15.999	13.1	11.2
O 1s b	534.065	1.564	1622.8	0.78	15.999	2.1	1.8
Si 2p 3/2	99.033	0.519	5948	0.328	28.086	22.7	34
Si 2p 1/2	99.643	0.565	3478.5	0.328	28.086	13.2	19.9
Si 2p 3/2 ox	102.135	0.948	325.1	0.328	28.086	1.2	1.9
Si 2p 1/2 ox	103.197	0.845	198.9	0.328	28.086	0.8	1.1

E.2 H-Terminated n-Si Microwires: Day 1

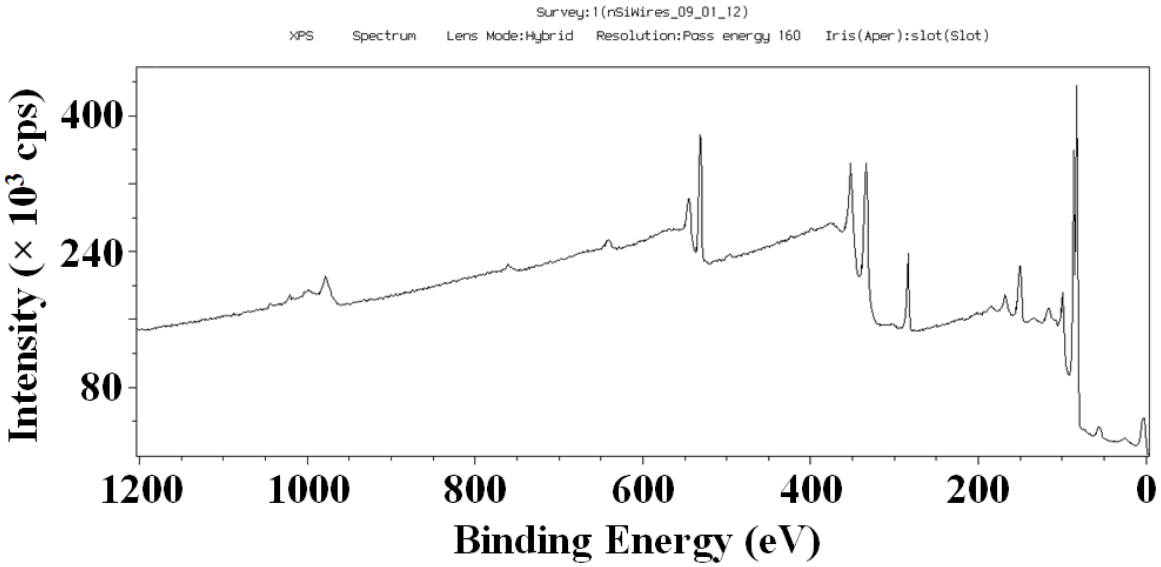

Figure E.5: The XPS survey of freshly etched H-terminated n-Si microwires at day 1.

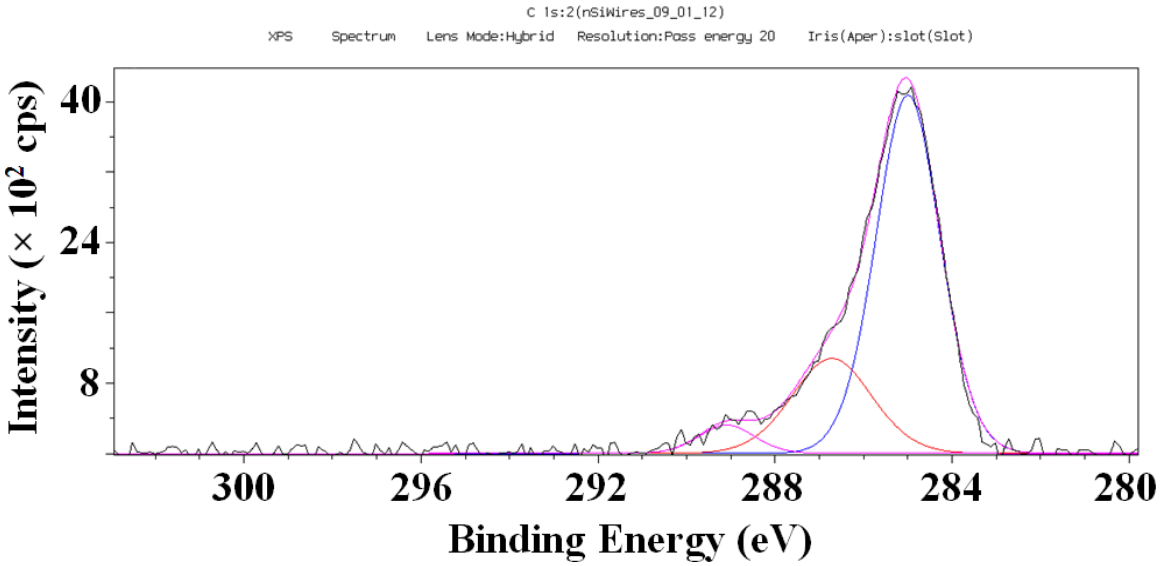

Figure E.6: C1s region of the XPS survey for H-terminated n-Si microwires at day 1.

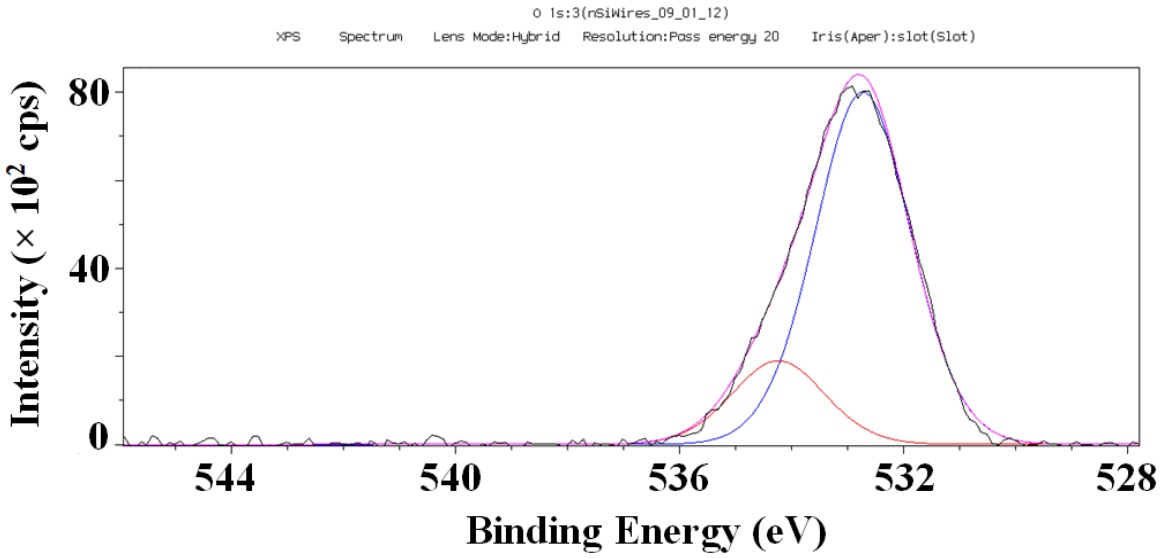

Figure E.7: O1s region of the XPS survey for H-terminated n-Si microwires at day 1.

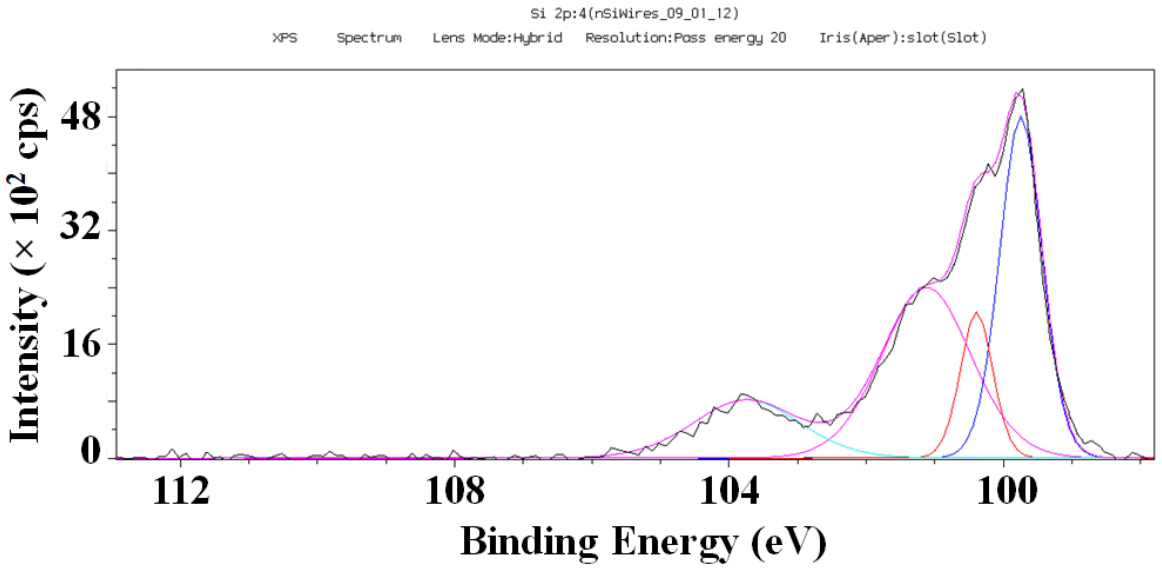

Figure E.8: Si2p region of the XPS survey for H-terminated n-Si microwires at day 1.

Table E.2: Details of the XPS analysis results on the freshly etched H-terminated n-Si microwires.

Peak	BE (eV)	FWHM (eV)	Raw Area (cps eV)	RSF	Atomic Mass	Atomic Conc. (%)	Mass Conc. (%)
C 1s	284.945	1.968	9901.4	0.278	12.011	37.5	23.7
O 1s	532.945	2.413	21435.4	0.78	15.999	25.5	21.6
Si 2p	99.745	1.36	10377.2	0.328	28.086	36.9	54.8
C 1s a	285	1.586	7068.1	0.278	12.011	26.6	16.8
C 1s b	286.422	1.643	2099.5	0.278	12.011	7.9	5
C 1s c	288.345	2.212	810.2	0.278	12.011	3	1.9
O 1s a	532.713	1.913	15817.7	0.78	15.999	18.9	16
O 1s b	534.076	1.984	5545.8	0.78	15.999	6.6	5.6
Si 2p 3/2	99.749	0.655	3360.9	0.328	28.086	11.9	17.7
Si 2p 1/2	100.371	0.709	2010.2	0.328	28.086	7.1	10.6
Si 2p hemi-ox	101.244	1.335	3280.5	0.328	28.086	11.6	17.2
Si 2p ox	103.706	1.909	1774.4	0.328	28.086	6.3	9.3

E.3 Methyl-Terminated n-Si Microwires: Day 30

Samples of CH_3-terminated and H-terminated n-Si microwires were kept under the lab conditions for one month prior to the analysis being repeated.

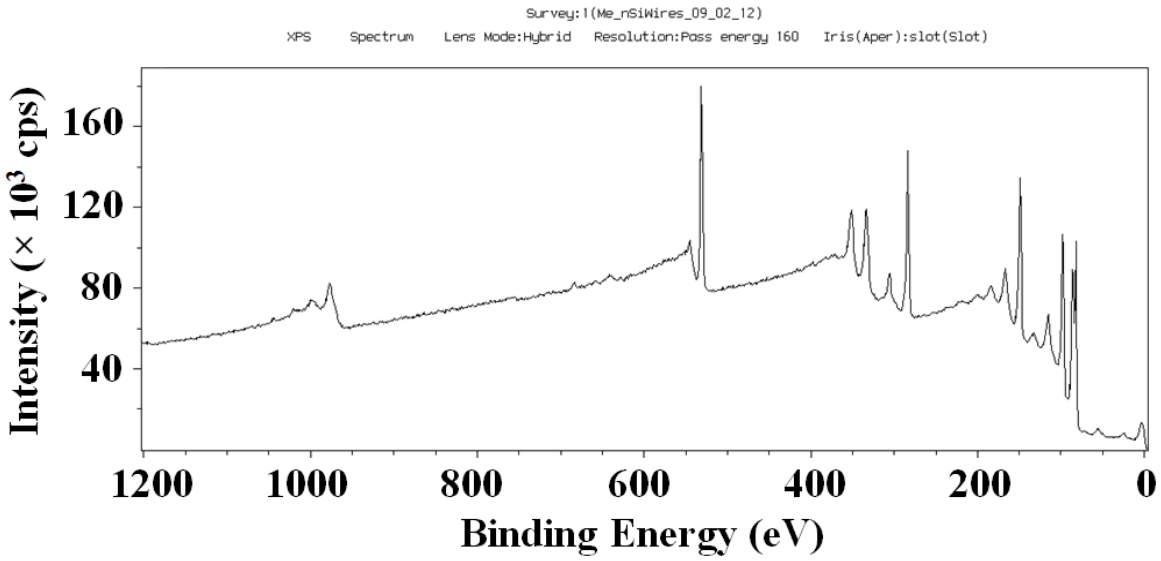

Figure E.9: The XPS survey for a batch of methylated n-Si microwires at day 30.

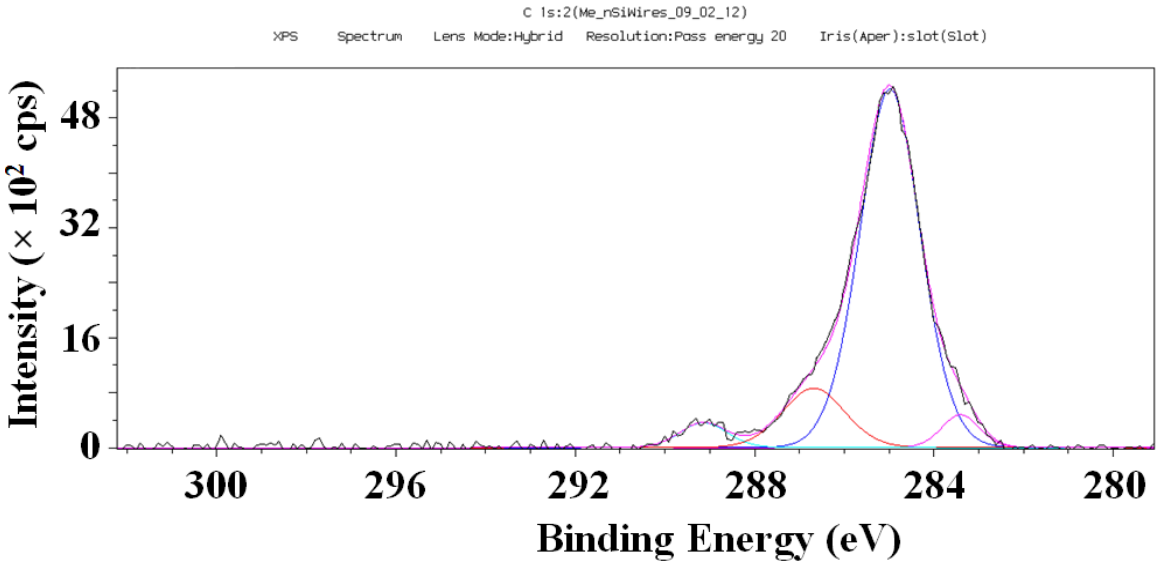

Figure E.10: C1s region of the XPS survey for CH_3-terminated microwires at day 30.

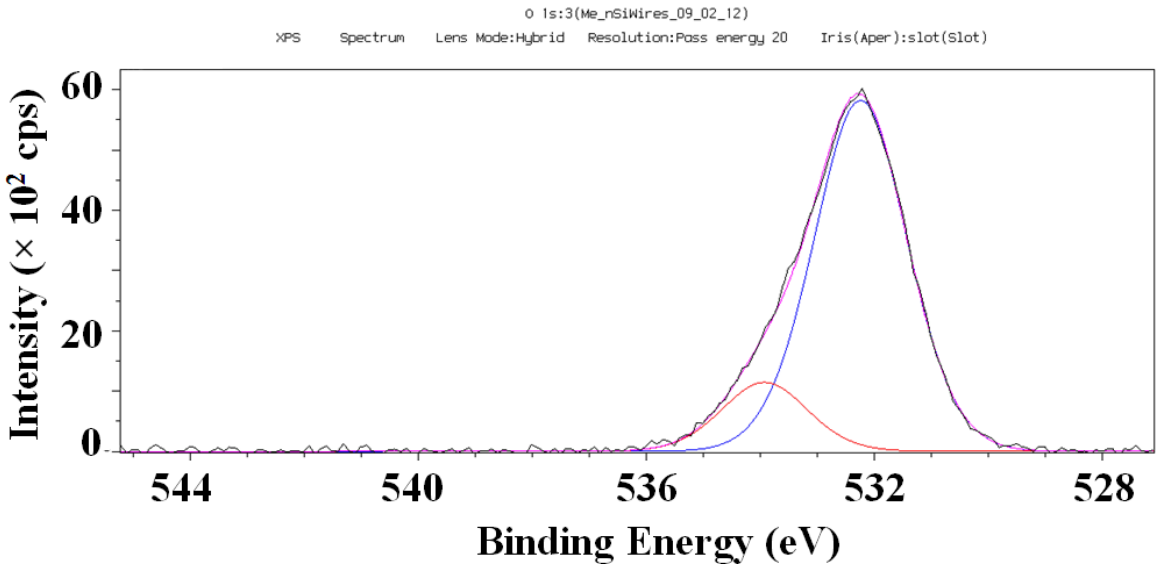

Figure E.11: O1s region of the XPS survey for CH_3-terminated microwires at day 30.

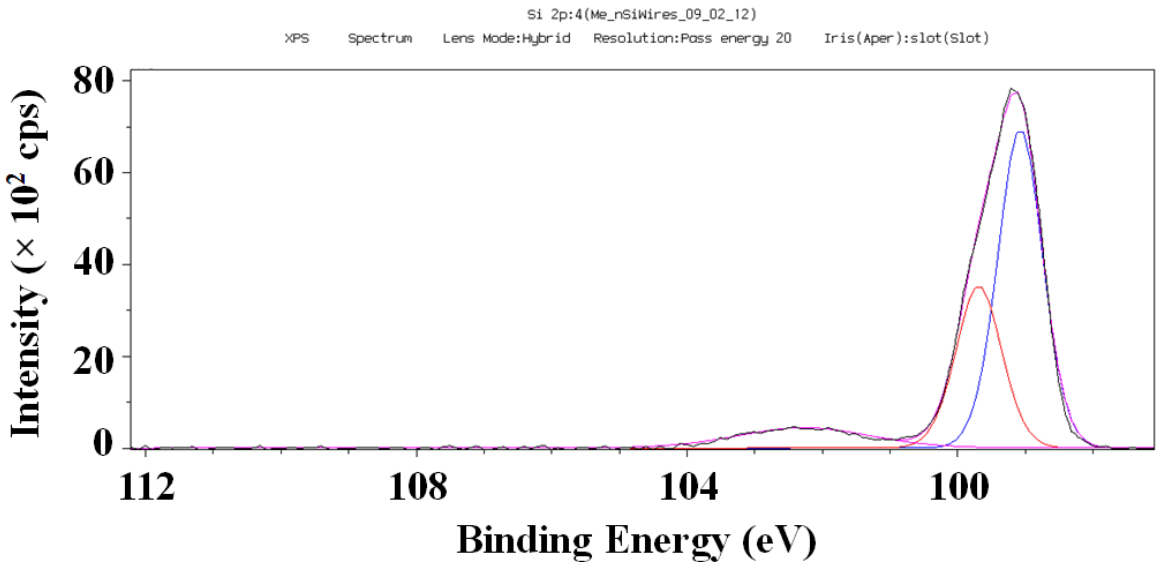

Figure E.12: Si2p region of the XPS survey for CH_3-terminated microwires at day 30.

Table E.3: Details of the XPS analysis results on the methylated n-Si microwires at day 30.

Peak	BE (eV)	FWHM (eV)	Raw Area (cps eV)	RSF	Atomic Mass	Atomic Conc. (%)	Mass Conc. (%)
C 1s	284.924	1.731	11836.8	0.278	12.011	46.6	30.3
O 1s	532.224	2.184	13898.7	0.78	15.999	17.2	14.9
Si 2p	99.224	1.118	9469.8	0.328	28.086	36.3	55
C 1s a	285	1.595	9160.6	0.278	12.011	35.6	23.1
C 1s b	286.724	1.627	1694.7	0.278	12.011	6.6	4.3
C 1s c	283.368	1.004	538.1	0.278	12.011	2.1	1.4
C 1s d	289.165	1.308	579.3	0.278	12.011	2.3	1.5
O 1s a	532.262	1.807	11499	0.78	15.999	14.2	12.3
O 1s b	533.891	1.677	2428.1	0.78	15.999	3	2.6
Si 2p 3/2	99.086	0.73	5801.1	0.328	28.086	21.3	32.3
Si 2p 1/2	99.723	0.705	2973.8	0.328	28.086	10.9	16.5
Si 2p ox	102.178	2.441	1107.8	0.328	28.086	4.1	6.2

E.4 H-Terminated n-Si Microwires: Day 30

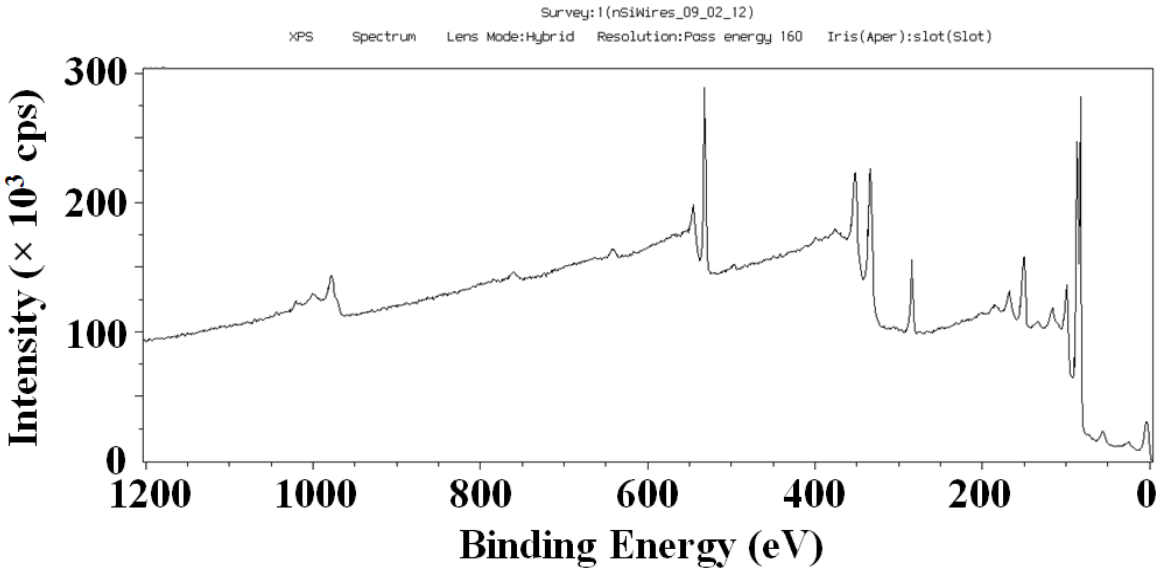

Figure E.13: The XPS survey of H-terminated n-Si microwires at day 30.

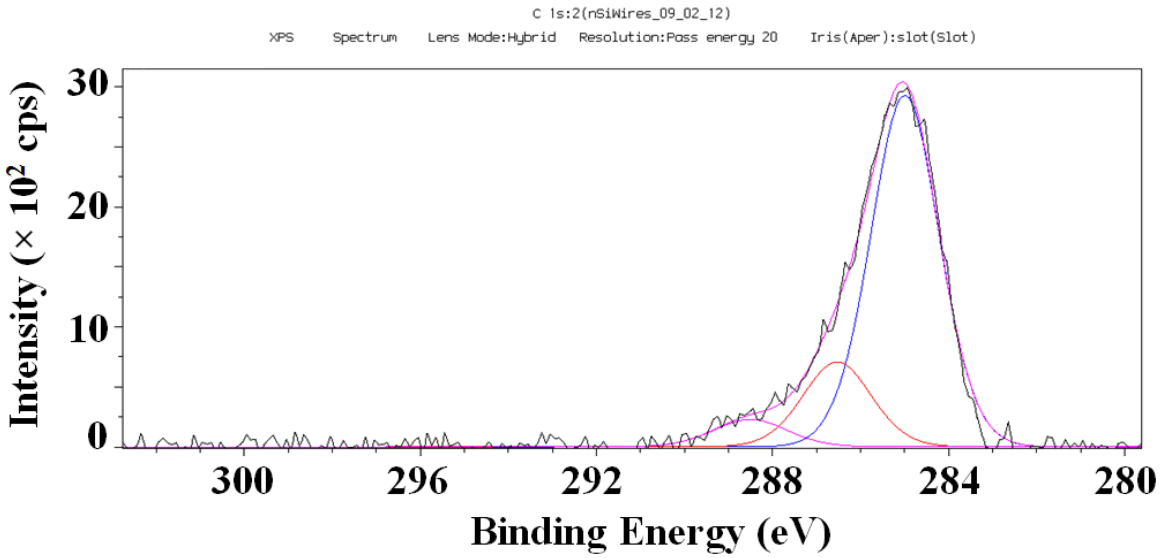

Figure E.14: C1s region of the XPS survey for H-terminated n-Si microwires at day 30.

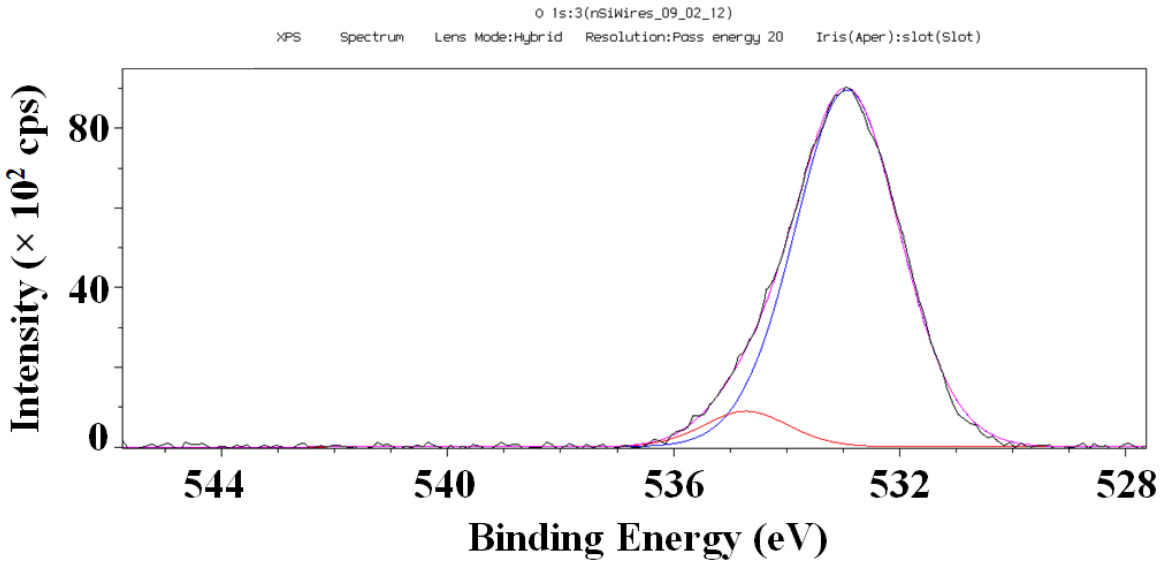

Figure E.15: O1s region of the XPS survey for H-terminated n-Si microwires at day 30.

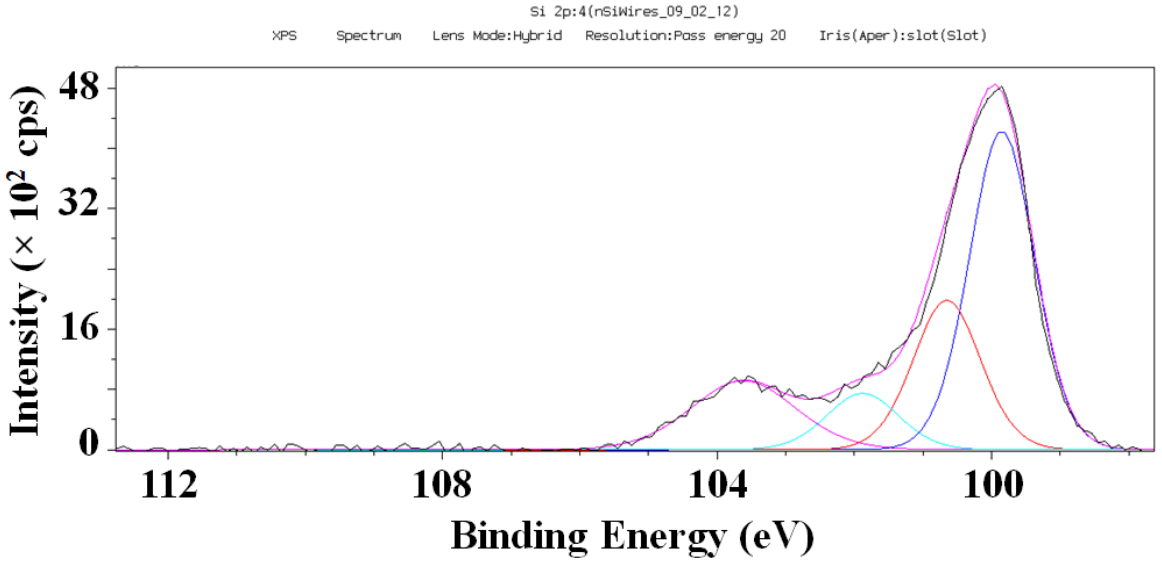

Figure E.16: Si2p region of the XPS survey for H-terminated n-Si microwires at day 30.

Table E.4: Details of the XPS analysis results on the H-terminated n-Si microwires at day 30.

Peak	BE (eV)	FWHM (eV)	Raw Area (cps eV)	RSF	Atomic Mass	Atomic Conc. (%)	Mass Conc. (%)
C 1s	285.009	2.362	8337.7	0.278	12.011	33	20.7
O 1s	533.009	2.355	23188.4	0.78	15.999	29.7	24.8
Si 2p	99.909	1.418	10190.4	0.328	28.086	37.3	54.7
C 1s a	285	1.804	5585	0.278	12.011	22	13.8
C 1s b	286.424	2.231	1909.1	0.278	12.011	7.5	4.7
C 1s c	288.673	2.996	880.2	0.278	12.011	3.5	2.2
O 1s a	532.825	2.039	17470.1	0.78	15.999	22	18.3
O 1s b	534.054	2.335	6159.8	0.78	15.999	7.7	6.5
Si 2p 3/2	99.834	0.961	4038.8	0.328	28.086	15.1	22
Si 2p 1/2	100.463	0.919	1864	0.328	28.086	6.9	10.2
Si 2p hemi-ox	101.328	1.676	2347.9	0.328	28.086	8.7	12.8
Si 2p ox	103.672	1.778	1777	0.328	28.086	6.6	9.7

References

[1] M. I. Hoffert, K. Caldeira, A. K. Jain, E. F. Haites, L. D. D. Harvey, S. D. Potter, M. E. Schlesinger, S. H. Schneider, R. G. Watts, T. M. L. Wigley, and D. J. Wuebbles, "Energy implications of future stabilization of atmospheric CO_2 content," *Nature*, vol. 395, no. 6705, pp. 881-884, 1998.

[2] Energy Information Administration, "Annual energy outlook 2005 with projections to 2025," First ed. Washington, DC: US Department of Energy, 2005.

[3] N. S. Lewis and D. G. Nocera, "Powering the planet: chemical challenges in solar energy utilization," *Proceedings of the National Academy of Sciences*, vol. 103, no. 43, pp. 15729-15735, 2006.

[4] D. Y. Goswami, F. Kreith, and J. F. Kreider, *Principles of Solar Engineering*, Second ed. Philadelphia, PA: CRC Press, 2000.

[5] M. G. Walter, E. L. Warren, J. R. McKone, S. W. Boettcher, Q. X. Mi, E. A. Santori, and N. S. Lewis, "Solar water splitting cells," *Chemical Reviews*, vol. 110, no. 11, pp. 6446-6473, 2010.

[6] R. E. Bird, R. L. Hulstrom, and L. J. Lewis, "Terrestrial solar spectral data sets," *Solar Energy*, vol. 30, no. 6, pp. 563-573, 1983.

[7] E. G. Laue, "The measurement of solar spectral irradiance at different terrestrial elevations," *Solar Energy*, vol. 13, no. 1, pp. 43-57, 1970.

[8] A. McEvoy, T. Markvart, and L. Castaner, *Practical Handbook of Photovoltaics: Fundamentals and Applications*, Second ed. Saint Louis, MO: Academic Press, 2011.

[9] H. K. V. Lotsch, A. Goetzberger, and V. U. Hoffmann, *Photovoltaic Solar Energy Generation*, First ed. vol. 112. New York, NY: Springer-Verlag, 2005.

[10] A. Luque and S. Hegedus, *Handbook of Photovoltaic Science and Engineering*, Second ed. West Sussex, UK: John Wiley & Sons Ltd., 2011.

[11] R. K. Clayton, *Photosynthesis: physical mechanisms and chemical patterns*, First ed. New York, NY: Cambridge University Press, 1980.

[12] A. S. Raghavendra, *Photosynthesis : A Comprehensive Treatise*, First ed. New York, NY: Cambridge University Press, 1998.

[13] A. J. Bard and M. A. Fox, "Artificial photosynthesis: solar splitting of water to hydrogen and oxygen," *Accounts of Chemical Research,* vol. 28, no. 3, pp. 141-145, 1995.

[14] J. Barber, "Biological solar energy," *Philosophical Transactions of the Royal Society A: Mathematical, Physical and Engineering Sciences,* vol. 365, no. 1853, pp. 1007-1023, April 15, 2007 2007.

[15] N. S. Lewis, "Light work with water," *Nature,* vol. 414, no. 6864, pp. 589-590, 2001.

[16] J. A. Turner, "A realizable renewable energy future," *Science,* vol. 285, no. 5428, pp. 687-689, 1999.

[17] A. Heller, "Conversion of sunlight into electrical power and photoassisted electrolysis of water in photoelectrochemical cells," *Accounts of Chemical Research,* vol. 14, no. 5, pp. 154-162, 1981/05/01 1981.

[18] R. A. Marcus, "Electron transfer reactions in chemistry: theory and experiment (Nobel lecture)," *Angewandte Chemie International Edition in English,* vol. 32, no. 8, pp. 1111-1121, 1993.

[19] H. Taube, "Electron transfer between metal complexes — a retrospective view (Nobel lecture)," *Angewandte Chemie International Edition in English,* vol. 23, no. 5, pp. 329-339, 1984.

[20] E. H. Thorndike, *Energy and Environment: A Primer for Scientists and Engineers*, First ed. Reading, MA: Addison-Wesley Publishing Company, 1976.

[21] D. A. Walker, *Energy, Plants and Man*, First ed. Chichester, UK: Packard Publishing, 1979.

[22] M. D. Archer and J. Barber, *Molecular to Global Photosynthesis*, First ed. London, UK: Imperial College Press, 2004.

[23] W. D. Clark, K. R. Stern, D. Vodopich, and R. Moore, *Botany*. Dubuque, IA: Wm. C. Brown Publishers, 1995.

[24] J. R. Bolton, S. J. Strickler, and J. S. Connolly, "Limiting and realizable efficiencies of solar photolysis of water," *Nature,* vol. 316, no. 6028, pp. 495-500, 1985.

[25] A. J. Nozik, "Photochemical diodes," *Applied Physics Letters*, vol. 30, no. 11, pp. 567-569, 1977.

[26] M. F. Weber and M. J. Dignam, "Efficiency of splitting water with semiconducting photoelectrodes," *Journal of The Electrochemical Society*, vol. 131, no. 6, pp. 1258-1265, 1984.

[27] W. Shockley and H. J. Queisser, "Detailed balance limit of efficiency of p-n junction solar cells," *Journal of Applied Physics*, vol. 32, no. 3, pp. 510-519, 1961.

[28] A. W. Bett, F. Dimroth, W. Guter, R. Hoheisen, E. Oliva, S. P. Philipps, J. Schöne, G. Siefer, M. Steiner, A. Wekkeli, E. Welser, M. Meusel, W. Köstler, and G. Strobl, "Highest efficiency multi-junction solar cell for terrestrial and space applications," in *24th European Photovoltaic Solar Energy Conference*, Hamburg, Germany, 2009, pp. 1-6.

[29] W. Guter, J. Schone, S. P. Philipps, M. Steiner, G. Siefer, A. Wekkeli, E. Welser, E. Oliva, A. W. Bett, and F. Dimroth, "Current-matched triple-junction solar cell reaching 41.1% conversion efficiency under concentrated sunlight," *Applied Physics Letters*, vol. 94, no. 22, p. 223504, 2009.

[30] J. F. Geisz, D. J. Friedman, J. S. Ward, A. Duda, W. J. Olavarria, T. E. Moriarty, J. T. Kiehl, M. J. Romero, A. G. Norman, and K. M. Jones, "40.8% efficient inverted triple-junction solar cell with two independently metamorphic junctions," *Applied Physics Letters*, vol. 93, no. 12, p. 123505, 2008.

[31] R. R. King, A. Boca, W. Hong, X.-Q. Liu, D. Bhusari, D. Larrabee, K. M. Edmondson, D. C. Law, C. M. Fetzer, S. Mesropian, and N. H. Karam, "Band-gap-engineered architectures for high-efficiency multijunction concentrator solar cells," in *24th European Photovoltaic Solar Energy Conference*, Hamburg, Germany, 2009, pp. 55-61.

[32] S. Kurtz, D. Myers, W. E. McMahon, J. Geisz, and M. Steiner, "A comparison of theoretical efficiencies of multi-junction concentrator solar cells," *Progress in Photovoltaics: Research and Applications*, vol. 16, no. 6, pp. 537-546, 2008.

[33] S. Kurtz and J. Geisz, "Multijunction solar cells for conversion of concentrated sunlight to electricity," *Optics Express*, vol. 18, no. S1, pp. A73-A78, 2010.

[34] A. De Vos, "Detailed balance limit of the efficiency of tandem solar cells," *Journal of Physics D: Applied Physics*, vol. 13, no. 5, pp. 839-846, 1980.

[35] A. B. Bocarsly, D. C. Bookbinder, R. N. Dominey, N. S. Lewis, and M. S. Wrighton, "Photoreduction at illuminated p-type semiconducting silicon photoelectrodes: evidence for Fermi level pinning," *Journal of the American Chemical Society*, vol. 102, no. 11, pp. 3683-3688, 1980.

[36] A. Heller, D. E. Aspnes, J. D. Porter, T. T. Sheng, and R. G. Vadimsky, "Transparent metals preparation and characterization of light-transmitting platinum films," *The Journal of Physical Chemistry,* vol. 89, no. 21, pp. 4444-4452, 1985.

[37] E. Aharon-Shalom and A. Heller, "Efficient p-InP(Rh-H alloy) and p-InP(Re-H alloy) hydrogen evolving photocathodes," *Journal of The Electrochemical Society,* vol. 129, no. 12, pp. 2865-2866, 1982.

[38] J. Sato, N. Saito, Y. Yamada, K. Maeda, T. Takata, J. N. Kondo, M. Hara, H. Kobayashi, K. Domen, and Y. Inoue, "RuO_2-loaded β-Ge_3N_4 as a non-oxide photocatalyst for overall water splitting," *Journal of the American Chemical Society,* vol. 127, no. 12, pp. 4150-4151, 2005/03/01 2005.

[39] A. Fujishima and K. Honda, "Electrochemical photolysis of water at a semiconductor electrode," *Nature,* vol. 238, no. 5358, pp. 37-38, 1972.

[40] L. Fornarini, A. J. Nozik, and B. A. Parkinson, "The energetics of p/n photoelectrolysis cells," *The Journal of Physical Chemistry,* vol. 88, no. 15, pp. 3238-3243, 1984.

[41] A. J. Nozik, "p-n photoelectrolysis cells," *Applied Physics Letters,* vol. 29, no. 3, pp. 150-153, 1976.

[42] H. Yoneyama, H. Sakamoto, and H. Tamura, "A photo-electochemical cell with production of hydrogen and oxygen by a cell reaction," *Electrochimica Acta,* vol. 20, no. 5, pp. 341-345, 1975.

[43] H. Mettee, J. W. Otvos, and M. Calvin, "Solar induced water splitting with p/n heterotype photochemical diodes: n-Fe_2O_3/p-GaP," *Solar Energy Materials,* vol. 4, no. 4, pp. 443-453, 1981.

[44] R. C. Kainthla, B. Zelenay, and J. O. M. Bockris, "Significant efficiency increase in self-driven photoelectrochemical cell for water photoelectrolysis," *Journal of The Electrochemical Society,* vol. 134, no. 4, pp. 841-845, 1987.

[45] R. C. Kainthla, S. U. M. Khan, and J. O. M. Bockris, "The theory of electrode matching in photoelectrochemical cells for the production of hydrogen," *International Journal of Hydrogen Energy,* vol. 12, no. 6, pp. 381-392, 1987.

[46] J. Akikusa and S. U. M. Khan, "Photoelectrolysis of water to hydrogen in p-SiC/Pt and p-SiC/ n-TiO_2 cells," *International Journal of Hydrogen Energy,* vol. 27, no. 9, pp. 863-870, 2002.

[47] M. S. Wrighton, A. B. Ellis, P. T. Wolczanski, D. L. Morse, H. B. Abrahamson, and D. S. Ginley, "Strontium titanate photoelectrodes. Efficient photoassisted

electrolysis of water at zero applied potential," *Journal of the American Chemical Society,* vol. 98, no. 10, pp. 2774-2779, 1976.

[48] J. William B. Ingler and S. U. M. Khan, "A self-driven p/n-Fe_2O_3 tandem photoelectrochemical cell for water splitting," *Electrochemical and Solid-State Letters,* vol. 9, no. 4, pp. G144-G146, 2006.

[49] H. Wang, T. Deutsch, and J. A. Turner, "Direct water splitting under visible light with nanostructured hematite and WO_3 photoanodes and a $GaInP_2$ photocathode," *Journal of The Electrochemical Society,* vol. 155, no. 5, pp. F91-F96, 2008.

[50] Y. Nakato, H. Yano, S. Nishiura, T. Ueda, and H. Tsubomura, "Hydrogen photoevolution at p-type silicon electrodes coated with discontinuous metal layers," *Journal of Electroanalytical Chemistry and Interfacial Electrochemistry,* vol. 228, no. 1–2, pp. 97-108, 1987.

[51] R. N. Dominey, N. S. Lewis, J. A. Bruce, D. C. Bookbinder, and M. S. Wrighton, "Improvement of photoelectrochemical hydrogen generation by surface modification of p-type silicon semiconductor photocathodes," *Journal of the American Chemical Society,* vol. 104, no. 2, pp. 467-482, 1982/01/01 1982.

[52] Y. Hou, B. L. Abrams, P. C. K. Vesborg, M. E. Björketun, K. Herbst, L. Bech, A. M. Setti, C. D. Damsgaard, T. Pedersen, O. Hansen, J. Rossmeisl, S. Dahl, J. K. Nørskov, and I. Chorkendorff, "Bioinspired molecular co-catalysts bonded to a silicon photocathode for solar hydrogen evolution," *Nat Mater,* vol. 10, no. 6, pp. 434-438, 2011.

[53] K. S. Raja, V. K. Mahajan, and M. Misra, "Determination of photo conversion efficiency of nanotubular titanium oxide photo-electrochemical cell for solar hydrogen generation," *Journal of Power Sources,* vol. 159, no. 2, pp. 1258-1265, 2006.

[54] S. Licht, "Efficient solar generation of hydrogen fuel – a fundamental analysis," *Electrochemistry Communications,* vol. 4, no. 10, pp. 790-795, 2002.

[55] S. Licht, S. Ghosh, H. Tributsch, and S. Fiechter, "High efficiency solar energy water splitting to generate hydrogen fuel: Probing RuS_2 enhancement of multiple band electrolysis," *Solar Energy Materials and Solar Cells,* vol. 70, no. 4, pp. 471-480, 2002.

[56] S. Licht, B. Wang, S. Mukerji, T. Soga, M. Umeno, and H. Tributsch, "Efficient solar water splitting, exemplified by RuO_2-catalyzed AlGaAs/Si photoelectrolysis," *The Journal of Physical Chemistry B,* vol. 104, no. 38, pp. 8920-8924, 2000.

[57] K. Jun, Y. S. Lee, T. Buonassisi, and J. M. Jacobson, "High photocurrent in silicon photoanodes catalyzed by iron oxide thin films for water oxidation," *Angewandte Chemie,* vol. 124, no. 2, pp. 438-442, 2012.

[58] E. R. Young, R. Costi, S. Paydavosi, D. G. Nocera, and V. Bulovic, "Photo-assisted water oxidation with cobalt-based catalyst formed from thin-film cobalt metal on silicon photoanodes," *Energy & Environmental Science,* vol. 4, no. 6, pp. 2058-2061, 2011.

[59] S. Y. Reece, J. A. Hamel, K. Sung, T. D. Jarvi, A. J. Esswein, J. J. H. Pijpers, and D. G. Nocera, "Wireless solar water splitting using silicon-based semiconductors and earth-abundant catalysts," *Science,* vol. 334, no. 6056, pp. 645-648, November 4, 2011 2011.

[60] D. G. Nocera, "The artificial leaf," *Accounts of Chemical Research,* vol. 45, no. 5, pp. 767-776, 2012/05/15 2012.

[61] X. Yang, A. Wolcott, G. Wang, A. Sobo, R. C. Fitzmorris, F. Qian, J. Z. Zhang, and Y. Li, "Nitrogen-doped ZnO nanowire arrays for photoelectrochemical water splitting," *Nano Letters,* vol. 9, no. 6, pp. 2331-2336, 2009.

[62] K. Shankar, J. I. Basham, N. K. Allam, O. K. Varghese, G. K. Mor, X. Feng, M. Paulose, J. A. Seabold, K.-S. Choi, and C. A. Grimes, "Recent advances in the use of TiO_2 nanotube and nanowire arrays for oxidative photoelectrochemistry," *The Journal of Physical Chemistry C,* vol. 113, no. 16, pp. 6327-6359, 2009/04/23 2009.

[63] M. J. Price and S. Maldonado, "Macroporous n-GaP in nonaqueous regenerative photoelectrochemical cells," *The Journal of Physical Chemistry C,* vol. 113, no. 28, pp. 11988-11994, 2009.

[64] J. H. Park, S. Kim, and A. J. Bard, "Novel carbon-doped TiO_2 nanotube arrays with high aspect ratios for efficient solar water splitting," *Nano Letters,* vol. 6, no. 1, pp. 24-28, 2005.

[65] A. P. Goodey, S. M. Eichfeld, K. K. Lew, J. M. Redwing, and T. E. Mallouk, "Silicon nanowire array photoelectrochemical cells," *Journal of the American Chemical Society,* vol. 129, no. 41, pp. 12344-12345, 2007.

[66] N. Beermann, L. Vayssieres, S.-E. Lindquist, and A. Hagfeldt, "Photoelectrochemical studies of oriented nanorod thin films of hematite," *Journal of The Electrochemical Society,* vol. 147, no. 7, pp. 2456-2461, 2000.

[67] A. Kay, I. Cesar, and M. Grätzel, "New benchmark for water photooxidation by nanostructured α-Fe_2O_3 films," *Journal of the American Chemical Society,* vol. 128, no. 49, pp. 15714-15721, 2006.

[68] S. O. Kasap, *Principles of Electronic Materials and Devices*, Third ed. New York, NY: McGraw Hill, 2006.

[69] S. M. Sze and K. K. Ng, *Physics of Semiconductor Devices*, Third ed. New York, NY: John Wiley & Sons Ltd., 2007.

[70] J. R. Maiolo, H. A. Atwater, and N. S. Lewis, "Macroporous silicon as a model for silicon wire array solar cells," *The Journal of Physical Chemistry C,* vol. 112, no. 15, pp. 6194-6201, 2008.

[71] B. M. Kayes, H. A. Atwater, and N. S. Lewis, "Comparison of the device physics principles of planar and radial p-n junction nanorod solar cells," *Journal of Applied Physics,* vol. 97, no. 11, pp. 114302-11, 2005.

[72] J. M. Spurgeon, K. E. Plass, B. M. Kayes, B. S. Brunschwig, H. A. Atwater, and N. S. Lewis, "Repeated epitaxial growth and transfer of arrays of patterned, vertically aligned, crystalline Si wires from a single Si(111) substrate," *Applied Physics Letters,* vol. 93, no. 3, p. 032112, 2008.

[73] M. X. Tan, C. N. Kenyon, O. Krüger, and N. S. Lewis, "Behavior of Si photoelectrodes under high level injection conditions. 1. Steady-state current−voltage properties and quasi-Fermi level positions under illumination," *The Journal of Physical Chemistry B,* vol. 101, no. 15, pp. 2830-2839, 1997.

[74] O. Krüger, C. N. Kenyon, M. X. Tan, and N. S. Lewis, "Behavior of Si photoelectrodes under high level injection conditions. 2. Experimental measurements and digital simulations of the behavior of quasi-Fermi levels under illumination and applied bias," *The Journal of Physical Chemistry B,* vol. 101, no. 15, pp. 2840-2849, 1997.

[75] C. N. Kenyon, M. X. Tan, O. Krüger, and N. S. Lewis, "Behavior of Si photoelectrodes under high level injection conditions. 3. Transient and steady-state measurements of the quasi-Fermi levels at Si/CH_3OH contacts," *The Journal of Physical Chemistry B,* vol. 101, no. 15, pp. 2850-2860, 1997.

[76] M. X. Tan, C. N. Kenyon, and N. S. Lewis, "Experimental measurement of quasi-Fermi levels at an illuminated semiconductor/liquid contact," *The Journal of Physical Chemistry,* vol. 98, no. 19, pp. 4959-4962, 1994.

[77] M. D. Kelzenberg, S. W. Boettcher, J. A. Petykiewicz, D. B. Turner-Evans, M. C. Putnam, E. L. Warren, J. M. Spurgeon, R. M. Briggs, N. S. Lewis, and H. A. Atwater, "Enhanced absorption and carrier collection in Si wire arrays for photovoltaic applications," *Nature Materials,* vol. 9, no. 3, pp. 239-244, 2010.

[78] CCI Powering the Planet: An NSF Center for Chemical Innovation; California Institute of Technology. *http://ccisolar.caltech.edu (Retrieved May 2012).*

[79] H. B. Gray, "Powering the planet with solar fuel," *Nature Chemistry,* vol. 1, no. 1, pp. 7-7, 2009.

[80] S. Licht, "Multiple band gap semiconductor/electrolyte solar energy conversion," *The Journal of Physical Chemistry B,* vol. 105, no. 27, pp. 6281-6294, 2001.

[81] O. Khaselev and J. A. Turner, "A monolithic photovoltaic-photoelectrochemical device for hydrogen production via water splitting," *Science,* vol. 280, no. 5362, pp. 425-427, 1998.

[82] J. M. Spurgeon and N. S. Lewis, "Proton exchange membrane electrolysis sustained by water vapor," *Energy & Environmental Science,* vol. 4, no. 8, pp. 2993-2998, 2011.

[83] B. D. Alexander, P. J. Kulesza, I. Rutkowska, R. Solarska, and J. Augustynski, "Metal oxide photoanodes for solar hydrogen production," *Journal of Materials Chemistry,* vol. 18, no. 20, 2008.

[84] X. Hu, B. S. Brunschwig, and J. C. Peters, "Electrocatalytic hydrogen evolution at low overpotentials by cobalt macrocyclic glyoxime and tetraimine complexes," *Journal of the American Chemical Society,* vol. 129, no. 29, pp. 8988-8998, 2007.

[85] F. Jiao and H. Frei, "Nanostructured cobalt oxide clusters in mesoporous silica as efficient oxygen-evolving catalysts," *Angewandte Chemie International Edition,* vol. 48, no. 10, pp. 1841-1844, 2009.

[86] S. Trasatti, "Work function, electronegativity, and electrochemical behaviour of metals: III. Electrolytic hydrogen evolution in acid solutions," *Journal of Electroanalytical Chemistry and Interfacial Electrochemistry,* vol. 39, no. 1, pp. 163-184, 1972.

[87] S. L. McFarlane, B. A. Day, K. McEleney, M. S. Freund, and N. S. Lewis, "Designing electronic/ionic conducting membranes for artificial photosynthesis," *Energy & Environmental Science,* vol. 4, no. 5, pp. 1700-1703, 2011.

[88] M. D. Kelzenberg, D. B. Turner-Evans, M. C. Putnam, S. W. Boettcher, R. M. Briggs, J. Y. Baek, N. S. Lewis, and H. A. Atwater, "High-performance Si microwire photovoltaics," *Energy & Environmental Science,* vol. 4, no. 3, pp. 866-871, 2011.

[89] O. Gunawan, K. Wang, B. Fallahazad, Y. Zhang, E. Tutuc, and S. Guha, "High performance wire-array silicon solar cells," *Progress in Photovoltaics: Research and Applications,* vol. 19, no. 3, pp. 307-312, 2011.

[90] S. W. Boettcher, J. M. Spurgeon, M. C. Putnam, E. L. Warren, D. B. Turner-Evans, M. D. Kelzenberg, J. R. Maiolo, H. A. Atwater, and N. S. Lewis, "Energy-

conversion properties of vapor-liquid-solid–grown silicon wire-array photocathodes," *Science,* vol. 327, no. 5962, pp. 185-187, 2010.

[91] I. Yahyaie, K. McEleney, M. Walter, D. R. Oliver, D. J. Thomson, M. S. Freund, and N. S. Lewis, "Electrical characterization of Si microwires and of Si microwire/conducting polymer composite junctions," *Journal of Physical Chemistry Letters,* vol. 2, no. 6, pp. 675-680, 2011.

[92] I. Yahyaie, K. McEleney, M. G. Walter, D. R. Oliver, D. J. Thomson, M. S. Freund, and N. S. Lewis, "Characterization of the electrical properties of individual p-Si microwire/polymer/n-Si microwire assemblies," *The Journal of Physical Chemistry C,* vol. 115, no. 50, pp. 24945-24950, 2011.

[93] M. B. McDonald and M. S. Freund, "Novel conducting polymer-heteropoly acid hybrid material for artificial photosynthetic membranes," *ACS Applied Materials & Interfaces,* vol. 3, no. 4, pp. 1003-1008, 2011.

[94] K. A. Mauritz and R. B. Moore, "State of understanding of Nafion," *Chemical Reviews,* vol. 104, no. 10, pp. 4535-4586, 2004.

[95] Y. Álvarez-Gallego and M. P. de Heer, "Sub-freezing conductivity of PFSA membranes," *Fuel Cells,* vol. 9, no. 4, pp. 421-431, 2009.

[96] A. Siu, J. Schmeisser, and S. Holdcroft, "Effect of water on the low temperature conductivity of polymer electrolytes," *The Journal of Physical Chemistry B,* vol. 110, no. 12, pp. 6072-6080, 2006.

[97] A. Eisenberg and J.-S. Kim, *Introduction to Ionomers,* First ed. New York, NY: John Wiley & Sons Ltd., 1998.

[98] T. A. Skotheim and J. Reynolds, *Handbook of Conducting Polymers,* Third ed. London, UK: CRC Press, 2007.

[99] J. H. Burroughes, D. D. C. Bradley, A. R. Brown, R. N. Marks, K. Mackay, R. H. Friend, P. L. Burns, and A. B. Holmes, "Light-emitting diodes based on conjugated polymers," *Nature,* vol. 347, no. 6293, pp. 539-541, 1990.

[100] D. Braun and A. J. Heeger, "Visible light emission from semiconducting polymer diodes," *Applied Physics Letters,* vol. 58, no. 18, pp. 1982-1984, 1991.

[101] Z. Bao, "Materials and fabrication needs for low-cost organic transistor circuits," *Advanced Materials,* vol. 12, no. 3, pp. 227-230, 2000.

[102] M. S. Freund and B. A. Deore, *Self-Doped Conducting Polymers,* First ed. Chichester, UK: John Wiley & Sons Ltd., 2007.

[103] T. H. Jozefiak, E. J. Ginsburg, C. B. Gorman, R. H. Grubbs, and N. S. Lewis, "Voltammetric characterization of soluble polyacetylene derivatives obtained from the ring-opening metathesis polymerization (ROMP) of substituted cyclooctatetraenes," *Journal of the American Chemical Society*, vol. 115, no. 11, pp. 4705-4713, 1993.

[104] C. B. Gorman, E. J. Ginsburg, and R. H. Grubbs, "Soluble, highly conjugated derivatives of polyacetylene from the ring-opening metathesis polymerization of monosubstituted cyclooctatetraenes: synthesis and the relationship between polymer structure and physical properties," *Journal of the American Chemical Society,* vol. 115, no. 4, pp. 1397-1409, 1993.

[105] G. B. Street, T. C. Clarke, M. Krounbi, K. Kanazawa, V. Lee, P. Pfluger, J. C. Scott, and G. Weiser, "Preparation and characterization of neutral and oxidized polypyrrole films," *Molecular Crystals and Liquid Crystals,* vol. 83, no. 1, pp. 253-264, 1982.

[106] A. Deronzier and J. C. Moutet, "Functionalized polypyrroles. New molecular materials for electrocatalysis and related applications," *Accounts of Chemical Research,* vol. 22, no. 7, pp. 249-255, 1989.

[107] H. S. O. Chan and S. C. Ng, "Synthesis, characterization and applications of thiophene-based functional polymers," *Progress in Polymer Science,* vol. 23, no. 7, pp. 1167-1231, 1998.

[108] S.-H. Ahn, M.-z. Czae, E.-R. Kim, H. Lee, S.-H. Han, J. Noh, and M. Hara, "Synthesis and characterization of soluble polythiophene derivatives containing electron-transporting moiety," *Macromolecules,* vol. 34, no. 8, pp. 2522-2527, 2001.

[109] A. G. MacDiarmid and A. J. Epstein, "Polyanilines: a novel class of conducting polymers," *Faraday Discussions of the Chemical Society,* vol. 88, pp. 317-332, 1989.

[110] N. L. D. Somasiri and A. G. Macdiarmid, "Polyaniline: characterization as a cathode active material in rechargeable batteries in aqueous electrolytes," *Journal of Applied Electrochemistry,* vol. 18, no. 1, pp. 92-95, 1988.

[111] T. Yamamoto and M. Abla, "Synthesis of non-doped poly(3,4-ethylenedioxythiophene) and its spectroscopic data," *Synthetic Metals,* vol. 100, no. 2, pp. 237-239, 1999.

[112] L. Groenendaal, F. Jonas, D. Freitag, H. Pielartzik, and J. R. Reynolds, "Poly(3,4-ethylenedioxythiophene) and its derivatives: past, present, and future," *Advanced Materials,* vol. 12, no. 7, pp. 481-494, 2000.

[113] L. Groenendaal, G. Zotti, P. H. Aubert, S. M. Waybright, and J. R. Reynolds, "Electrochemistry of poly(3,4-alkylenedioxythiophene) derivatives," *Advanced Materials*, vol. 15, no. 11, pp. 855-879, 2003.

[114] J. Roncali, P. Blanchard, and P. Frere, "3,4-Ethylenedioxythiophene (EDOT) as a versatile building block for advanced functional π-conjugated systems," *Journal of Materials Chemistry*, vol. 15, no. 16, pp. 1589-1610, 2005.

[115] G. M. Suppes, B. A. Deore, and M. S. Freund, "Porous conducting polymer/heteropolyoxometalate hybrid material for electrochemical supercapacitor applications," *Langmuir*, vol. 24, no. 3, pp. 1064-1069, 2007.

[116] S. L. McFarlane, B. A. Deore, N. Svenda, and M. S. Freund, "A one-step, organic-solvent processable synthesis of PEDOT thin films via in situ metastable chemical polymerization," *Macromolecules*, vol. 43, no. 24, pp. 10241-10245, 2010.

[117] G. Li and P. G. Pickup, "Ion transport in poly(3,4-ethylenedioxythiophene)-poly(styrene-4-sulfonate) composites," *Physical Chemistry Chemical Physics*, vol. 2, no. 6, pp. 1255-1260, 2000.

[118] J. Ouyang, C. W. Chu, F. C. Chen, Q. Xu, and Y. Yang, "High-conductivity poly(3,4-ethylenedioxythiophene):poly(styrene sulfonate) film and its application in polymer optoelectronic devices," *Advanced Functional Materials*, vol. 15, no. 2, pp. 203-208, 2005.

[119] F. Jonas, W. Krafft, and B. Muys, "Poly(3, 4-ethylenedioxythiophene): conductive coatings, technical applications and properties," *Macromolecular Symposia*, vol. 100, no. 1, pp. 169-173, 1995.

[120] B. M. Kayes, M. A. Filler, M. C. Putnam, M. D. Kelzenberg, N. S. Lewis, and H. A. Atwater, "Growth of vertically aligned Si wire arrays over large areas (> 1 cm^2) with Au and Cu catalysts," *Applied Physics Letters*, vol. 91, no. 10, pp. 103110–110113, 2007.

[121] Z. Huang, H. Fang, and J. Zhu, "Fabrication of silicon nanowire arrays with controlled diameter, length, and density," *Advanced Materials*, vol. 19, no. 5, pp. 744-748, 2007.

[122] R. S. Wagner and W. C. Ellis, "Vapor-liquid-solid mechanism of single crystal growth," *Applied Physics Letters*, vol. 4, no. 5, pp. 89-90, 1964.

[123] E. I. Givargizov, "Fundamental aspects of VLS growth," *Journal of Crystal Growth*, vol. 31, no. 0, pp. 20-30, 1975.

[124] H. J. Fan, P. Werner, and M. Zacharias, "Semiconductor nanowires: from self-organization to patterned growth," *Small*, vol. 2, no. 6, pp. 700-717, 2006.

[125] T. Martensson, M. Borgstrom, W. Seifert, B. J. Ohlsson, and L. Samuelson, "Fabrication of individually seeded nanowire arrays by vapour–liquid–solid growth," *Nanotechnology,* vol. 14, no. 12, pp. 1255-1258, 2003.

[126] T. Kawano, Y. Kato, M. Futagawa, H. Takao, K. Sawada, and M. Ishida, "Fabrication and properties of ultrasmall Si wire arrays with circuits by vapor–liquid–solid growth," *Sensors and Actuators A: Physical,* vol. 97–98, no. 0, pp. 709-715, 2002.

[127] J. Westwater, D. P. Gosain, and S. Usui, "Control of the size and position of silicon nanowires grown via the vapor-liquid-solid technique," *Japanese Journal of Applied Physics,* vol. 36, pp. 6204-6209, 1997.

[128] L. Tsakalakos, J. Balch, J. Fronheiser, M. Y. Shih, S. F. LeBoeuf, M. Pietrzykowski, P. J. Codella, B. A. Korevaar, O. Sulima, J. Rand, A. Davuluru, and U. Rapol, "Strong broadband optical absorption in silicon nanowire films," *Journal of Nanophotonics,* vol. 1, pp. 1355/2–1355/10, 2007.

[129] K. Q. Peng, Y. Xu, Y. Wu, Y. J. Yan, S. T. Lee, and J. Zhu, "Aligned single-crystalline Si nanowire arrays for photovoltaic applications," *Small,* vol. 1, no. 11, pp. 1062-1067, 2005.

[130] L. Hu and G. Chen, "Analysis of optical absorption in silicon nanowire arrays for photovoltaic applications," *Nano Letters,* vol. 7, no. 11, pp. 3249-3252, 2007.

[131] B. Z. Tian, X. L. Zheng, T. J. Kempa, Y. Fang, N. F. Yu, G. H. Yu, J. L. Huang, and C. M. Lieber, "Coaxial silicon nanowires as solar cells and nanoelectronic power sources," *Nature,* vol. 449, pp. 885-889, 2007.

[132] W. U. Huynh, J. J. Dittmer, and A. P. Alivisatos, "Hybrid nanorod-polymer solar cells," *Science,* vol. 295, pp. 2425-2427, 2002.

[133] J. R. Maiolo, B. M. Kayes, M. A. Filler, M. C. Putnam, M. D. Kelzenberg, H. A. Atwater, and N. S. Lewis, "High aspect ratio silicon wire array photoelectrochemical cells," *Journal of the American Chemical Society,* vol. 129, no. 41, pp. 12346-12347, 2007.

[134] S. W. Boettcher, E. L. Warren, M. C. Putnam, E. A. Santori, D. Turner-Evans, M. D. Kelzenberg, M. G. Walter, J. R. McKone, B. S. Brunschwig, H. A. Atwater, and N. S. Lewis, "Photoelectrochemical hydrogen evolution using Si microwire arrays," *Journal of the American Chemical Society,* vol. 133, no. 5, pp. 1216-1219, 2011.

[135] E. L. Warren, S. W. Boettcher, M. G. Walter, H. A. Atwater, and N. S. Lewis, "pH-independent, 520 mV open-circuit voltages of Si/methyl viologen$^{2+/+}$ contacts

through use of radial n^+p-Si junction microwire array photoelectrodes," *The Journal of Physical Chemistry C,* vol. 115, no. 2, pp. 594-598, 2010.

[136] A. Kumar, W. C. A. Wilisch, and N. S. Lewis, "The electrical properties of semiconductor/metal, semiconductor/liquid, and semiconductor/conducting polymer contacts," *Critical Reviews in Solid State and Materials Sciences,* vol. 18, no. 4, pp. 327-353, 1993.

[137] T. Skotheim, O. Inganäs, J. Prejza, and I. Lundström, "Polypyrrole - semiconductor photovoltaic devices," *Molecular Crystals and Liquid Crystals,* vol. 83, no. 1, pp. 329-339, 1982.

[138] O. Inganäs, T. Skotheim, and I. Lundström, "Schottky barrier formation between polypyrrole and crystalline and amorphous hydrogenated silicon," *Physica Scripta,* vol. 25, no. 6A, 1982.

[139] G. Nagasubramanian, S. DiStefano, and J. Moacanin, "Effect of counterions on the formation of ohmic contact between p-Si and poly(pyrrole) film," *Journal of The Electrochemical Society,* vol. 133, no. 2, pp. 305-309, 1986.

[140] G. Nagasubramanian, S. Distefano, and J. Moacanin, "Electrochemical evaluation of the p-Si/conducting polymer interfacial properties," presented at the IUPAC International Symposium on Polymers for Advanced Technologies, Jerusalem, Israel, 1987.

[141] C. R. Crowell and S. M. Sze, "Current transport in metal-semiconductor barriers," *Solid-State Electronics,* vol. 9, no. 11–12, pp. 1035-1048, 1966.

[142] P. H. Schmidt, S. R. Forrest, and M. L. Kaplan, "Organic-inorganic contact barrier heights," *Journal of The Electrochemical Society,* vol. 133, no. 4, pp. 769-771, 1986.

[143] R. A. Simon and M. S. Wrighton, "Stabilization of n-type silicon photoanodes against photoanodic decomposition with thin films of polyacetylene," *Applied Physics Letters,* vol. 44, no. 9, pp. 930-932, 1984.

[144] M. J. Sailor, F. L. Klavetter, R. H. Grubbs, and N. S. Lewis, "Electronic properties of junctions between silicon and organic conducting polymers," *Nature,* vol. 346, no. 6280, pp. 155-157, 1990.

[145] M. J. Sailor, E. J. Ginsburg, C. B. Gorman, A. Kumar, R. H. Grubbs, and N. S. Lewis, "Thin films of n-Si/poly-$(CH_3)_3$Si-cyclooctatetraene: conducting-polymer solar cells and layered structures," *Science,* vol. 249, no. 4973, pp. 1146-1149, 1990.

[146] M. D. Kelzenberg, D. B. Turner-Evans, B. M. Kayes, M. A. Filler, M. C. Putnam, N. S. Lewis, and H. A. Atwater, "Photovoltaic measurements in single-nanowire silicon solar cells," *Nano Letters*, vol. 8, no. 2, pp. 710-714, 2008.

[147] Y. Gu, J. P. Romankiewicz, J. K. David, J. L. Lensch, L. J. Lauhon, E.-S. Kwak, and T. W. Odom, "Local photocurrent mapping as a probe of contact effects and charge carrier transport in semiconductor nanowire devices," *Journal of Vacuum Science & Technology B*, vol. 24, no. 4, pp. 2172-2177, 2006.

[148] Y. Cui, Z. Zhong, D. Wang, W. U. Wang, and C. M. Lieber, "High performance silicon nanowire field effect transistors," *Nano Letters*, vol. 3, no. 2, pp. 149-152, 2003.

[149] E. C. Garnett and P. Yang, "Silicon nanowire radial p–n junction solar cells," *Journal of the American Chemical Society*, vol. 130, no. 29, pp. 9224-9225, 2008.

[150] J. M. Spurgeon, S. W. Boettcher, M. D. Kelzenberg, B. S. Brunschwig, H. A. Atwater, and N. S. Lewis, "Flexible, polymer-supported, Si wire array photoelectrodes," *Advanced Materials*, vol. 22, no. 30, pp. 3277-3281, 2010.

[151] J. M. Spurgeon, M. G. Walter, J. Zhou, P. A. Kohl, and N. S. Lewis, "Electrical conductivity, ionic conductivity, optical absorption, and gas separation properties of ionically conductive polymer membranes embedded with Si microwire arrays," *Energy & Environmental Science*, vol. 4, no. 5, 2011.

[152] M. C. Putnam, S. W. Boettcher, M. D. Kelzenberg, D. B. Turner-Evans, J. M. Spurgeon, E. L. Warren, R. M. Briggs, N. S. Lewis, and H. A. Atwater, "Si microwire-array solar cells," *Energy & Environmental Science*, vol. 3, no. 8, 2010.

[153] E. Koren, Y. Rosenwaks, J. E. Allen, E. R. Hemesath, and L. J. Lauhon, "Nonuniform doping distribution along silicon nanowires measured by kelvin probe force microscopy and scanning photocurrent microscopy," *Applied Physics Letters*, vol. 95, no. 9, pp. 092105–092107, 2009.

[154] J. E. Allen, D. E. Perea, E. R. Hemesath, and L. J. Lauhon, "Nonuniform nanowire doping profiles revealed by quantitative scanning photocurrent microscopy," *Advanced Materials*, vol. 21, no. 30, pp. 3067-3072, 2009.

[155] T. Umesaka, H. Ohnaka, Y. Ohno, S. Kishimoto, K. Maezawa, and T. Mizutani, "Surface potential measurement of carbon nanotube field-effect transistors using kelvin probe force microscopy," *Japanese Journal of Applied Physics*, vol. 46, pp. 2496-2500, 2007.

[156] S. Cabrini, *Nanofabrication Handbook*, First ed. New York, NY: CRC Press, 2012.

[157] J. N. Helbert, *Handbook of VLSI Microlithography - Principles, Technology and Applications*. Norwich, NY: William Andrew Publishing/Noyes, 2001.

[158] S. Reyntjens and R. Puers, "A review of focused ion beam applications in microsystem technology," *Journal of Micromechanics and Microengineering,* vol. 11, no. 4, pp. 287-300, 2001.

[159] Y. H. Ahn, B. H. Son, and J. K. Park, "Investigation of metal contact properties in silicon nanowire field-effect transistors by using scanning photocurrent microscopy," *Journal of the Korean Physical Society,* vol. 51, no. 6, pp. 2040-2044, 2007.

[160] M. Freitag, J. C. Tsang, A. Bol, D. Yuan, J. Liu, and P. Avouris, "Imaging of the Schottky barriers and charge depletion in carbon nanotube transistors," *Nano Letters,* vol. 7, no. 7, pp. 2037-2042, 2007.

[161] D. Gupta, D. Kabra, N. Kolishetti, S. Ramakrishnan, and K. S. Narayan, "An efficient bulk-heterojunction photovoltaic cell based on energy transfer in graded-bandgap polymers," *Advanced Functional Materials,* vol. 17, no. 2, pp. 226-232, 2007.

[162] D. Kabra and K. S. Narayan, "Direct estimate of transport length scales in semiconducting polymers," *Advanced Materials,* vol. 19, no. 11, pp. 1465-1470, 2007.

[163] Y. Gu, J. P. Romankiewicz, J. K. David, J. L. Lensch, and L. J. Lauhon, "Quantitative measurement of the electron and hole mobility–lifetime products in semiconductor nanowires," *Nano Letters,* vol. 6, no. 5, pp. 948-952, 2006.

[164] W. Paul and G. L. Pearson, "Pressure dependence of the resistivity of silicon," *Physical Review,* vol. 98, no. 6, pp. 1755-1757, 1955.

[165] P. W. Bridgman, "The effect of pressure on the electrical resistance of certain semi-conductors," *Proc. Am. Acad. Arts Sci.,* vol. 79, pp. 127–148, 1951.

[166] J. E. Bradby, J. S. Williams, and M. V. Swain, "In situ electrical characterization of phase transformations in Si during indentation," *Physical Review B,* vol. 67, no. 8, pp. 085205–085209, 2003.

[167] S. Ruffell, J. E. Bradby, N. Fujisawa, and J. S. Williams, "Identification of nanoindentation-induced phase changes in silicon by in situ electrical characterization," *Journal of Applied Physics,* vol. 101, no. 8, p. 083531, 2007.

[168] J. D. L. Shapley and D. A. Barrow, "Novel patterning method for the electrochemical production of etched silicon," *Thin Solid Films,* vol. 388, no. 1-2, pp. 134-137, 2001.

[169] S. S. Perry, H. C. Galloway, P. Cao, E. J. R. Mitchell, D. C. Koeck, C. L. Smith, and M. S. Lim, "The influence of chemical treatments on tungsten films found in integrated circuits," *Applied Surface Science,* vol. 180, no. 1–2, pp. 6-13, 2001.

[170] W. Zhou and Z. L. Wang, *Scanning Microscopy for Nanotechnology - Techniques and Applications*, First ed. New York, NY: Springer, 2007.

[171] M. A. Green, K. Emery, Y. Hishikawa, W. Warta, and E. D. Dunlop, "Solar cell efficiency tables (version 39)," *Progress in Photovoltaics: Research and Applications,* vol. 20, no. 1, pp. 12-20, 2012.

[172] M. C. Putnam, D. B. Turner-Evans, M. D. Kelzenberg, S. W. Boettcher, N. S. Lewis, and H. A. Atwater, "10 μm minority-carrier diffusion lengths in Si wires synthesized by Cu-catalyzed vapor-liquid-solid growth," *Applied Physics Letters,* vol. 95, no. 16, pp. 163116–163118, 2009.

[173] R. C. Chiechi, E. A. Weiss, M. D. Dickey, and G. M. Whitesides, "Eutectic gallium–indium (EGaIn): a moldable liquid metal for electrical characterization of self-assembled monolayers," *Angewandte Chemie,* vol. 120, no. 1, pp. 148-150, 2008.

[174] H. C. Card and E. H. Rhoderic, "Studies of tunnel MOS diodes I. Interface effects in silicon schottky diodes," *Journal of Physics D-Applied Physics,* vol. 4, no. 10, pp. 1589-1601, 1971.

[175] S. H. Lo, D. A. Buchanan, Y. Taur, and W. Wang, "Quantum-mechanical modeling of electron tunneling current from the inversion layer of ultra-thin-oxide nMOSFET's," *IEEE Electron Device Lett.*, vol. 18, no. 5, pp. 209-211, 1997.

[176] R. Grünwald and H. Tributsch, "Mechanisms of instability in Ru-based dye sensitization solar cells," *The Journal of Physical Chemistry B,* vol. 101, no. 14, pp. 2564-2575, 1997/04/01 1997.

[177] B. Macht, M. Turrión, A. Barkschat, P. Salvador, K. Ellmer, and H. Tributsch, "Patterns of efficiency and degradation in dye sensitization solar cells measured with imaging techniques," *Solar Energy Materials and Solar Cells,* vol. 73, no. 2, pp. 163-173, 2002.

[178] W. J. Royea, A. Juang, and N. S. Lewis, "Preparation of air-stable, low recombination velocity Si(111) surfaces through alkyl termination," *Applied Physics Letters,* vol. 77, no. 13, pp. 1988-1990, 2000.

[179] S. F. Bent, "Organic functionalization of group IV semiconductor surfaces: principles, examples, applications, and prospects," *Surface Science,* vol. 500, no. 1–3, pp. 879-903, 2002.

[180] L. J. Webb and N. S. Lewis, "Comparison of the electrical properties and chemical stability of crystalline silicon(111) surfaces alkylated using grignard reagents or olefins with Lewis acid catalysts," *The Journal of Physical Chemistry B,* vol. 107, no. 23, pp. 5404-5412, 2003.

[181] E. J. Nemanick, P. T. Hurley, B. S. Brunschwig, and N. S. Lewis, "Chemical and electrical passivation of silicon (111) surfaces through functionalization with sterically hindered alkyl groups," *The Journal of Physical Chemistry B,* vol. 110, no. 30, pp. 14800-14808, 2006.

[182] S. A. Mitchell, R. Boukherroub, and S. Anderson, "Second harmonic generation at chemically modified Si(111) surfaces," *The Journal of Physical Chemistry B,* vol. 104, no. 32, pp. 7668-7676, 2000.

[183] H.-Z. Yu, R. Boukherroub, S. Morin, and D. D. M. Wayner, "Facile interfacial electron transfer through n-alkyl monolayers formed on silicon (111) surfaces," *Electrochemistry Communications,* vol. 2, no. 8, pp. 562-566, 2000.

[184] A. Bansal, X. Li, I. Lauermann, N. S. Lewis, S. I. Yi, and W. H. Weinberg, "Alkylation of Si surfaces using a two-step halogenation/grignard route," *Journal of the American Chemical Society,* vol. 118, no. 30, pp. 7225-7226, 1996.

[185] M. R. Linford and C. E. D. Chidsey, "Alkyl monolayers covalently bonded to silicon surfaces," *Journal of the American Chemical Society,* vol. 115, no. 26, pp. 12631-12632, 1993.

[186] M. R. Linford, P. Fenter, P. M. Eisenberger, and C. E. D. Chidsey, "Alkyl monolayers on silicon prepared from 1-alkenes and hydrogen-terminated silicon," *Journal of the American Chemical Society,* vol. 117, no. 11, pp. 3145-3155, 1995.

[187] J. Terry, M. R. Linford, C. Wigren, R. Cao, P. Pianetta, and C. E. D. Chidsey, "Determination of the bonding of alkyl monolayers to the Si(111) surface using chemical-shift, scanned-energy photoelectron diffraction," *Applied Physics Letters,* vol. 71, no. 8, pp. 1056-1058, 1997.

[188] J. Terry, R. Mo, C. Wigren, R. Cao, G. Mount, P. Pianetta, M. R. Linford, and C. E. D. Chidsey, "Reactivity of the H-Si (1 1 1) surface," *Nuclear Instruments and Methods in Physics Research Section B: Beam Interactions with Materials and Atoms,* vol. 133, no. 1–4, pp. 94-101, 1997.

[189] R. Boukherroub and D. D. M. Wayner, "Controlled functionalization and multistep chemical manipulation of covalently modified Si(111) surfaces," *Journal of the American Chemical Society,* vol. 121, no. 49, pp. 11513-11515, 1999.

[190] F. Effenberger, G. Götz, B. Bidlingmaier, and M. Wezstein, "Photoactivated preparation and patterning of self-assembled monolayers with 1-alkenes and

aldehydes on silicon hydride surfaces," *Angewandte Chemie International Edition,* vol. 37, no. 18, pp. 2462-2464, 1998.

[191] R. L. Cicero, M. R. Linford, and C. E. D. Chidsey, "Photoreactivity of unsaturated compounds with hydrogen-terminated silicon(111)," *Langmuir,* vol. 16, no. 13, pp. 5688-5695, 2000.

[192] A. B. Sieval, R. Linke, G. Heij, G. Meijer, H. Zuilhof, and E. J. R. Sudhölter, "Amino-terminated organic monolayers on hydrogen-terminated silicon surfaces," *Langmuir,* vol. 17, no. 24, pp. 7554-7559, 2001.

[193] M. M. Sung, G. J. Kluth, O. W. Yauw, and R. Maboudian, "Thermal behavior of alkyl monolayers on silicon surfaces," *Langmuir,* vol. 13, no. 23, pp. 6164-6168, 1997.

[194] R. Boukherroub, J. T. C. Wojtyk, D. D. M. Wayner, and D. J. Lockwood, "Thermal hydrosilylation of undecylenic acid with porous silicon," *Journal of The Electrochemical Society,* vol. 149, no. 2, pp. H59-H63, 2002.

[195] J. M. Buriak, M. P. Stewart, T. W. Geders, M. J. Allen, H. C. Choi, J. Smith, D. Raftery, and L. T. Canham, "Lewis acid mediated hydrosilylation on porous silicon surfaces," *Journal of the American Chemical Society,* vol. 121, no. 49, pp. 11491-11502, 1999.

[196] L. A. Zazzera, J. F. Evans, M. Deruelle, M. Tirrell, C. R. Kessel, and P. McKeown, "Bonding organic molecules to hydrogen-terminated silicon wafers," *Journal of The Electrochemical Society,* vol. 144, no. 6, pp. 2184-2189, 1997.

[197] J. M. Schmeltzer, L. A. Porter, M. P. Stewart, and J. M. Buriak, "Hydride abstraction initiated hydrosilylation of terminal alkenes and alkynes on porous silicon," *Langmuir,* vol. 18, no. 8, pp. 2971-2974, 2002.

[198] A. B. Sieval, A. L. Demirel, J. W. M. Nissink, M. R. Linford, J. H. van der Maas, W. H. de Jeu, H. Zuilhof, and E. J. R. Sudhölter, "Highly stable Si–C linked functionalized monolayers on the silicon (100) surface," *Langmuir,* vol. 14, no. 7, pp. 1759-1768, 1998.

[199] A. Bansal and N. S. Lewis, "Electrochemical properties of (111)-oriented n-Si surfaces derivatized with covalently-attached alkyl chains," *The Journal of Physical Chemistry B,* vol. 102, no. 7, pp. 1067-1070, 1998.

[200] M. P. Stewart and J. M. Buriak, "Photopatterned hydrosilylation on porous silicon," *Angewandte Chemie International Edition,* vol. 37, no. 23, pp. 3257-3260, 1998.

[201] P. Bhattacharya, *Semiconductor Optoelectronic Devices*, Second ed. New Delhi, India: Prentice Hall of India, 2005.

[202] S. M. Sze, *Semiconductor Devices: Physics and Technology*, Second ed. New York, NY: John Wiley & Sons Ltd., 2002.

[203] H. H. Silvestri, "Diffusion in silicon isotope heterostructures," Ph.D Thesis, Dept. Materials Science and Engineering, University of California, Berkeley, Berkeley, CA, 2004.

[204] A. Fick, "On liquid diffusion," *Philosophical Magazine Series 4,* vol. 10, no. 63, pp. 30-39, 1855.

[205] S. K. Ghandhi, *The Theory and Practice of Microelectronics*, First ed. New York, NY: John Wiley & Sons Ltd., 1968.

[206] R. B. Fair and J. C. C. Tsai, "A quantitative model for the diffusion of phosphorus in silicon and the emitter dip effect," *Journal of The Electrochemical Society,* vol. 124, no. 7, pp. 1107-1118, 1977.

[207] R. B. Fair, "Concentration Profiles of Diffused Dopants in Silicon," in *Impurity Doping Processes in Silicon*. vol. 2, F. F. Y. Wang, Ed., First ed Amsterdam, NL: North-Holland Publishing Company, 1981.

[208] A. I. Hochbaum and P. Yang, "Semiconductor nanowires for energy conversion," *Chemical Reviews,* vol. 110, no. 1, pp. 527-546, 2010/01/13 2009.

[209] I. Yahyaie, D. A. Buchanan, G. E. Bridges, D. J. Thomson, and D. R. Oliver, "High resolution imaging of GHz polarization response arising from the interference of reflected surface acoustic waves," *IEEE Transactions on Ultrasonics, Ferroelectrics and Frequency Control,* vol. 59, no. 6, pp. 1212-1218, 2012.

[210] S. J. Paddison, D. W. Reagor, and T. A. Zawodzinski Jr, "High frequency dielectric studies of hydrated Nafion®," *Journal of Electroanalytical Chemistry,* vol. 459, no. 1, pp. 91-97, 1998.